

MXene Materials based Printed Flexible Devices for Healthcare, Biomedical and Energy Storage Applications

Sithara P. Sreenilayam¹, Inam Ul Ahad¹, Valeria Nicolosi², and Dermot Brabazon^{1}*

¹I-Form, Advanced Manufacturing Research Centre, & Advanced Processing Technology Research Centre, School of Mechanical and Manufacturing Engineering, Dublin City University, Glasnevin, Dublin-9, Ireland

²I-Form and AMBER research centers, School of Chemistry, Trinity College Dublin, Dublin 2, Ireland

The advent of cost effective printed smart devices has revolutionized the healthcare sector by allowing disease prediction and timely treatment through non-invasive real time and continuous health monitoring. Future advancements in printed electronic (PE) materials will continue to enhance the quality of human living. For any PE application, materials should possess proper mechanical integrity and resistivity while being non-toxic. In the case of sensing devices for physiological and biochemical signals, excellent conductivity is an essential requirement for obtaining high response signals. The emergence of the novel class of 2D materials called MXenes and their composites has resulted in structures and materials hugely relevant for healthcare devices. Exploiting solution based 2D MXene materials can expedite their practical application in PE devices by overcoming the present limitations of conductive inks such as poor conductivity and the high cost of alternative functional inks. There has been much progress in the MXene functional ink generation and its PE device applications since its discovery in 2011. This review summarises the MXene ink formulation for additive patterning and the development of PE devices enabled by them in healthcare, biomedical and related power provision applications.

Corresponding author E-mail address: dermot.brabazon@dcu.ie

Sreenilayam, S.P., Ul Ahad, I., Nicolosi, V., Brabazon, D., MXene materials based printed flexible devices for healthcare, biomedical and energy storage applications, Materials Today, 2021, <https://doi.org/10.1016/j.mattod.2020.10.025>

1. Introduction

In the past decade, the scientific community has invested much attention toward the development of 2 dimensional (2D) MXene nanomaterials, which incorporate transition metal nitrides, [1-3] carbides, [4-7] or carbonitrides, [4] as these exhibit excellent mechanical and thermal properties, high conductivity, high surface area, layered structure, unique morphology and hydrophilic nature. [4, 7, 8] Since the introduction of this class of materials with the structural formula of $M_{n+1}X_nT_x$, (M= transition metal, [4, 7, 9-13] X= carbon or nitrogen and T= terminal group (e.g., -O, -OH, or -F) [14-17] in 2011 by Gogotsi *et al.*, [7] numerous computational [10, 18-37] and experimental studies have been conducted on this material system. From the experimentally synthesised MXenes to date, over 25 of them are based on carbides, only three are from the nitride family ($Ti_4N_3T_x$, [2] Ti_2NT_x , [3] and Mo_2NT_x [38]) and two are based on carbonitrides (Ti_3CN) [4, 39]. MXenes have been synthesized by the exfoliation of layered hexagonal MAX phases (Fig. 1) having $P6_3/mmc$ symmetry by the selective removal of atomic layers (of the A group element, e.g. silicon or aluminium) using hydrofluoric acid (HF) [14, 40, 41], solution of hydrochloric acid (HCl) and lithium fluoride (LiF), [7, 42, 43] solution of HF and lithium chloride (LiCl), [42] ammonium hydrogen fluoride (NH_4HF_2) [43, 44], and ammonium fluoride (NH_4F) [45] at room temperature (Fig. 1). The molecular formula of the artificially synthesised layered MAX phase is $M_{n+1}AX_n$, here $n = 1, 2, 3$ (Fig. 1). The A group elements are mostly from the boron (group 13) and carbon (group 14) in the periodic table. Here, the name 'MXene' denotes as MAX phase with the removal of A-element atomic layers and the suffix 'ene' emphasize its 2D behaviour and graphene (GR) (discovered in 2004 [46]) resemblance. The first developed MXene was $Ti_3C_2T_x$. [7] When compared to the strong M-X bond in the chemically stable MAX phases that are combined with ionic, metallic, and covalent bonding, [47] the bonding between the atomic layers of A-element is relatively weak and hence they are more chemically reactive, forming a molecular structure suitable for exfoliation. Most of the MXene materials are generated from the aluminium containing MAX phases as aluminium exhibits high chemical activity [5, 7, 42].

An extensively studied material exhibiting layered configuration is graphite and the first developed 2D material is GR, a single-layer of graphite atoms in a 2D hexagonal lattice. The unique characteristics of graphene and associated 2D materials or single-layer materials offer huge opportunities for future technologies. The synthesis methods for 2D materials include liquid-phase exfoliation, mechanical cleavage exfoliation, wet chemistry, electrochemical metal ion intercalation and exfoliation, as well as chemical and physical vapor deposition. Along with hexagonal boron nitride (h-BN), black phosphorus (BP), and transition metal dichalcogenides (TMDs), MXenes are another example of 2D materials. [49-54] In the past number of years, evidently GR has dominated as the most investigated material from the 2D family. However, the main limitation of GR for the practical application is its simple layered network structure only with carbon atoms. The composition of materials having a more complex layered structure by the attachment of more than one element provides new possibilities due to the wide structural varieties which can be altered for particular characteristics and specific applications. [55-63] In recent years, there are a great deal of advances in the development of MXene 2D nanomaterials due to their excellent performances (Fig. 2). According to the theoretical investigations, the electronic properties of layered MXenes can be tailored or engineered by the chemical functionalisation process. [7, 12, 14, 64]

MXenes have shown significant potential for numerous applications including electromagnetic shielding [65-69], energy storage devices such as super capacitors (SCs) [70-72] and lithium ion batteries (LIB) [73-77], CO₂ capture [78-80], all-optical switching, [498-503] polymer conductive reinforcement fillers [81], field-effect transistors [82], photocatalysis [83-89], water purification [90-94], gas sensing [95-100], fluorescence imaging and heavy metal ions sensing [101], and electromechanical actuators [102, 103]. In medical applications it has been used in photothermal therapy [104-106, 497], biosensing [107-109], implants [110], tissue engineering [111], drug delivery [112, 113] and drug detection [504], antimicrobial formulations [114, 115], and diagnostic imaging [15, 104, 116].

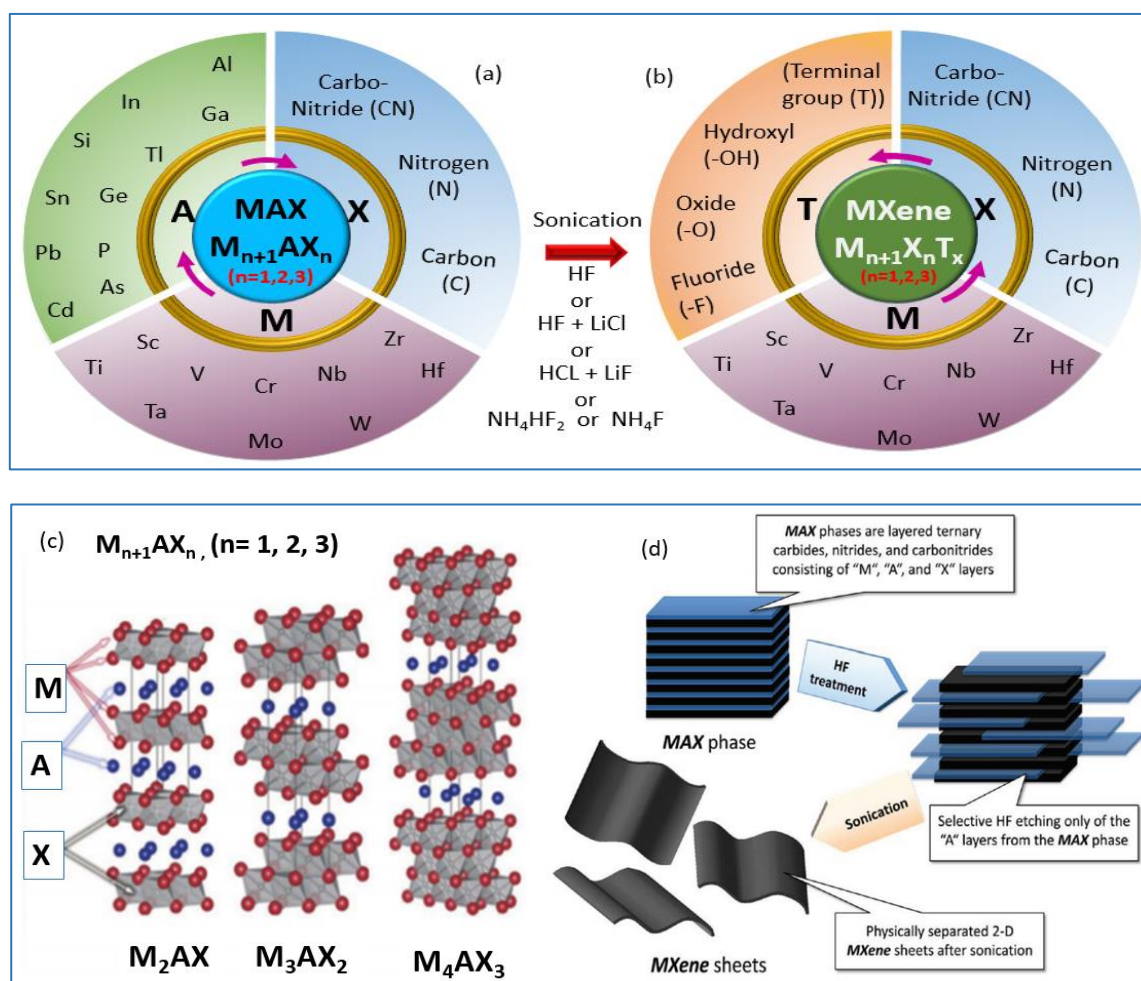


FIGURE 1. Max phase components and MXene formation. The components that create (a) MAX phase of the general molecular formula $M_{n+1}AX_n$, (b) MXene having the general molecular formula $M_{n+1}X_nT_x$, (c) MAX molecular structure with $n=1, 2, 3$, and (d) schematic illustration of MXene formation. Reprinted from the Ref. [4], Copyright © 2012 with permission from American Chemical Society.

“Smart MXene” terminology has been used by a number of researchers, for MXene based hybrid materials, exhibiting unique application based properties. Such unique combinations make MXene potential candidate for fabrication of transparent conductors. MXene can provide up to 95% transmittance in the visible and ultraviolet regions with extremely low sheet resistance (up to 0.01 k Ω per square). With excellent mechanical properties and tuneable optical properties, MXene can be used as transparent conductive electrodes for applications in touch screens, flexible displays, light emitting diodes, and range of sensors. [503, 552] For

optoelectronics, MXenes have demonstrated applications in non-linear optics [499, 501] photothermal agent [500, 497], and biosensors [343]. Particularly for biomarker quantification during Dialysis, MXene-Ti₃C₂T_x electrode was used for detection of uric acid, urea and creatinine. MXene electrode was screen printed and the electrochemical sensing mechanism was used to record the measurements to provide continuous and on-line detection [337]. MXenes have been investigated for development of all-optical switcher. MXene optical light-control-light system was built to modulate the pump light into probe light. Ti₃C₂T_x MXenes demonstrated nonlinear refractive index ($n_2 \approx 10^{-4}$) with multiple times higher magnitude when compared to GR and MoS₂. [498] Another non-linear optics application for MXenes is to be used as saturable absorbers. MXenes demonstrate reduced absorption loss at high optical intensities. Therefore, for ultrashort optical pulses produced by femtosecond lasers, MXenes have been used as saturable absorbers for passive mode locking. Feng *et al.* [553] demonstrated MXene Ti₃C₂T_x application as saturable absorber with high damage threshold and high modulation depth and achieved Q-switching in a Nd: YAG ceramic laser with 359 ns pulse width at 186 kHz repetition rate.

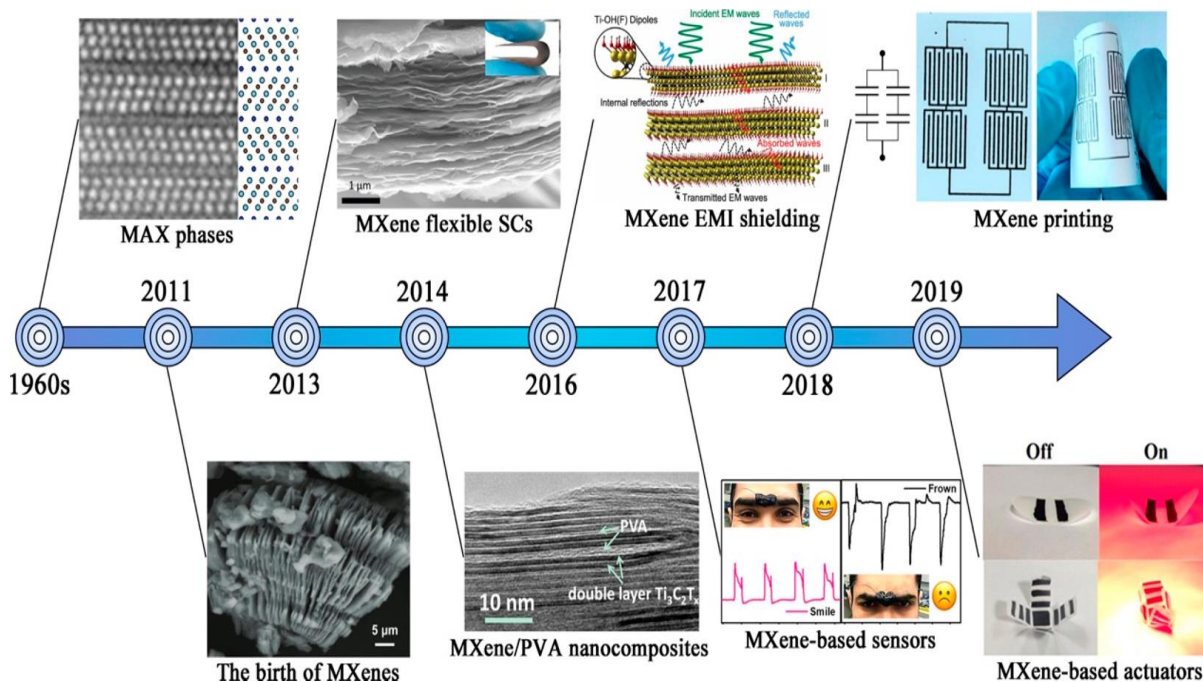


FIGURE 2. Emergence of MXene material and its PE applications in the chronological order. Reprinted from the Ref. [487] Copyright © 2019 with permission from American Chemical Society. Reprinted from the Ref. [5], Copyright © 2013 with permission from AAAS. Reprinted from the Ref. [7], Copyright © 2011 with permission from WILEY-VCH Verlag GmbH & Co. KGaA, Weinheim. Reprinted from the Ref. [65], Copyright © 2016 with permission from AAAS. Reprinted from the Ref. [312], Copyright © 2019 with permission from AAAS. Reprinted from the Ref. [140], Copyright © 2019 with permission from Springer Nature. Reprinted from the Ref. [492], Copyright © 2010 with permission from Elsevier. Reprinted from the Ref. [493], Copyright © 2018 with permission from AAAS. Reprinted from the Ref. [563], Copyright © 2014 with permission from National Academy of Sciences.

Generally, from the layered parent molecular structure, the exfoliation of 2D materials, for *e.g.*, GR, [117-122] hBN, [123-125] TMDs, [123, 124, 126-128] BP, [52, 129-131] MXenes [7, 12, 14,

64] *etc.* can be formed through the solution processing method. A number of fabrication techniques have been developed for manufacturing flexible devices using such solution processed 2D nano materials based inks. Therefore, considerable research interest has been focused on solution-processed 2D materials using this class of materials as functional inks. [132, 133] Among the flexible device fabrication techniques, printing methods have attracted much attention as they can enable mass scale economic production. [134]

Since the development of inkjet-printed transistors using solution processed GR in 2012, there has been significant progress in the formulation of functional inks and printable device applications based on 2D materials. Figure 3 shows the printed electronic (PE) applications of 2D solution processed materials: GR, [135, 136] hBN, [137, 567] BP, [52, 138] TMD, [139] and MXenes. [140, 141] Atomically planar GR has already received much popularity as a conductive ink in the flexible device fabrication field due to its exceptional electrical, mechanical, and thermal, properties. [142-146] Nevertheless, an ultimate aim for the development of GR functional inks is for them to completely replace the currently used very expensive metallic (*e.g.*, silver (Ag) [147-152], gold (Au) [142, 153-156], copper (Cu) [157-162] *etc.*) nanoparticle (NP) based conductive inks in PEs and flexible devices. However, any of the available ink formulation techniques are not capable for producing high quality mass scale GR functional ink for practical large scale PE application. Therefore, the development of new functional ink formulation methods and materials are necessary. Another representative from the large 2D family, GR-analogous MXenes, are low dimensional non-planar materials, exhibiting excellent electronic conductivity appropriate for sensing and biosensing applications

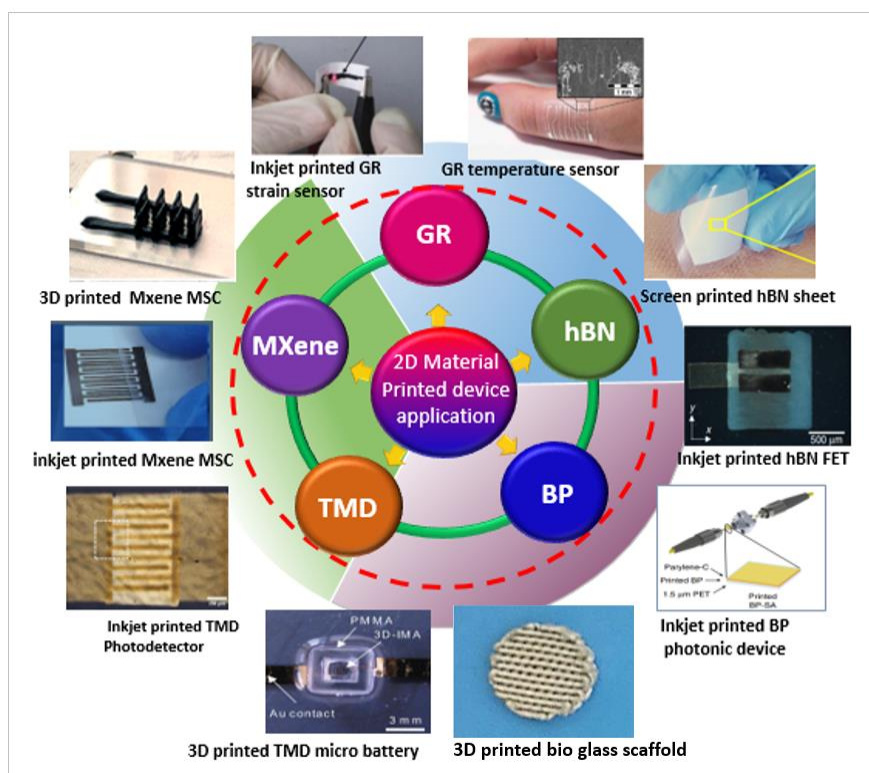


FIGURE 3. Printed electronics application of 2D materials: GR (Reprinted from the Ref. [135] Copyright © 2017 with permission from Elsevier. Reprinted from the Ref. [136] Copyright © 2016 with permission from Springer Nature), hBN (Reprinted from the Ref. [567] Copyright © 2018 WILEY-VCH Verlag GmbH & Co. KGaA, Weinheim), BP (Reprinted from the Ref. [52] Copyright © 2017 from Springer Nature. Reprinted from the Ref. [138] Copyright © 2018 from Royal Society of Chemistry), TMD (Reprinted from the Ref. [139] Copyright © 2018 from IOP Publishing Ltd), and MXene (Reprinted from the Ref. [140] Copyright © 2019 with permission from Springer Nature. Reprinted from the Ref. [141] Copyright © 2020 with permission from American Chemical Society).

in healthcare have attracted much research attention and represent an alternate candidate for various applications for highly conductive ink formulation.

Application sector areas include healthcare, aerospace, automotive, environmental and clean energy. MXenes in the 2D family, with an exceptional combination of excellent electronic and mechanical properties have already proved successfully in some printed and flexible electronic devices. MXene materials are composed of abundant and non-toxic elements (Ti, N or C). The generation of by-products N_2 and CO_2 after their degradation are also not toxic. Therefore, MXene materials have been widely

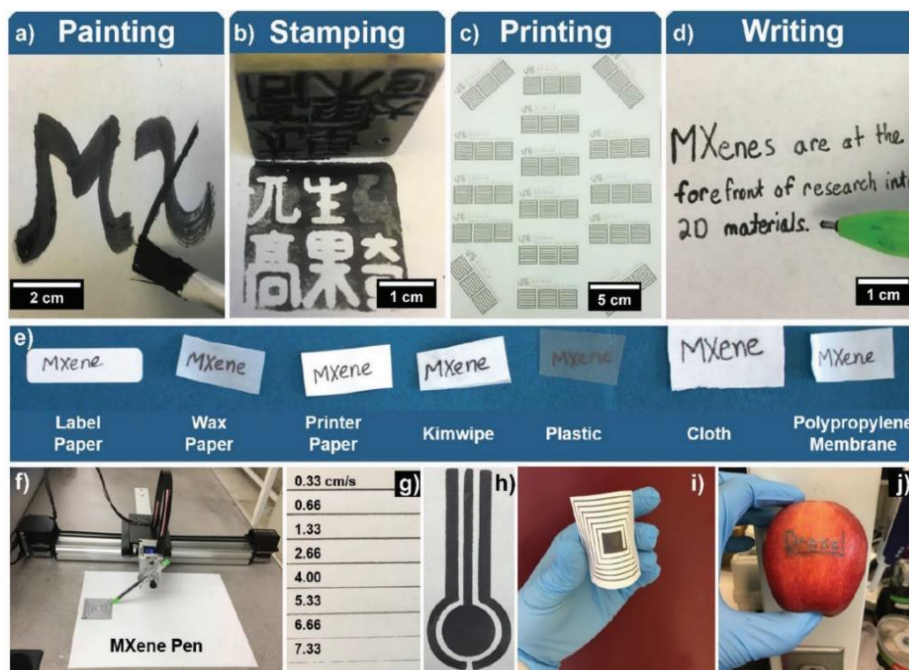


FIGURE 4. Different deposition methods of MXene ink, (a) painting (b) stamping, (c), printing and (d) writing. (e, j) MXene ink writing on various substrates including paper, plastic, cloth, polypropylene membrane and fruit. (f) Computer controlled patterning using automated writing apparatus, AxiDraw. (g) MXene lines deposited at different speeds. (h, i) Patterns deposited using the apparatus AxiDraw. Reprinted from the Ref. [169] Copyright © 2018 with permission from WILEY-VCH Verlag GmbH & Co. KGaA, Weinheim.

investigating for environmentally friendly applications. [163] The peculiarity of the aqueous based MXene ink is that it can be formulated for different deposition methods (such as painting, stamping, printing and writing (Fig. 4a-d) and made suitable for different substrates (such as paper, plastic, cloth and polypropylene membrane (Fig. 4e), even it is possible to write on a fruit (Fig. 4j) [169]. The automated direct writing of MXene inks is shown as implemented by attaching a Ti_3C_2 ink filled pen into a computer controllable robotic arm (AxiDraw, IJ Instruments Ltd.) (Fig. 4f) to make patterns (Fig. 4h, i) at adjustable speeds. Depending on the substrate surface smoothness, patterns having thickness in the range of ≈ 0.5 – $10 \mu m$ and line widths in the range of ≈ 0.3 – $1 mm$ can be deposited by adjusting MXene inks concentration and writing speed. Figure 4g shows lines deposited at different speeds. [169]

This specific 2D family is of significant research interest as proven by the growing research efforts and progress. Review papers to date reported on MXene synthesis [518, 519], application in electrocatalysis [520], water purification and environmental applications [521-524], and energy storage devices [523, 525-528]. The applications of Mxene nanosheets in biomedical sciences for therapeutic and biosensing purposes have been also reviewed. [107,

529]. A recent review on MXene PE application discuss work on printing and patterned coating of MXenes in terms of applications in electronics and optoelectronics, sensing and actuation and energy storage [378]. However, a detailed summary of PE applications of MXenes in the healthcare and biomedical sectors has not yet been reported. Therefore, recent advancement in the development of 2D MXenes, formulation of inks for specific printing techniques such as inkjet printing, screen printing, and 3D printing and MXene PE applications specifically in healthcare and biomedical areas are highlighted in this review article. MXenes materials certainly will open up more new opportunities by virtue of their tunable surface and transition metal chemistries when compared to other materials such as GR, carbon nanotubes (CNT) and C60. The broad fascinating properties and potential for their usage in promising technologies indicate that the development of MXenes will remain a significant area of research for years to come.

2. MXene based Flexible Electronics Fabrication Method and Ink Formulation

2.1. Printing Techniques

The emerging and fascinating PE technology, which brings the application of printing methods to fabricate electronic components and devices is leading to the mass scale production of lightweight, flexible, and cost effective electronic parts and components for numerous applications. [164, 170-174] The global market of flexible device technology, obtaining significant advancements over the past decade offering a diverse and wide range of commercial products is estimated to increase from \$ 31.7 billion US dollars in 2018 to over \$77.3 billion by 2029. [165] This technology first started to advance as a cost-effective potential replacement of electronic systems based on silicon and the manufacture of integrated electronic devices instead of using complex and expensive integrated circuit (IC) fabrication technology. The processing steps involved in the printing methods for the development of an electronic device are simple and fewer when compared to the conventional silicon based manufacturing methods that consist of several hundred processing steps in a production line. [175] Advancements in the PEs are necessary as the manufacturing market is growing very fast. The printing methods, commonly used for making conductive patterns with solution based functional inks onto the flexible and conformable substrates are screen printing, inkjet printing, flexographic printing, and roll-to-roll gravure printing. [215-220] There are three important factors that need to be considered when fabricating PE components and devices: (i) substrates, (ii) methods for the functional ink deposition, and (iii) the materials for the generation of the functional ink.

Flexible substrates and post printing process for PE devices: Generally, substrate selection depends on the requirements of a particular application where the printed component or part is intended to be used. PE technology is capable for printing components on paper, [176-178] textile, [179-182] and plastic [183-187] substrates. In this technology, commonly used plastic substrates are polyurethane (PU), polyethylene (PE), polyacrylate (Pacr), polycarbonate (PC), polyethylene terephthalate (PET), polyether imide (PEI), and polydimethylsiloxane (PDMS). [188-190] In these popular substrates, PC, [191] PU [192] and PET [193-196] are highly deformable and optically well transparent. The substrate based on PDMS [197-200] can be formulated to exhibits super elasticity and biocompatibility as well. Several parameters of the selected substrates including surface roughness, surface energy, thickness, thermal stability, mechanical stability and surface treatment affect the functional ink selection and print quality.

Most PEs prefer to use flexible substrates having excellent surface energy (γ_{SV}) and low porosity. A high γ_{SV} of the substrate indicates its nature of high hydrophilicity, leading to a strong adhesion of functional inks to the surface. However, if the γ_{SV} is low, the substrate surface will exhibit high hydrophobicity, *i.e.*, more hydrophobicity indicates the reduced lateral spread of the ink on the surface of the substrate which leads to an increased resolution of the print patterns. Both these hydrophilic and hydrophobic natures of the surface of the substrates have bad and good influences on the quality of printing. Gas-impermeability and dimensional stability of flexible substrates are vital factors for all PE applications. Other important properties are heat resistance as the fabrication of a flexible device involves high temperature processing steps (~ 300 °C) and flexibility. Therefore, careful selection of suitable materials as substrates for a particular PE application is vital to meet the mechanical, physical, optical, thermal, and functional ink requirements.

After printing, post printing process such as curing or sintering of the printed patterns that is similar to drying in the conventional printing method, needs to be carried out for improving conductivity and microstructure and thereby mechanical performances of the printed tracks. [221] In this post processing treatment, a reduction in electrical barrier will occur by the removal of surfactants and as a result, the resistance of the printed track decreases through the coalesce of the printed ink particles, forming a continuous electric conductor. Depending on the material that is used for ink formulation and substrate, different curing methods such as pressure assisted, [222] thermal energy, [222] mechanical, [223] non-thermal chemical process [224] *etc.* have been used. For flexible polymer substrates having low glass transition temperature, the conventional thermal curing is not possible. In such cases, either laser assisted or intense pulsed light curing methods are commonly used. [225, 226]

2.2. Printable ink Formulation

Inks to use in PE technology should keep a particular viscosity, not clog print nozzles, and exhibits other characteristics specific to the chosen particular method and kind of printer. The materials used in such inks exhibits dielectric, [201-203] semiconducting, [183, 204-206] or conducting, [207-209] properties and it can be either inorganic (*e.g.*, Cu, Au, Ag, aluminium (Al), carbon and GR) or organic (*e.g.*, polymers, and RGO) materials. [210, 211] A high level knowledge in physics and chemistry is required for the ink formulation appropriate to the chosen substrate to be patterned on and printing method. Ink composition strongly influences the homogeneity of the patterns and their characteristics. The ink composition of a particular organic or inorganic material in aqueous or appropriate organic solvent contains several additives such as rheology and surface tension modifiers, active agents (functional material either conducting, semiconducting or dielectric), [134, 212] binders and defoamers. [213] One significant property of the PEs ink is its viscosity which has a direct influence on the printed pattern, *i.e.*, layer thickness of the printed patterns will be more if the ink is highly viscous and the flow of ink droplets (*e.g.*, in the inkjet printing) will not be controllable if the ink is less viscous. The selection of printing method depends on the parameters such as ink curing properties, process speed, accuracy, web tension, *etc.* The materials used as inks determine the PE device operation and its functionality. The suitable rheology and viscosity of the ink for a particular printing method must be optimized when formulating inks. To make sure proper wetting conditions, to obtain an ink surface tension (γ_{LV}) that matches the substrate, the ink

needs to be adjusted by adding surfactants/additives and appropriate solvents. For controlling the wetting properties, one should know the values of γ_{LV} and γ_{SV} . [214] The condition for a substrate that wet partially is $\gamma_{LV} > \gamma_{SV}$ and it is properly wet if $\gamma_{LV} < \gamma_{SV}$. [214] Lower values of γ_{SV} lead to a finite contact angle (θ_c) *i.e.* $\cos\theta_c < 1$ in between the chosen substrate and fluidic ink when the ink drop touches the surface of the substrate.

MXene inks for PE devices: In recent years, MXene has received much attraction in the flexible device fabrication due to its excellent mechanical and thermal properties, high ion adsorption abilities, excellent hydrophilicity, high surface area, and super electric conductivities. [7] MXene materials are mostly generated by the selective removal of “A” layers from their MAX phases using strong etching solutions that contain fluoride ions. It is possible to produce MXenes from non-MAX phases as well, in such case, the synthesis process involves the etching out of diatomic multilayers. [71] In both cases, strong etchants are used. A number of top-down etching and delamination techniques have been developed to produce MXenes. [377-379] The etching process suits well for MXene production as the chemical bond M-A is chemically more active when compared to the bond M-X and therefore, wet-chemical etching technique has been generally used for generating MXenes. Fluoride based acidic solutions are mainly used for MXene production. However, through the electrochemical selective etching, fluoride free etching steps are also possible, for example, Ti_2AlC etching in solutions which contain chloride. [511, 512] Mass scale MXene production easily achievable through the selective chemical etching technique, which is the advantage of the MXene materials over many other 2D materials. Depending on the crystal structures, particle size and strength of the atomic bonding, the conditions for the optimal etching vary with the MAX phases, *i.e.*, for example, transition metal, M, having large atomic number requires strong etchants and take longer time for etching. [64] MXene multi-layered materials form after the selective A-layer etching process. Multilayered MXene particles have been used for applications in LIBs and adsorption. Delamination techniques are performed to make single MXene nanosheets. A single layer of MXene contains a single crystalline layer with a number of atomic layers. Single-sheet 2D materials which is generated *via* delamination method often show very different characteristics when compared to their counterparts having bulk layers. In MXenes, the delamination of multi-layers to single or few layer nano MXene flakes strongly affects their characteristics. For instance, the energy storage device applications based on the delaminated MXene nanosheets exhibited good electrochemical performances. [5, 9, 42, 332, 546] Therefore, it is vital to delaminate MXenes successfully into single-layers for obtaining their unique 2D characteristics. For MXene delamination, intercalation is required to separate MXene flakes well. Different organic molecules and metal cations (*e.g.*, Al^{3+} , Na^+ , Li^+ , and Ca^{2+}) are used as intercalants either through electrochemical or chemical reactions. MXene inks, that can be printed, have been developed by dispersing MXene suspension well using intercalation and delamination. [43, 75, 378, 379] Through the delamination, MXene flakes having lateral size in the nano-meter to micro-meter ranges can be produced. Centrifugation is generally used for obtaining uniform 2D flake size distribution. [380] This sheet/flake size strongly affects the properties of MXenes. [381] Eventhough the bottom-up techniques for developing surface-termination-free 2D nitrides and carbides have been developed, they are not much explored for MXene. The main problem is the generation of bulk 2D carbides and non-2D carbides. The bottom-up approach for the MXene generation involves the two step processes such as MAX phase thin film epitaxy and following MXene thin film development

by the A layer's removal. [382-385] Nanometer thick (~2-3 nm) W_2C and Mo_2C have been generated *via* pulsed laser deposition and chemical vapor deposition. Another bottom up route is the salt templating method. [545] However, the direct MXene growth by using thermal deposition methods has not been developed yet. Each MXene synthesis method, top-down and bottom up, still needs to be advanced and perfected towards low-cost, high efficient, high-quality and reproducible because MXene materials properties significantly depend on the synthesis and processing conditions. In the near future, emerging processing techniques, for example, computer numerical controlled deposition (CNC) [543] and 3D printing [544] could be applied to engineer precisely MXene based composite materials.

Different characterization techniques are performed to understand the A layer removal, surface groups attachments, MXene flakes formation and flakes dimensions. The Al- layer removal can be confirmed using x-ray diffraction (XRD) studies (Fig. 5a) and Raman spectroscopic studies (Fig. 5b). [496] The disappearance of Al-layer peak and the peak emergence ([0 0 0 l]) of $Ti_3C_2T_x$ is clearly visible in the XRD patterns of Ti_3AlC_2 , as- $Ti_3C_2T_x$, d-a- $Ti_3C_2T_x$, d-D- $Ti_3C_2T_x$, in Fig 5a. The Raman studies of the same materials given in Fig. 5b shows the disappearance of peaks of Ti_3AlC_2 at 185, 200 and 270 cm^{-1} after the treatments in HF. The surface conditions such as the attachments of functional terminal groups can be clarified by X-ray photoelectron spectroscopic (XPS) study (Fig. 5c). [496] The high resolution XPS spectrum O1s shown in Fig. 5c explains the attachment of -O atoms in all the three materials as- $Ti_3C_2T_x$, d-a- $Ti_3C_2T_x$, and d-D- $Ti_3C_2T_x$. [496] Fourier-transform infra red (FTIR) spectroscopy helps to obtain the details of new surface terminations in MXene beyond the conventional terminal O, F, and OH groups (Fig. 5d). [551] Internal surface terminations of MXenes and the confirmation of intercalation mechanism can be investigated using Nuclear Magnetic Resonance (NMR) spectroscopy. [549, 564-566] Hope *et al.*, reported the ^{13}C NMR spectra of MXene Ti_3C_2 and MAX. The broad signals recorded at -227 ppm for HF etched sample and at -255 ppm for the LiF-HCl etched samples indicates the -F terminations on the flakes. [549] One of the recent Solid-state (SS) NMR spectroscopic study of MXenes (particularly 1H SSNMR) shows different types of -OH group terminations that reside on the internal and external surfaces, in a $Ti_3C_2T_x$ MXene (Fig. 5e). [566] This work also reports the interactions of water- flake surface and de-intercalation mechanism of water upon annealing (Fig. 5e). [566] Terminal groups attachments can also be investigated using Electron Energy-Loss Spectroscopy (EELS) (Fig. 5f). [550] MXene flake morphologies can be characterized using Scanning electron microscopic (SEM), Transmission electron microscopy (TEM) and atomic force microscopy (AFM). Figure 5g shows the SEM image of MXene flakes having size ranging from from 4 to 15 μm . [548] These MXene flakes are generated using LiF etchant and non- sonication. The SEM image shows the same brightness on the surface suggesting the formation of MXene flakes having same thickness. Further characterization using TEM confirms the production of hole free MXene flakes with well-defined and clean edges (Fig. 5h). [548] The shapes and thickness of the MXene flakes can be studied by AFM. Figure 5i shows the AFM image of a folded $Ti_3C_2T_x$ flake having 2.7 nm height. [548]

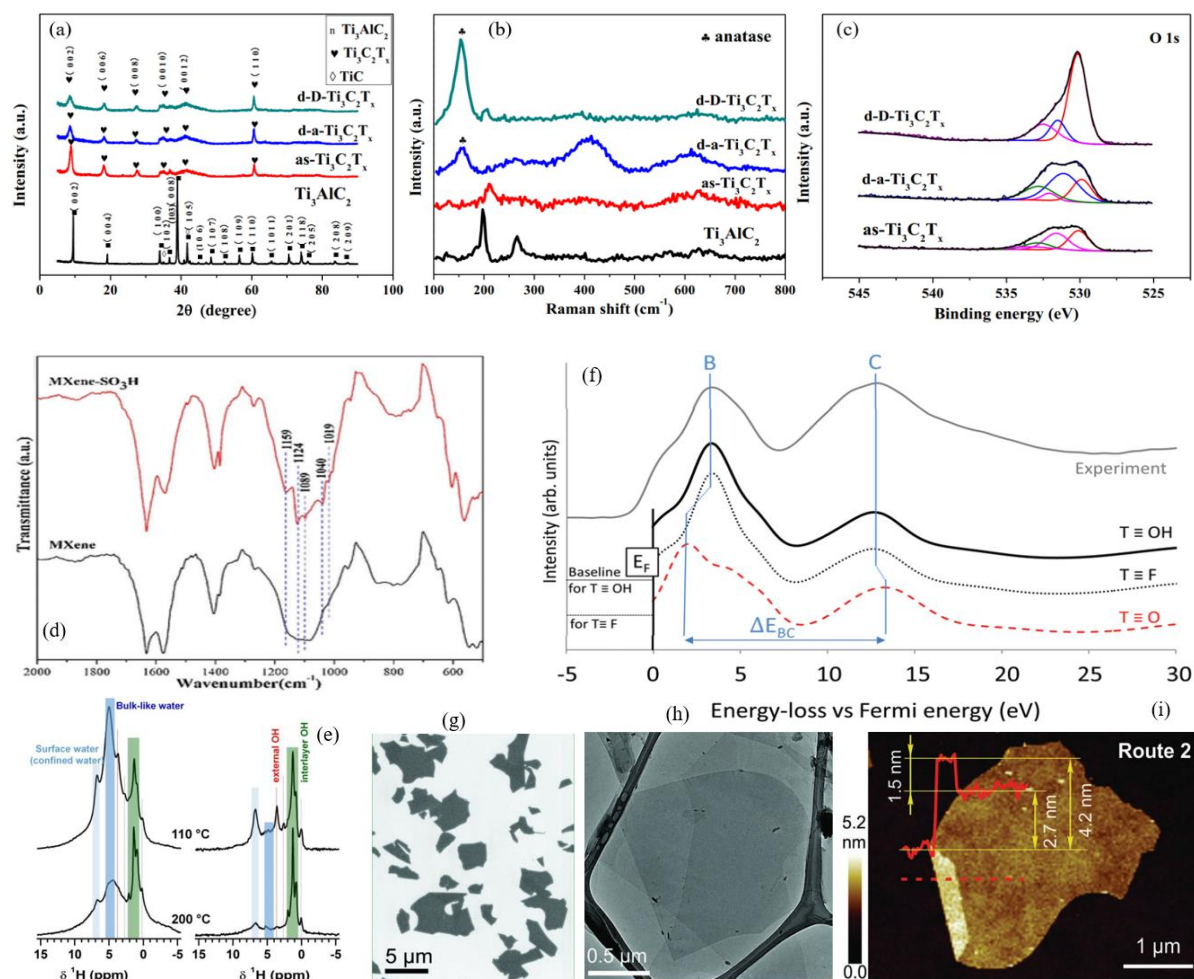


FIGURE 5. (a) X-ray diffraction (XRD) patterns and (b) Raman spectra of Ti_3AlC_2 , as- $\text{Ti}_3\text{C}_2\text{T}_x$, d-a- $\text{Ti}_3\text{C}_2\text{T}_x$, d-D- $\text{Ti}_3\text{C}_2\text{T}_x$. (c) The high resolution XPS spectrum O1s of as- $\text{Ti}_3\text{C}_2\text{T}_x$, d-a- $\text{Ti}_3\text{C}_2\text{T}_x$, and d-D- $\text{Ti}_3\text{C}_2\text{T}_x$. Reprinted from the Ref. [496] Copyright © 2018 with permission from Elsevier. (d) Fourier-transform IR spectra of an MXene and after surface modifications of an MXene with diazonium salt groups. Reprinted from the Ref. [551] Copyright © 2016 with permission from Elsevier. (e) 1D ^1H SSNMR spectra (1D magic-angle spinning (MAS) (left side) and MAS with spin-echo (MAS_{echo}) (right side)) of MXene $\text{Ti}_3\text{C}_2\text{T}_x$ recorded at 110 °C and 200 °C annealed temperatures. Reprinted from the Ref. [566] Copyright © 2020 with permission from American Chemical Society. (f) Electron Energy-Loss Spectroscopy (EELS) of MXene with OH, O and F terminations. Reprinted from the Ref. [550] Copyright © 2016 with permission from Royal Society of Chemistry. (g) Scanning electron microscopy (SEM) and (h) Transmission electron microscopy (TEM) images of MXene flakes. (i) Atomic force microscopy (AFM) image showing the few-layer behaviour of an MXene flake. (h) and (i) Reprinted from the Ref. [548] Copyright © 2016 with permission from WILEY-VCH Verlag GmbH & Co. KGaA, Weinheim.

For MXene synthesis, HF etching is considered as the best approach. However, HCl/LiF etchants have been generally used for synthesis of 2D MXene, [515] because the etchants which contains a high concentration HF will lead to high fluorine attachments on MXene nanosheet surfaces. An increase in the development of defects on the MXene nanosheets is observed with the use of more aggressive etching agents like HF. The use of fluorine based etchants prohibits safe synthesis of MXene inks and poses challenges to the research community to develop non-toxic and environmentally friendly routes for MXene synthesis. A couple of research studies have been performed to demonstrate fluorine free synthesis of

MXenes, [530-532] however, these have not been demonstrated for large scale applications. Beside etching, increase in the lateral size of the 2D MXene layers also need urgent attention of the research community. [533]

Micro-meter to nano-meter thick MXene patterns deposition from the colloidal MXene inks are necessary for the practical application. This material especially in the colloidal form provide the potential to fabricate flexible devices on flexible substrates including paper, plastic and textiles using various printing [140, 166, 167], coating [168] and direct writing [140, 169] techniques. The main advantage of these techniques is their capability to produce high density large-area electronic surfaces. When compared to traditional colloidal inks, the rheological characteristics of the MXene based inks can be effectively tuned for wet processing as MXene nanolayers exhibit a high-aspect-ratio with higher surface charge. The rheological characteristics of MXene inks are strongly depends on nanolayers aspect ratio, degree of functionalization and particle size distribution. The other parameter that affects the rheological behaviour is its concentration. [513] Generally, different regimes of rheological properties can be obtained for different MXene ink concentrations. For example, the dispersion of a m-MXene having medium sized particles (*e.g.* 5 μm) at low (10-30 wt.%) concentrations lead to the random dispersion of particles with reduced particles interaction. However, at medium/moderate (40-60 wt.%) concentrations, a sol-gel transition can be formed and at higher (>60 wt.%) concentrations, the percolated nanolayers network forms colloidal gels having substantial yield strength. [513] When formulating MXene inks for different liquid phase techniques including printing methods, each of these behavioral regimes of inks can be used.

MXene based inks, shows high levels of elastic behavior even at its low concentration suspension ($<0.36 \text{ mg.ml}^{-1}$). [513] Such ink formulations can be used for particular printing techniques such as inkjet printing, that use inks having low-viscosity. Generally, MXenes are developed in water and disperse well in water compared to any other solvent. However, other alternative solvents for MXene dispersion and ink formulation are necessary for printing applications as the additive-free aqueous inks exhibits high surface tension. [547] This leads to poor ink jetting and wetting. Recently, Zhang *et al.*, formulated inkjet printable MXene inks in various organic solvents such as ethanol, dimethylformamide (DMF), N-Methyl-2-pyrrolidone (NMP) and dimethyl sulfoxide (DMSO). [140] The viscosities of all the formulated inks were appropriate for inkjet printing and MSCs were fabricated on flexible substrates. The performance of the printed MSCs were different for different ink formulation and best results were obtained from the NMP ink. The printed tracks showed excellent adhesion to the chosen substrate and high mechanical integrity even without the use of binder in ink generation, that is because of the strong functional groups interaction. Aqueous $\text{Ti}_3\text{C}_2\text{T}_x$ ink based MSC printed on paper substrate via 2D extrusion printing [140] shows high value of figure of merit ($66996 \text{ S.cm}^{-1} \cdot \text{mg.ml}^{-1}$) when compared to GR ink ($6000 \text{ S.cm}^{-1} \cdot \text{mg.ml}^{-1}$). Yang *et al.* studied the nanoflake aspect ratio and size dependencies on MXene inks rheological behaviour by formulating additive free extrusion printable ink that contains ultrahigh aspect ratio nano flakes (~ 4000). [327] The ink developed was shown viscosity with the same order of magnitude as the inks reported with three orders of higher concentration magnitude. These high aspect ratio nano flakes were developed using a mild etching method. The formulated inks in different concentrations were exhibited high yield strength that is required for 3D printing technique. For the retention of proper shape and interlayer connection in printed patterns, the viscoelastic characteristics of the inks should be precisely adjusted. In aqueous media, MXene layers are less

stable, that limits the formulation of MXene based printable inks. For overcoming this limitation, more studies are required for capping MXene nanosheets and improving oxidation resistance. For example, Wu *et al.*, reported MXene aqueous ink having good oxidation resistance by using sodium ascorbate as capping agent to $Ti_3C_2T_x$ nanolayers. [289] Such inks exhibited high dispersibility and stability over 80 days. [289] The challenges for precise printing using MXene inks lie in the ink formulation including the kinetics of solvent evaporation as well.

Even though, several printing technologies have been available for flexible device manufacturing from the colloidal functional inks, [181, 209, 227-229] so far screen printing, extrusion type 3D printing, and inkjet printing are the main three techniques used for colloidal MXene printing.

MXene inks for Inkjet printing: The main attraction of this non-contact inkjet printing technique [230, 231] suitable for the large area flexible electronics fabrication is, small fluid droplets of materials can be repeatedly deposited with a higher accuracy to a specific place in a controlled manner through the limited processing steps and reduced material waste. [232] Substrates compatibility, production at low temperature, digital and additive functional structure development, and high printing speed are its other benefits. [233] All these properties make this method capable for direct printing of electronic components including wearable sensors, [234, 235] solar cells, [236, 237] thin film transistors, [238, 239] electroluminescent displays, [240] transparent electrodes [241] and complementary ring oscillators [242]. This method can be categorized as Continuous Inkjet printing (CIJ) and Drop-on-Demand (DoD) Inkjet printing. [232, 243-245] Using this method, patterns having higher thickness (up to 20 μm) can be printed. The viscosity of the ink used in this technology is in the range of 0.001-0.04 Pa.s. [246] Numerous conductive inks based on nanomaterials have been already developed for using in this printing method. [247-252]

For inkjet printing of MXenes colloidal ink, the printing factors such as print height, waveform of ink jetting, ink jetting frequency, ink viscosity, ink density, surface tension, ink jetting temperature, inkjet printer nozzle diameter, stable ink jetting, substrate wetting, ability to dry and form spatially well uniform MXene deposited patterns *etc.* have to be optimized. [245] One of the important requirement is the stable jetting of a single ink droplet without any satellite or secondary ink droplet creation [243, 262-265] as this deviate ink drops from the jetting path and make deposition in the areas that are even not targeted. [266] The ink fluidic features that are represented by the dimensionless constants such as Weber number(W), [267] Reynolds number (R), [268] and Ohnesorge number(Oh), [269] determines the ink droplets jetting nature as, [270, 271, 230]

$$R = \frac{\nu \rho a}{\eta}, \quad W = \frac{\nu^2 \rho a}{\gamma}, \quad Oh = \frac{\sqrt{W}}{R} = \frac{\eta}{\sqrt{\gamma \rho a}} = \frac{1}{Z} \quad (1)$$

where, v (ms^{-1}) = average travel velocity of ink droplets, ρ (g/cm^3) = density, a (μm) = diameter of ink jetting nozzle, γ (mJ/m^2) = surface tension of the printable ink, and η (mPa s) = dynamic viscosity of the ink. According to the numerical studies that conducted in 1984, the required condition for obtaining stable ink jetting without satellite drops is $Z > 2$ [270] and the computational fluid dynamics studies later on conducted in 2000 by Reis *et al.* have reported this inverse Ohnesorge number, Z , which is independent of ink velocity but relates to the density of the fluid, surface tension, and viscosity, and it has been reported that it should be in the range of 1 - 10. [272] However,

experimentally, Daehwan Jang *et al.* have redefined this Z value range as $4 \leq Z \leq 14$ through the in-situ monitoring of dynamics of ink drops formation for different fluids. [273] Here, the values of Z that are less than 4, and greater than 14, point out the satellite drops formation. These are badly affecting the resolution and the positional accuracy of print patterns and therefore are not suitable for the inkjet printing technique. The Z values can be optimized by adjusting η , ρ , and γ .

Even though, various functional inks based on nanomaterials have been developed for inkjet printing technique, [247-252] they are very expensive (*e.g.*, Ag and Cu NP [253, 254] based inks) and facing lack of stability in solvents that are generally used (*e.g.*, ethanol, acetone, IPA, water). Due to this stability problem, these metallic NP dispersions in such solvents requires stabilizing agents. [262, 274] This kind of inks require post-processing treatment/sintering at high temperatures after printing, leading to them oxidizing very easily. [255] Even though the novel

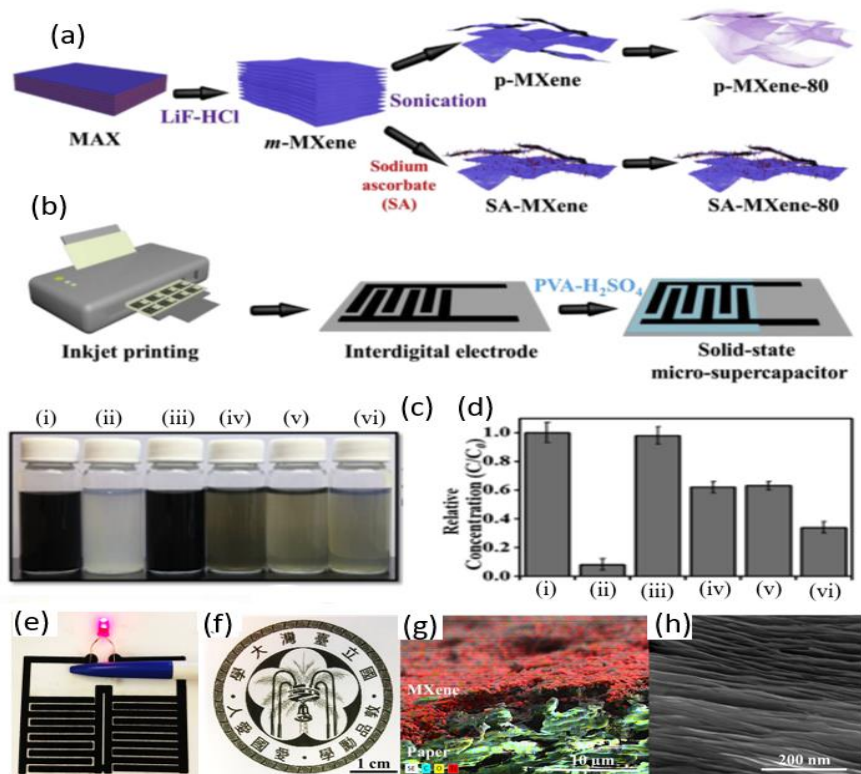


FIGURE 6. MXene inks and inkjet printing. Schematic demonstration of (a) MXene nanocomposite synthesis and (b) inkjet printing. (c) MXene inks (i) fresh and after 80 days (ii) MXene-80, (iii) SA-MXene-80, (iv) SC-MXene-80, (v) SO-MXene-80, and (vi) SP-MXene-80), (d) with the relative concentrations, (e) Picture of a planar two SA-MXene inkjet printed MSCs in series connection light up a LED. (f) Picture of an SA-MXene inkjet printed emblem of NTU. (g) SEM-EDS image of SA-MXene inkjet printed patterns cross section view on a paper substrate. Here, yellow color represents oxygen, blue color indicates carbon and red is for titanium. Scale bar is $10\mu\text{m}$. (h) SEM high magnification image of the layered SA-MXene structure on paper substrate. Scale bar is 200 nm . (e)-(h) from the supporting information. Reprinted from the Ref. [289] Copyright © 2019 with permission from Elsevier.

techniques in particular ‘enhanced NP photo-absorption’ permit these functional metallic inks to be treated more easily, [256] emerging 2D nanomaterials based inexpensive inks are considered as an alternative of these currently used expensive metallic NP based inks. [49, 257-261] The first attempts for generating 2D material based functional inks were using the graphene oxide (GO). [274-288] 2D MXenes have received much attention in recent years as these exhibit higher conductivity than graphene. Several MXene based inkjet printable (Fig. 6a, b) inks have been formulated. For example, Chien-Wei Wu *et al.* have formulated inkjet printable stable $\text{Ti}_3\text{C}_2\text{T}_x$ MXene inks with suitable surface tension modifiers and viscosity, through the etching method using $\text{LiF}+\text{HCl}$ solution. [289] They have shown the structural stability enhancement of MXene $\text{Ti}_3\text{C}_2\text{T}_x$ in liquid after its treatment with the capping ligand (Fig. 6c, d) *i.e.*, the capping ligand resists oxidation when it exposed to air or at the ambient temperature storage conditions. Among the capping ligands used in this study (sodium ascorbate (SA), sodium citrate (SC), sodium phosphate (SP) and sodium oxalate (SO)), SA exhibited the best results as the ions of ascorbate helped to increase the distance between MXene nanosheets and enhance the oxidative stability and dispersibility. The developed SA-MXene ink was stable for around 80 days. The ink density was $\sim 1100 \text{ kg m}^{-3}$ and the calculated Z value was 19.4. The MXene nanolayers lateral size is a very important factor for ink jetting, as larger values lead to clogging of the print nozzle. Therefore, for generating high performance print patterns *via* inkjet printing, the functional ink material size must be 1/10 that of the diameter of the print nozzle or even smaller. Here in this SA-MXene case, the lateral size of the nanosheets are approximately 200 nm ($>1/50^{\text{th}}$ of inkjet printer nozzle size) which were obtained after 4h MXene nanolayer delamination sonication treatment. The homogeneous patterns having thickness 1.5 μm have been inkjet printed on a photopaper using this SA-MXene ink without any clogging issues at the inkjet printer nozzle (Fig. 6e-h). In another example, additive free inkjet printable $\text{Ti}_3\text{C}_2\text{T}_x$ viscous inks (Fig. 7) in organic solvents (ethanol, dimethylformamide (DMF), N-Methyl-2-pyrrolidone (NMP) and dimethyl sulfoxide (DMSO)) have been formulated (Fig. 7a, e, c) and homogenous conductive patterns with higher resolution were inkjet printed (Fig. 7l) on untreated polymeric and paper substrates. [140] The TEM images (Fig. 7b, d, f) and TEM histograms (Fig. 7k) of these MXene DMF, ethanol and MXene DMSO inks reveal the formation of monolayers to few-layered MXene nanosheets having a mean lateral size in the range, $\sim 1\text{--}2.1 \mu\text{m}$ (Fig. 7k). Solvent-transfer strategy has been used to formulate these MXene organic inks having nanosheet lateral sizes within the suitable range for inkjet printing. The Z values of all these MXene organic inks are (ethanol=2.6, DMSO=2.5, and NMP=2.2) within the optimal range for producing a stable ink jetting. Even after 12 months, the MXene ink in NMP, DMF and ethanol were stable, however, DMSO ink had completely sedimented after 6 months (Fig. 7 g-i) which shows the homogeneity of MXene nano flakes in NMP, DMF and ethanol solvents. The viscosity–shear rate study (Fig. 7m) shows the shear-thinning behaviour and non-Newtonian characteristics of these organic inks and the SEM pictures of printed patterns having line gap, $\sim 410 \mu\text{m}$ and line width, $\sim 450 \mu\text{m}$, given in Fig. 7 n-r shows their ink jet printability. This work report that the inkjet printed patterns using the developed stable organic MXene inks were stable even at 24 months after production (Fig. 7s).

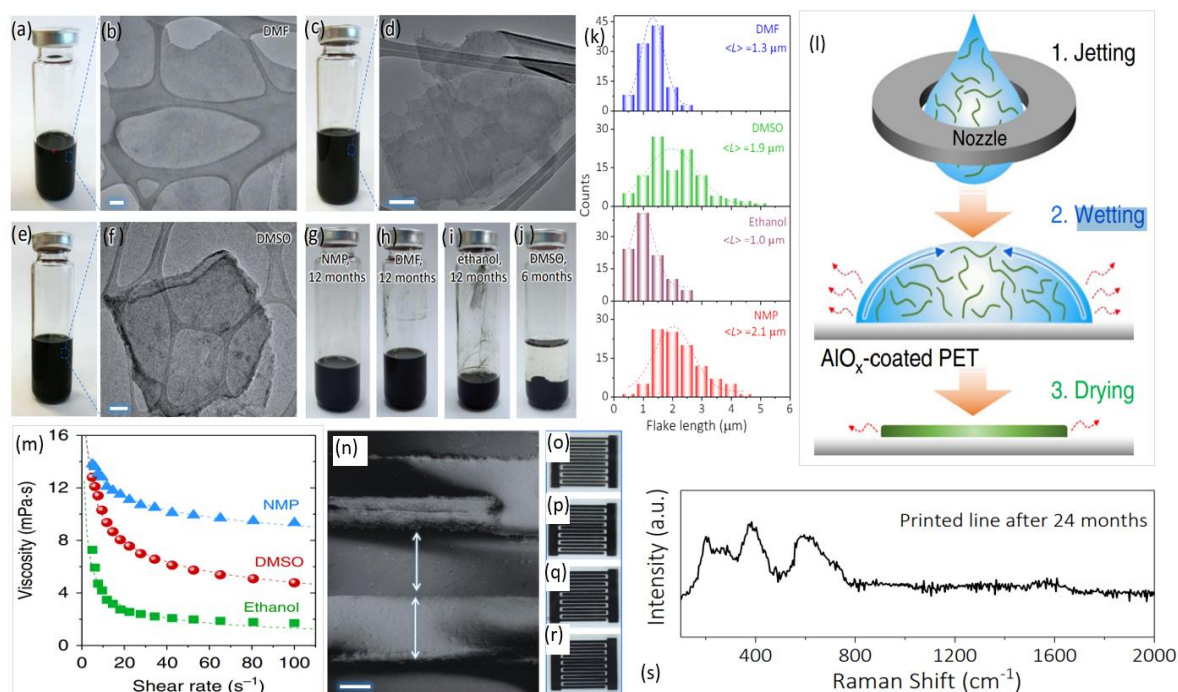


FIGURE 7. MXene inks in different solvents and inkjet printing. Photograph and SEM picture of (a, b) MXene DMF ink, (c, d) ethanol ink, (e, f) MXene DMSO ink. Optical of (g) NMP, (h) DMF and (i) ethanol inks after 12 months and (j) DMSO ink after 6 months. Scale bar in the images of (b, f) 200 nm and (d) 100 nm. (k) Histogram of the MXene $Ti_3C_2T_x$ nanolayer size from the statistics of transmission electron microscopy (TEM) of NMP ink (2.1 μm), DMF ink (1.3 μm), ethanol ink (1.0 μm), and DMSO ink (1.9 μm). (l) Schematic of organic MXene inks inkjet printing fine resolution, here, green line = MXene nanolayers, blue arrow = ink droplets inward flow, red arrow = ink droplets outward flow. (m) Viscosity of organic MXene inks (NMP, DMSO and ethanol) as a function of shear rate. (n) SEM of inkjet printed pattern and images of (o) ethanol, (p) DMSO, (q) DMF and (r) NMP. (s) Raman spectra of the inkjet printed patterns after 24 months, confirming stability. Reprinted from the Ref. [140] Copyright © 2019 with permission from Springer Nature.

MXene inks for Screen Printing: In the manufacturing industry, widely used simple, faster and mature method for developing PEs is screen printing, which is a contact process. [290-296] Screen printing method is compatible to both rigid (*e.g.*, silicon wafer, glass) and flexible (*e.g.*, plastic, paper, textile) substrates. [297] Print patterns quality and resolution are dependent

strongly on stencilling methods, ink printability and the compatibility of substrates and inks. [214, 300] Screen printable ink viscosity comes in between 0.5-50 Pa.s. The factors that decide the ink volume to deposit are, the screen thread count, screen thread diameter, D and, pressure. [238, 294, 298, 299] Using this method, conductive patterns having higher thickness up to 100 μm can be printed, that means, a large amount of ink material can be deposited per unit area, enhancing

electrochemical performance. This quality makes screen printing technique more versatile than the conventional printing methods, particularly in the large scale manufacturing of micro-sized and flexible energy storage systems. [301] One of the main limitations of this technique is that the required ink for screen printing must be highly viscous with an appropriate shear-thinning characteristics. Another factor that limit the cost effectiveness of the production process is the amount of the material that used for printing. Even though a number of flexible devices (*e.g.*, wearable sensors, [186, 302] energy storage devices, [303-305]) have already been screen printed, the availability of limited selection of screen printable ink and lack of ink standardization restricts screen printed device performances and therefore this method's cost effectiveness.

MXene based pure and composite screen printable inks have been developed for fabricating MSCs and sensors. An example of MXene $\text{Ti}_3\text{C}_2\text{T}_x$ based screen printable inks formulation,

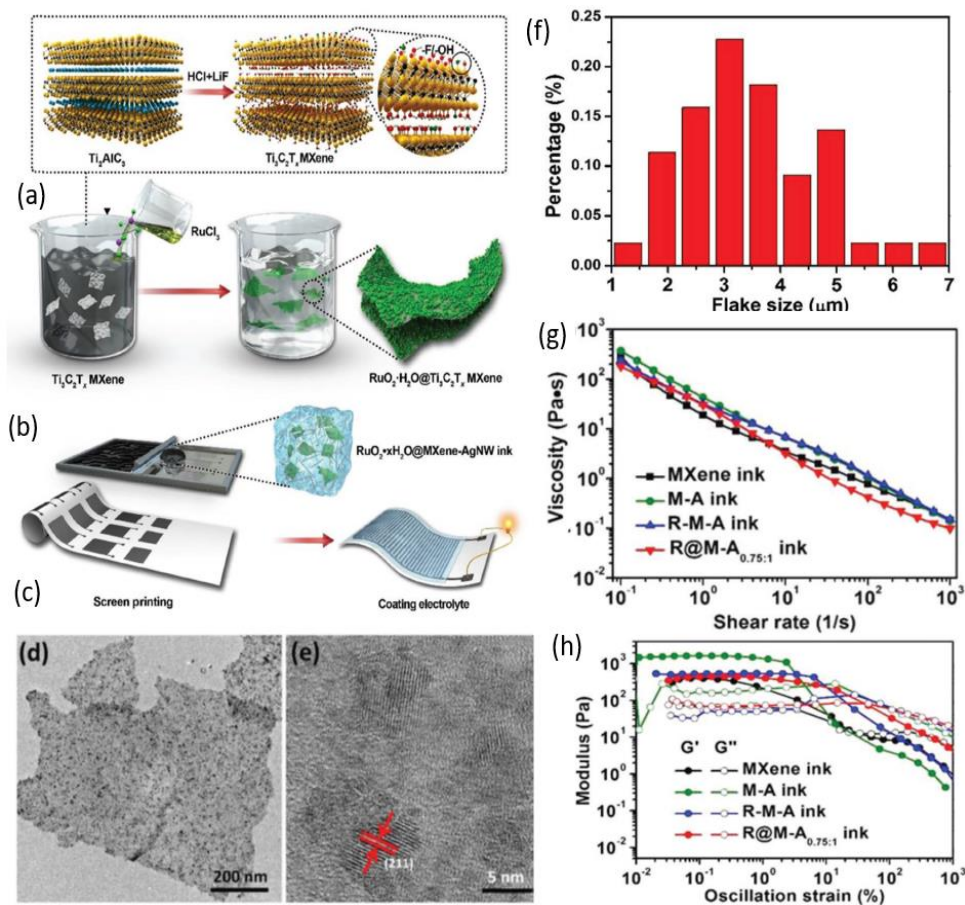


FIGURE 8 Screen printable MXene inks and properties. (a-c) Schematic explanation of screen printable MXene $\text{Ti}_3\text{C}_2\text{T}_x$ ink formulation and MXene screen printing. (d) the TEM and (e) high-resolution TEM (HRTEM) pictures of the developed nanocomposite $\text{RuO}_2 \cdot x\text{H}_2\text{O}@\text{MXene}$. (f) MXene nanolayers sideways size distribution from the atomic force microscopy (AFM) studies. (g) Viscosity as a function of shear rate. (h) Oscillation strain dependent storage modulus G' and loss modulus G'' variations. Reprinted from the Ref. [307] Copyright © 2019 with permission from WILEY-VCH Verlag GmbH & Co. KGaA, Weinheim.

characterization and their screen printing process are given in Fig. 8. [307] In printing process, rheological properties of MXene based inks plays an important role. The MXene ink viscosity is variable and can be tuned by adjusting shear rate as linear reduction in viscosity occurs with an increase in shear rate. That means, MXene ink is not following Newton's law of viscosity. As the ink is transferring through the mesh in screen printing method, the screen printable inks must fulfil the requirements such as suitable viscosity, and high yield stress, so that the ink can transfer through the screen mesh only with the pressure of squeegee and smoothly distributes. [306] With non-Newtonian inks, it is possible to control the ink flow via control of the processing conditions. The main factors that influence non-Newtonian fluids are shear thickening or shear thinning flow property and time. The loss modulus (G''), representing viscous response and storage modulus (G'), representing elastic solid like nature tell us the stress reaction in oscillatory shear for a viscoelastic fluid, which use to characterise printable inks rheological properties. The $G' > G''$ means the solid like nature, which enables the ink solidification during printing and $G'' > G'$ means the liquid like nature, enabling easy extrusion of inks at higher shear stresses. The rheological properties of the inks have a large influence on the parameters of the print pattern resolution, aspect ratios, wettability of inks on the substrates, and alignment of the material particles in inks. One of the recent work reports a fully screen printed strategy to develop flexible MSCs on paper substrates using the inks, MXene, MXene+AgNW (M-A), $\text{RuO}_2 \cdot x\text{H}_2\text{O}$ nanoparticles +MXene +AgNWs (R-M-A) and $\text{RuO}_2 \cdot x\text{H}_2\text{O}@\text{MXene}$ + AgNWs with the mass ratio 0.75:1 (R@M-A_{0.75:1}) (Fig. 9). [307] Aqueous-phase synthetic procedure has been used to generate $\text{RuO}_2 \cdot x\text{H}_2\text{O}@\text{MXene}$ nanocomposite (Fig. 8a). Schematics of MXene screen printing using the $\text{RuO}_2 \cdot x\text{H}_2\text{O}@\text{MXene}$ nanocomposite are shown in Fig. 8b, c. The homogenous anchoring of $\text{RuO}_2 \cdot x\text{H}_2\text{O}$ nanoparticles onto the MXene nanosheet surface has been confirmed by TEM study (Fig. 8d) and the high-resolution TEM (HRTEM) image indicate the amorphous and the polymorphic behaviours of the RuO_2 nanoparticles (Fig. 8e). In this case, the delaminated MXene nanolayers using HCL+LiF shows lateral size 2–5 μm and thickness ≈ 1.5 nm, confirms the monolayer formation (Fig. 8f). The study reveals that these screen printable inks are with ideal non-Newtonian fluid characteristics (Fig. 8g), appropriate for continuous MXene ink transfer *via* screen mesh and minimal spreading after printing. This work report that the developed MXene, M-A, R-M-A, and R@M-A_{0.75:1} inks were with appropriate shear-thinning characteristics and viscosity for screen printing process which is evidenced by the modulus results *i.e.*, all these reported inks were shown $G' > G''$ before the point of yield stress (which is the switching point of elastic deformation to the plastic deformation) and after this point, it was $G' > G''$ (Fig. 8h). The MSC patterns having uniform edges and well defined shapes have been screen printed using these developed pure MXene ink (Fig. 9a, e), M-A ink (Fig. 9b, f), R-M-A ink (Fig. 9c, g), and R@M-A_{0.75:1} ink (Fig. 9d, h). The MSC which is screen printed using R@M-A_{0.75:1} ink exhibit higher conductivity ($\sim 17\,800$ S cm^{-1}) than the other inks, that is because of the presence of AgNW network and the smaller $\text{RuO}_2@\text{MXene}$ nanocomposite size. When compared to previous works related to MSC, [308-311] this screen printed MSC based on R@M-A_{0.75:1} nanocomposite ink, shows the highest conductivity (as high as $17\,800$ S cm^{-1}). In this case, $\text{Ti}_3\text{C}_2\text{T}_x$ MXene nanolayers were separated by RuO_2 NPs that attached on the nanosheet surface *via* oxygenated functional groups. Incorporation of all the individual elements properties in this R@M-A_{0.75:1} ink leads to the development of flexible MSC with higher print resolution, enhanced electrochemical performance with respect to energy density, volumetric capacitance, and power density, super cycling stability, and robust and durable

mechanical properties (Fig. 9i-k). In another work, screen printable crumpled nitrogen doped MXene (MXene-N) exhibiting non-Newtonian shear-thinning fluid nature, has been reported [166] *i.e.*, a decrease in viscosity observed with an increase in shear rate (Fig. 9l) similar to the inks reported by H. Li *et al.* [307] This MXene-N ink with uniformly doped N has been formulated through a melamine formaldehyde templating method. Nitrogen doping leading to an enhanced electrochemical reactions and increased conductivity. To support fine patterns printing and prevent short circuiting of the entire printed device, this ink possesses higher viscosities greater than 10^4 Pa. s at the initial shear rate 0.05 s^{-1} (Fig. 9l). [166] The G'' domination at the increased values of shear stress *i.e.*, greater than 500 Pa indicate the smooth printability of the developed ink. The frequency decency study of G' and G'' shows lower values of G'' when compared to G' in the entire frequency region under interest, which suggest the developed ink stability (Fig. 9 m, n). [166]

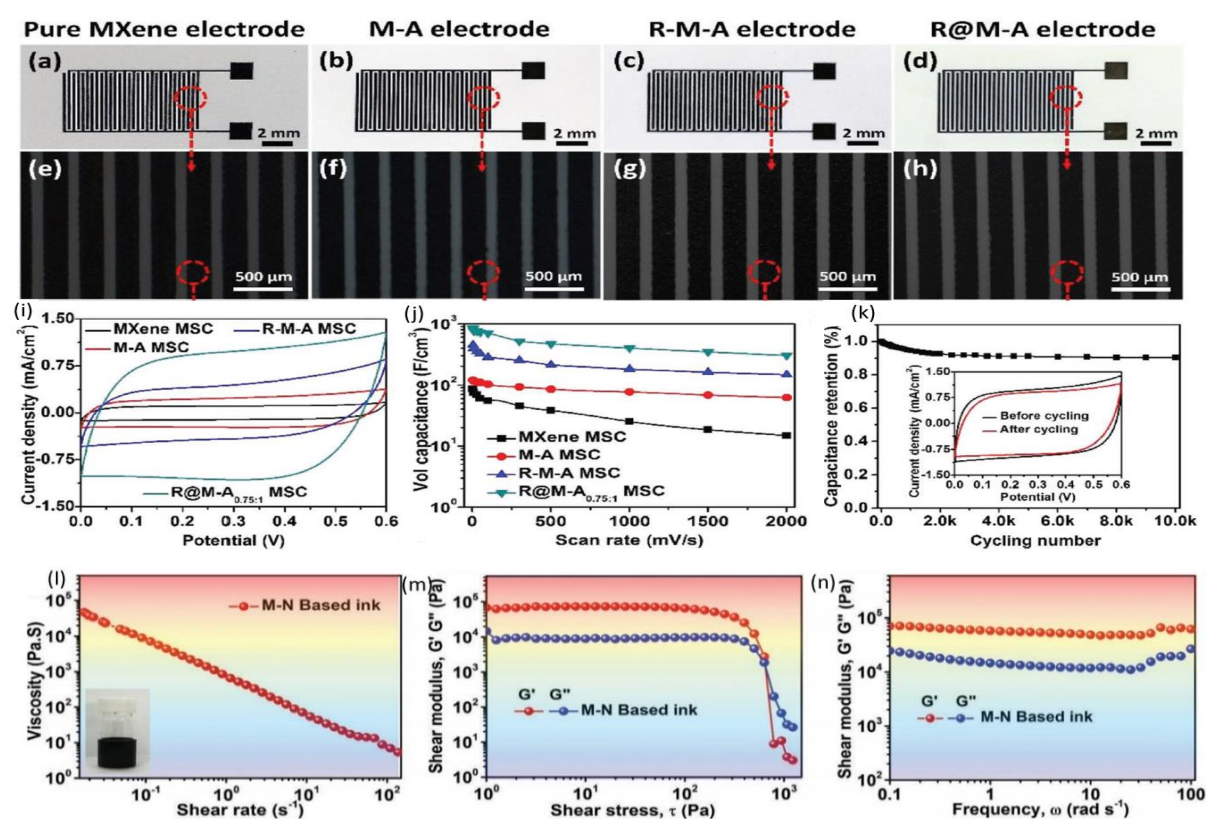


FIGURE 9. MXene based screen printable ink properties and screen printed MXene MSCs. Photographic and microscopic optical images of screen printed MSCs using the inks based on (a, e) MXene (b, f) MXene and AgNW nanocomposite (M-A), (c, g) $RuO_2 \cdot xH_2O$ nanoparticles, MXene and AgNWs (R-M-A) composite and (d, h) $RuO_2 \cdot xH_2O@MXene$ and AgNWs composite with the mass ratio 0.75:1 (R@M-A_{0.75:1}). (i) Current density as a function of potential for MSCs screen printed using the developed MXene and composite inks. (j) Scan rate dependent volumetric capacitance of the screen printed MSCs. (k) Capacitance retention as a function of cyclic number of the MSC screen printed using R@M-A_{0.75:1} ink. Reprinted from the Ref. [307] Copyright © 2019 with permission from WILEY-VCH Verlag GmbH & Co. KGaA, Weinheim. (l) Shear rate dependent viscosity of MXene-N. Modulus G' , G'' of MXene-N as a function of (m) shear stress and (n) frequency. Reprinted from the Ref. [166] Copyright © 2019 with permission from WILEY-VCH Verlag GmbH & Co. KGaA, Weinheim.

MXene inks for 3D Printing: 3D printing denotes the computer-controlled production of a complex 3D structure directly from the computer aided design (CAD) model, [313] in which deposition of material is in a layer-by-layer (additive) manner along the Z-axis as per the

required object's computer slicing. 3D printing is a bottom-up technique, which is capable for achieving rapid prototyping and offers much simplicity and flexibility in the manufacturing of very complex precise microstructures with super mechanical characteristics to satisfy all kinds of single requirements. Different 3D printing methods have been widely used to develop structural electronic systems with adaptive designs and personal customization through the integration of components such as conductors into the devices which are 3D printed. [234, 314, 315] Extrusion based 3D printing process has been widely used to produce wearable flexible devices including health monitoring sensors, and energy storage devices [316-324]. In this process, inks in the colloidal form are deposited in a layer-by layer or additive manner onto a chosen substrate by extruding them *via* nozzle and develop 3D objects. More viscous inks are required for extrusion based 3D printing process to keep the 3D printed structure without any damage or collapse. The structure and shape of the 3D printed objects on various substrates can be solidified immediately after the ink extrusion *via* nozzle, that promote precise and rapid prototyping. [325, 326] This method is in high demand to permit fast digital processing for customized super capacitor and sensor patterning. In this sense, to enable various printing protocols, the rheological characteristics of the 3D printable inks are very important *i.e.*, the physical characteristics of inks are determined by the ink components and their interactions, which strongly affects both printing process and the developed patterns.

MXene based 3D printable functional inks have been received much attention in recent years. Schematics in Fig. 10a-d show the fabrication strategy for MXene based freestanding architectures and MSC by 3D printing technique. [327] Here, in this example, the 3D printable MXene ink having specific rheological properties (Fig. 10b) was formulated with 2D $Ti_3C_2T_x$ flakes (Fig. 10a) and used to print freestanding, architectures of different shapes and sizes with high specific surface area, showing its suitability to fabricate high-performance symmetrical MSCs (Fig. 10c, d). The dimensions and shape of the developed 3D structures can be retained after freeze-drying process (Fig. 10c, d).

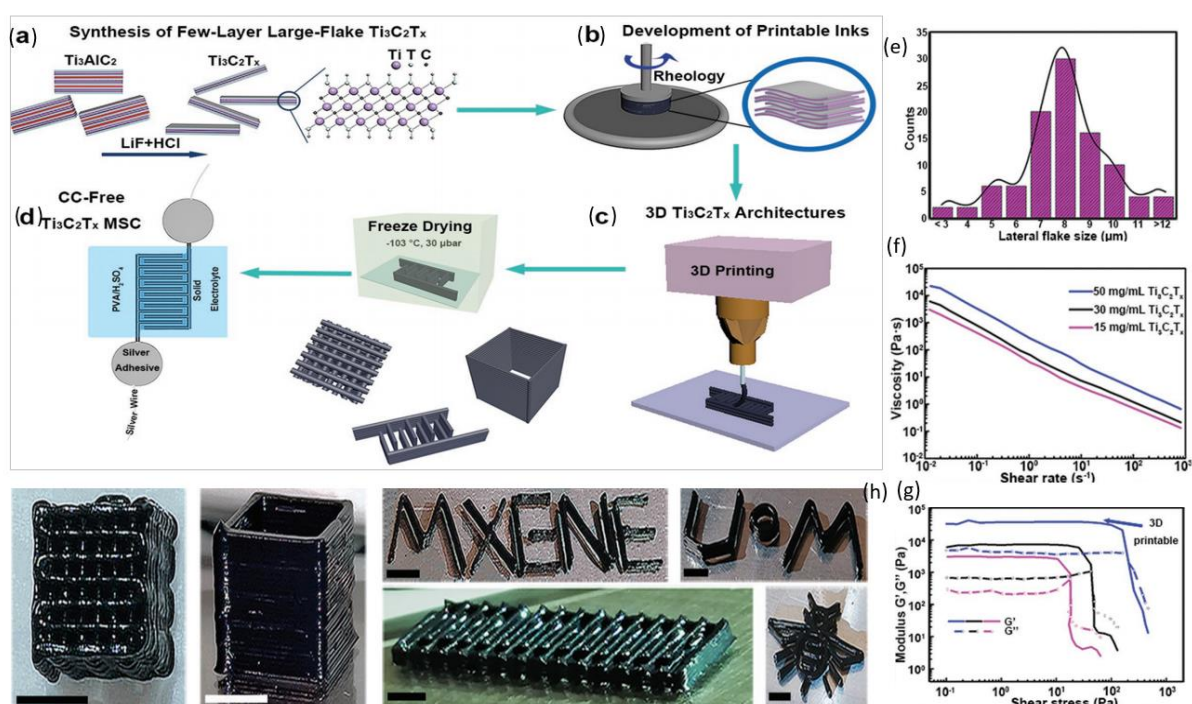


FIGURE 10. MXene 3D printing. Schematic illustration of the 3D printing fabrication strategy for freestanding architectures based on MXene inks. (a) development of 2D MXene $Ti_3C_2T_x$ without sonication, (b) production of aqueous $Ti_3C_2T_x$ ink and its rheological properties characterization to check the appropriateness to 3D printing technique, (c) 3D printing of MXene inks and following freeze-drying to make 3D freestanding structures, recollecting their dimensions and shape, and (d) MSCs fabrication. (e) Lateral flake size of MXene $Ti_3C_2T_x$. Histogram is obtained from SEM. (f) Ink viscosity as a function of shear rate. (g) Modulus G' , G'' of MXene ink as a function of shear stress. ((h) Images of 3D printed structures with different shapes and sizes using the developed MXene $Ti_3C_2T_x$ ink. Scale bars of all the images are 3mm. Reprinted from the Ref. [327] Copyright © 2019 with permission from WILEY-VCH Verlag GmbH & Co. KGaA, Weinheim.

The rheological properties of the developed aqueous additive free 3D printable MXene ink has been controlled with few-sheet thick large flakes having lateral size of $8\ \mu\text{m}$ (Fig. 10e). MXenes bidimensionality with more positive charges on edges and large negatively charged nanolayer surfaces provide them electrostatic properties and make them capable for water intercalation. [327] Here, MXene nanolayers were etched out using the mixture of LiF and HCl (Fig. 10a). It is reported that this MXene ink has rheological characteristics (Fig. 10f, g) suitable for the formation of “solid-like” strong $Ti_3C_2T_x$ networks and additive printing of freestanding 3D structures without any internal damage or collapse (Fig. 10h).

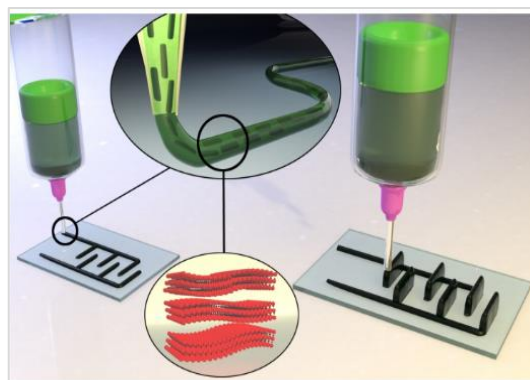


FIGURE 11. MXene ink printable mechanism through a 3D printer nozzle. Reprinted from the Ref. [141] Copyright © 2020 with permission from American Chemical Society.

Here, shear stress which is induced in the 3D printer nozzle has an important role in the MXene flake alignments which leads to their alignment horizontally in the direction of the 3D printer nozzle movement (Fig. 11). [141]

In the work reported by L. Yu *et al.*, a developed binder-free 3D printable MXene composite ink is presented, in addition to the binder-additive MXene aqueous screen printable ink, based on MXene-N. [166] Here, a 3D printable composite MXene-N ink was formed by mixing it with GO, carbon nanotubes (CNTs), and

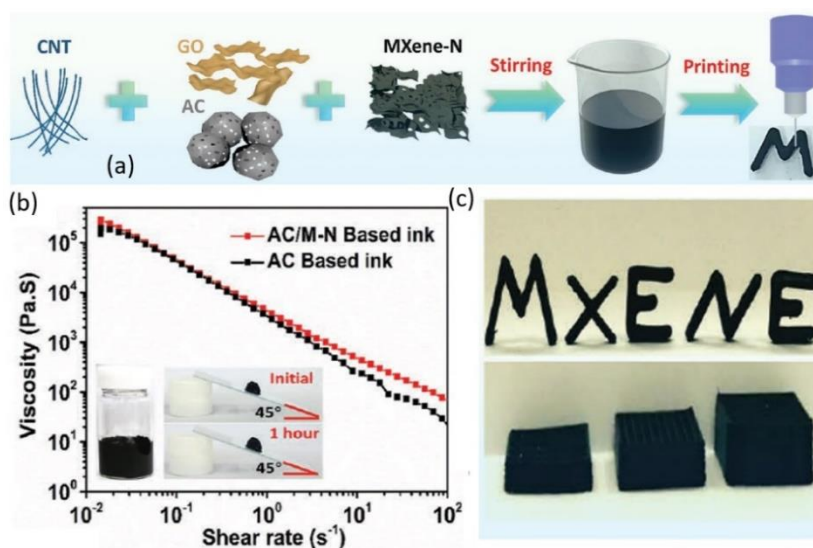


FIGURE 12. 3D printable MXene composite ink formation. (a) Schematic demonstration of 3D printable AC/CNT/MXene-N/GO ink formulation. (b) Shear rate dependent viscosities of AC/CNT/MXene-N/GO ink and (c) Optical images of the 3D printed free standing woodpile structure for three different heights and MXENE scaffolds having a height of ≈ 15 mm. Reprinted from the Ref. [166] Copyright © 2019 with permission from WILEY-VCH Verlag GmbH & Co. KGaA, Weinheim.

activated carbon (AC) for controlling the ink viscosities to be appropriate for extrusion printing (Fig. 12a). The 3D printable capability of this ink was demonstrated by successfully fabricating a freestanding and rigid woodpile structures and MXENE scaffold using this developed AC/CNT/MXene-N/GO ink (Fig. 12c). Rheological properties of this composite MXene-N ink show shear thinning nature and it exhibited high viscosity *i.e.*, $>10^4$ Pa. s at 0.06 s^{-1} shear rate (Fig. 12b) and yield stress *i.e.*, $G' \geq G''$ is of 300 Pa. The yield stress and viscosity values of this composite MXene-N ink enabled extrusion printing without any clogging during the printing process and generated stable freestanding 3D structures.

A comparison of functional ink properties of MXene and other some of the conventional materials of PE applications are given in Table 1.

Table 1. Comparison of Printable functional inks based on MXene and conventional materials.

Ref.	Material	solvent	Stability	Concentration	Viscosity	electronic conductivity	Fabrication Method	Application
[140]	MXene (Ti ₃ C ₂ T _x)	Water	12 months	36 mg mL ⁻¹	0.71 Pa.s	~ 10 ³ S cm ⁻¹	Extrusion 3D printing	MSC
		NMP	12 months	12.5 mg mL ⁻¹	13.8 mPa.s			
		DMF	12 months				Inkjet printing	MSC
		Ethanol	12 months	0.8 mg mL ⁻¹	7.3 mPa.s			
		DMSO	6 months	2.1 mg mL ⁻¹	12.8 mPa.s			
[166]	MXene-N	Water	-	-	$>10^4$ Pa s	-	Screen Printing	SC
	AC/CNT/MXene-N/GO		-	-	$>10^4$ Pa s	-	Extrusion 3D printing	

[307]	pure MXene	Water			High	2653 S cm ⁻¹	Screen printing	MSC
	M-A					7830 S cm ⁻¹		
	R-M-A					12182 S cm ⁻¹		
	R@M-A _{0.75:1}					17800 S cm ⁻¹		
[327]	2D Ti ₃ C ₂ T _x	Water		15 mg mL ⁻¹	>10 ³ Pa s		Extrusion 3D printing	MSC
				30 mg mL ⁻¹	>10 ³ Pa s			
				50 mg mL ⁻¹	>10 ⁴ Pa s			
[554]	RuO ₂ /PEDOT:PSS/Graphene	Water	-	-	10 ³ cP	1570 S cm ⁻¹	Screen printing	SC
[311]	GR	Water	-	-	8–12 mPa s	6.10 (± 0.92) × 10 ³ S m ⁻¹	Inkjet Printing	MSC
[556]	Ag	Water	-	-	2 mPa s	>10 ⁴ S m ⁻¹	Inkjet Printing	Conductive pattern
[556]	MWCNT/Ag	Water		160 mg mL ⁻¹	-	-	Inkjet Printing	Conductive pattern
[557]	GO/polyaniline (PANi) - PEDOT:PS	Water	-	25 mg mL ⁻¹	3.9 Pa s	64 S cm ⁻¹	Extrusion printing	fMSC
[558]	GR/ ethyl cellulose (EC)	cyclohexanone, terpineol, and di(ethylene glycol) methyl ether	>6 months	30 mg mL ⁻¹	-	-	Inkjet Printing	SC
[559]	Exfoliated graphene (EEG)	dimethylformamide (DMF)	>6 months	2.3 mg mL ⁻¹	4 mPa s	High	Inkjet Printing	MSC
[560]	Ag@PPy nanocomposites	Water	good stability	-	low viscosity	-	Screen printing	MSC
[561]	AgNW-MONW	Water	long-term stability	1 mg mL ⁻¹ GO/MXene and 1 mg mL ⁻¹ NW	80 000 Pa s	40 000 S cm ⁻¹	Extrusion 3D printing	MSC
[305]	N-doped rGO	polyvinylidene fluoride	-	4 : 1 in weight	-	-	Screen printing	MSC
[316]	V ₂ O ₅ /GO and GR-VNQDs/GO	-	-	50 mg mL ⁻¹	>10 ⁴ Pa. s	-	3D printing	MSC

3. MXene: PEs device Application

3.1. Biomedical Application

The unique features of MXenes such as the high surface area of MXene nanolayers, enhanced hydrophilicity, the presence of functional groups (-F, -OH or -O), excellent physicochemical, mechanical, and electronic characteristics, high absorbance of the electromagnetic radiation in the near-infrared (NIR) region (650–900 nm), and biocompatibility, make them suitable for biomedical and biosensing applications in the

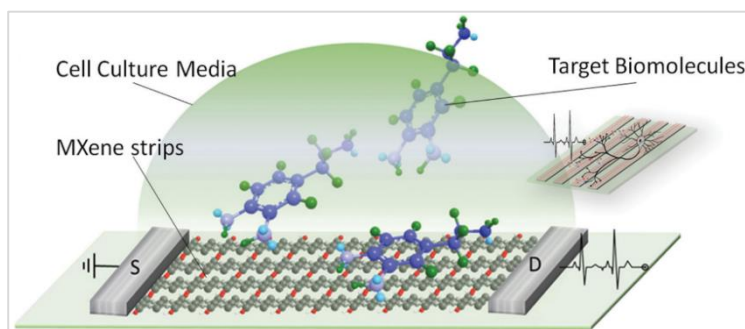


FIGURE 13. Schematic illustration of the MXene field effect transistor (FET) biosensing device. Reprinted from the Ref. [82] Copyright © 2016 with permission from WILEY-VCH Verlag GmbH & Co. KGaA, Weinheim.

medical field. [328-331] Another unique feature of MXene is the sufficient mesophase structure. The rich surface chemistry of MXene allow for targeting modifications. The combination of these properties with MXenes capability to functionalize the nanosheet surface easily with different NPs or polymers make them a favorable nanoplatform especially for bioimaging cancer therapy and accurate biosensing. In drug delivery application, the high surface area of MXenes leading easy attaching of versatile agents of therapeutics on the layered structure surface, similar to delivery approach of other 2D nanoplatforms. [508-510] Even though the metal oxide semiconductors (MOS) are currently a good choice for biosensing application, they produce high signal with very little noise simultaneously only at a higher temperature (300-450°C), which limits their practical application in portable sensor devices. [505-507] However, MXenes have a room temperature sensing ability of high signal with minimized noise due to the combination of fully functionalized layer surface and excellent metallic conductivity and therefore these are recommended as an alternative to MOS. The sensing mechanism in MOS systems is controlled by the conductivity of the surface which is strongly dependent on the atmosphere but in 2D MXenes, transfer of charges from the adsorbed molecules play a major role. This material has started to be used for biosensor applications only after the Ti_3C_2 MXene micropattern based field effect transistor (FET) was developed in 2016 for the label free high sensitive dopamine detection and the hippocampal neurons fast movement monitoring (Fig. 13). [82] In the sensor device developed by Xu *et.al.*, the semiconducting metallic characteristics of Ti_3C_2 MXene with an appropriate bandgap leads to very low off state leakage of current compared to that of 2D graphene (zero bandgap), offering excellent detection sensitivity. This work was a new opening for MXenes in the area of biosensing and since then, a number of research works started to immobilize biomaterials or enzymes on the MXene based electrode surfaces for biosensor applications, for example, hydrogen peroxide (H_2O_2) biosensor, [329, 331-335] nitrite biosensor, [328, 336] creatine, [337] adrenaline, [338] phenol, [339] carcinoembryonic antigen, [340] and glucose biosensor [341].

The MXene biosensor used to detect H_2O_2 , nitrite and phenol utilizes the multilayers of Ti_3C_2 MXene system for immobilizing electrochemically active protein molecules *via* physical adsorption. Even though, the biosensing *via* physical adsorption technique is effective, it is limited when sensing biomarkers of lower concentrations as this method is unable to use completely the huge potential of the nanolayer morphology of MXenes for combining surface functional groups having high density. Studies show the possibility of cancer biomarkers (*e.g.*, carcinoembryonic antigen, CEA, which is an important biomarker that could be observed in lung, pancreatic, breast, ovarian, liver and colorectal cancer patients) detection, [340] blood biomarkers (uric acid, creatinine and urea) detection, [337] and the detection of biochemical analytes in blood serum, [343] by anchoring antibodies using biofunctionalized MXene nanolayers. Such biosensor systems help clinicians to know the health states and treatment responses of their patients by delivering real time and continuous data of a range of bio/chemical molecules. Even though, most of the recent studies focus on to immobilize protein or enzyme on 2D MXene nano layers for making biological material sensing functional electrodes, another biosensor system, DNA sensors based on MXene, has also obtained much attention recently. [344, 345] Although, this new MXene-DNA sensor can solve the issues that face by the traditional DNA sensor such as high cost and the requirement of complex alteration to generate DNA nanostructures, the accuracy and the sensitivity of this technique must be confirmed.

Sweat analysis is a great way to monitor the activities of a person and it serves as a non-invasive continuous

monitoring method for several biomarkers coming off the skin (such as glucose, alcohols, electrolytes and pH). Lei *et al.*, [342] fabricated a 2D MXene ($\text{Ti}_3\text{C}_2\text{T}_x$) nanosheets based

biosensing system for detection of biomarkers such as glucose and lactate. MXene composite

electrode was combined with glucose oxidase (Gox) and lactate oxidase for glucose and lactate

monitoring. As prepared graphene/Prussian blue (PB) and CNTs/PB composites, and MXene/BP based composite sensors without enzyme immobilization were tested for detection of hydrogen peroxide for performance comparison analysis. The porous structure with a tri-phase interface and high electrochemical activity of $\text{Ti}_3\text{C}_2\text{T}_x$ resulted in high sensitivity, low limit of detection, enhanced linearity and accuracy comparing to those of graphene/Prussian

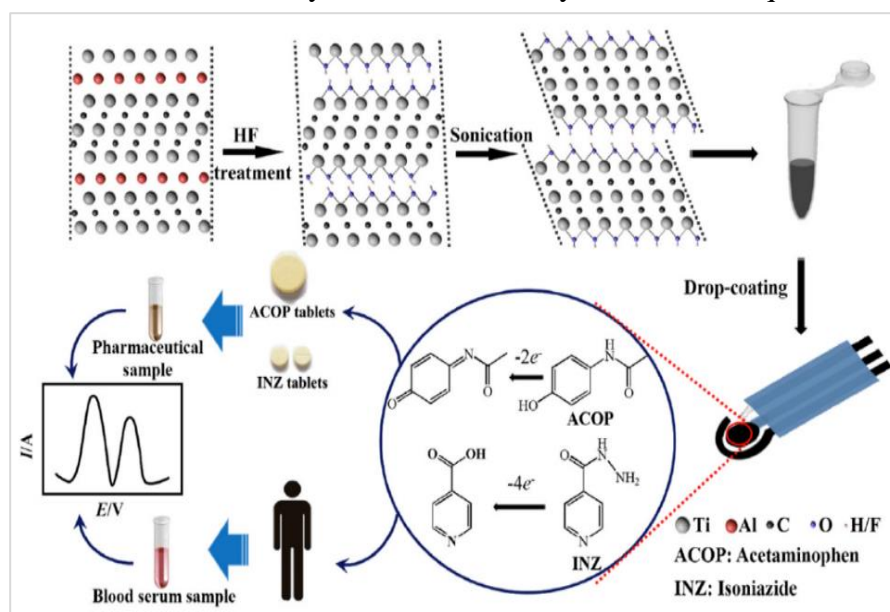


FIGURE 14. Schematic illustration of $\text{Ti}_3\text{C}_2\text{T}_x$ MXene synthesis and the detection of acetaminophen (ACOP) and isoniazid (INZ) drugs in human fluids using MXene modified screen printed electrode to understand the toxic liver disease condition. Reprinted from the Ref. [343] Copyright © 2019 with permission from Elsevier.

blue (PB) and CNTs/PB composites based sensors. Volatile Organic Compounds (VOCs) from human breath gas analysis could identify several biomarkers that represent pathological information about diabetes, lung cancer, asthma and other diseases. [516] Yuan *et al.* [517] demonstrated fabrication of a flexible VOC sensor based on 3D MXene framework that exhibited very low limit of detection up to 50 parts per billion for several VOCs including ethanol, methanol and acetone. The sensor was characterised for flexibility and demonstrated no performance change for 1000 bending cycles.

MXene based electrochemical sensor has been inkjet printed for detecting the chemical H_2O_2 , [333] which is generated through the oxidase reactions in the living biological cells, mitochondria. [346, 347] Monitoring of this chemical in the human body is important as this may lead to cancer, aging, biological damages and neurodegeneration if H_2O_2 is not keeping at a specific amount. [348-352] Hence, it is important to develop cost effective fast sensing platforms for this chemical detection. In the work by J. Zheng *et al.*, the inkjet printed H_2O_2 sensor showed excellent sensitivity and selectivity. [333] This was manufactured using the stable nanocomposite, Ti_3C_2 /graphene oxide (Ti_3C_2 -GO). In this inkjet printable nanocomposite, the presence of GO enhanced the stability and the electrochemical property of Ti_3C_2 MXene, which was in this case developed by the removal of Al from Ti_3AlC_2 using the LiF/HCl etchant. The detection limit of this developed sensor was 1.95 μ M. The dynamic range of this inkjet printed H_2O_2 sensor varies from 2 μ M to 1 Mm. In another work, Yu Zhanga *et al.*, developed an electrochemical sensor for selective and simultaneous detection of drugs (acetaminophen (ACOP) and isoniazid (INZ)) in the clinical environment to understand drug toxicity as this leads to toxic liver disease (known as, hepatotoxicity). [343] In health care, suitable dosage of medication in physiological fluids or plasma is very important for effective treatment and avoid drug toxicity. This sensing device resulted from the integration of Ti_3C_2Tx MXene and a screen printed electrode (SPE), in which delaminated Ti_3C_2Tx MXene solution was coated on the SPE to enhance the sensing signal (Fig. 14). [343] Here, Ti_3C_2Tx nanosheets were synthesized by the removal of Al using the HF etchant and simple drop casting method has been applied to obtain Ti_3C_2Tx -modified SPE. When compared to the other electrochemical sensors based on modified electrodes for ACOP and INZ detection, [353-359] this Ti_3C_2Tx -modified SPE exhibited either better performances or comparable features.

Most recently, S. Pan *et al.*, have first demonstrated the 3D printing of Ti_3C_2 MXene based bioactive glass scaffold (TBGS) for bone cancer treatment (Fig. 15). [360] Cells can be attached to the scaffolds and leads to the tissue formation. These can temporarily replace the extracellular matrix function of the human bones. Advancements in this scaffold development is necessary to provide bone material for the degenerated region. Several scaffold manufacturing techniques and materials have been reported. [361-364] The TBGS developed by S. Pan *et al.* exhibit dual functionalities *i.e.*, bone cancer tissue elimination through photonic hyperthermia and bone tissue regeneration *via* bioactive scaffolds. [360] The properties of Ti_3C_2 that utilize in cancer therapeutic application are their photothermal-conversion efficiency in the biowindow (near-infrared, NIR) and biocompatibility. [15, 365] Particularly, with the oxygen and water interaction, they degrade and release species based on Ti, promoting new bone tissue growth. [366]

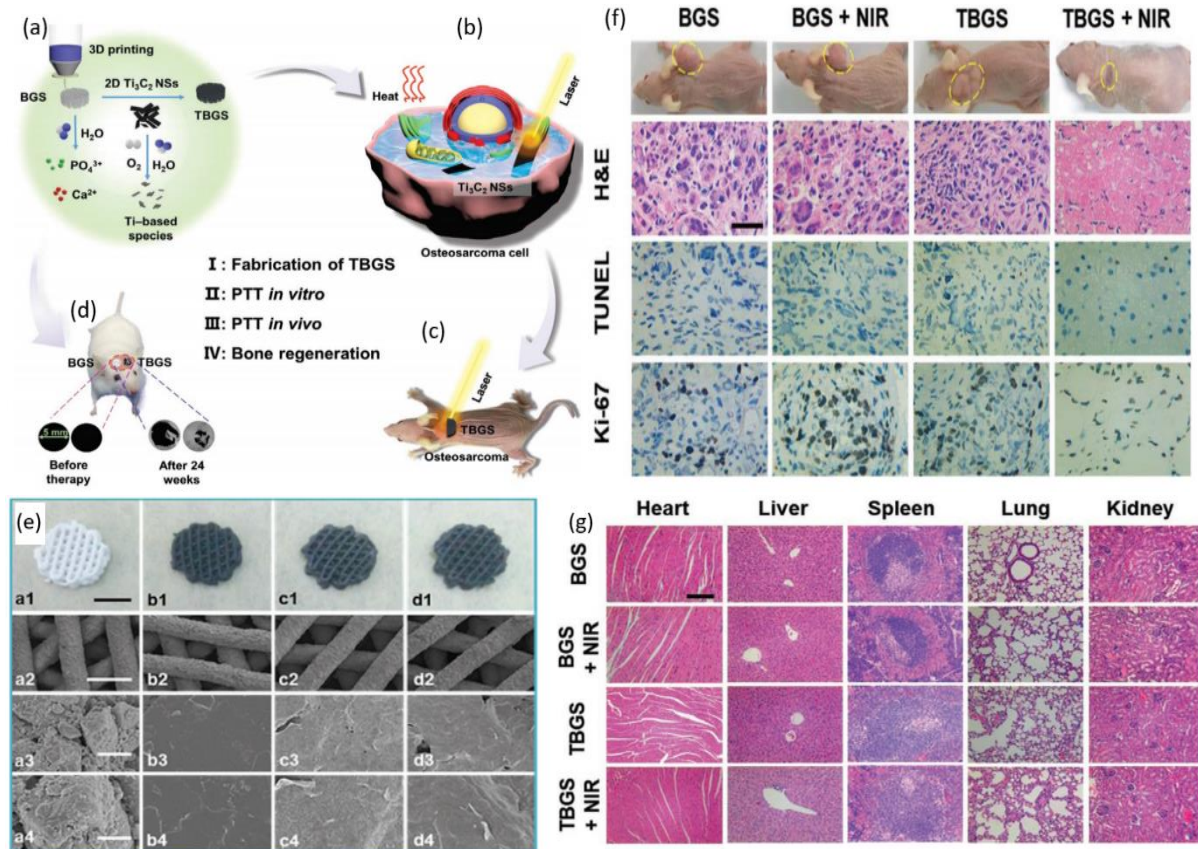


FIGURE 15. 3D printed MXene based bioscaffolds for bone cancer tissue elimination. Schematic presentation of (a) the generation of Ti_3C_2 -Bioactive glass scaffold (TBGS). Photothermal (laser) ablation of bone cancer cell (osteosarcoma cell) elimination (b) in-vitro and (c) in-vivo. (e) optical (a1) and SEM (a2-a4) images of pure BGS, optical (b1) and SEM (b2-b4) images of 1.0 TBGS, optical (c1) and SEM (c2-c4) images of 1.5 TBGS, optical (cb1) and SEM (c2-c4) images of 1.5 TBGS, and optical (d1) and SEM (d2-d4) images of 2.0 TBGS. Scale bars: (a1-d1) 3 mm, (a2-d2) 500 μ m, (a3-d3) 5 μ m, and (a4-d4) 1 μ m. (f) Images of the tumor (Saos-2) in mice after several treatments on fourteenth day and Saos-2 tumor tissue stained using Ki-67 (proliferation), TUNEL (apoptosis), and H&E, the next day after those treatments. Scale bars of all the pictures are 10 μ m. (g) The organs, kidney, lung, spleen, liver, and heart, of Saos-2 tumor tissue bearing mice's staining using H&E after several treatments on the fourteenth day. Scale bars of all the pictures are 100 μ m. Reprinted from the Ref. [360] Copyright © 2019 with permission from WILEY-VCH Verlag GmbH & Co. KGaA, Weinheim.

3.2 Wearable device Application

Wearables in the healthcare sector are becoming an essential part of physiological parameters recording (*e.g.*, body temperature, [367, 368] physical pressure, [369, 370] blood pressure, [199, 371] respiratory rate, [372, 373] heart rate [374, 375] and skin conductance [376]), personal analytics, physical status measurements, informing medication schedule or timely treatment. In recent years, wearable flexible pressure sensors, which convert deformations or mechanical forces into electric signals, have received much attention. The wearable pressure sensors for human activity monitoring must be very sensitive to detect the signals from forceful movements (*e.g.*, movements of muscle, walking and bending of joints) to subtle movements (*e.g.*, heartbeat, wrist pulse and speaking). [386-390] The sensing mechanism of the developed wearable and flexible pressure sensors are piezoelectricity, piezoresistivity, triboelectricity and

capacitance. [387, 391-394] Both the triboelectric and piezoelectric pressure sensors measure signals that arise only from the dynamic distortions. The pressure sensor based on capacitance ($C = \epsilon A/d$, where, C = capacitance, ϵ = dielectric constant of the sandwiched dielectric layer, A = area between two conductive plates and d = sandwiched dielectric layer thickness) [386] measures the change in capacitance under pressure using a dielectric layer which is placed in between conductive plates. [395-397] The piezoresistive devices shows a simple sensing mechanism, which convert applied pressure into resistance signals. This cost effective pressure sensor having broad detection range can measure both transient and static deformation and acquire signals very easily and moreover, it exhibits fast response. [398-401] Due to these advantages, piezoresistive pressure sensors are widely studied and in recent years, a number of works have been reported on piezoresistive sensor materials, methods and sensor devices for printed flexible pressure sensor systems. The microstructure and the morphology of the materials used for sensing are the two features that helps to enhance pressure sensor sensitivity (S), which is defined as,

$$S = \frac{\Delta I/I_{off}}{\Delta P} \quad (2)$$

where, ΔI is the current in loading, I_{off} is the current under unloading, and ΔP is the change in pressure.

Materials currently used for this pressure sensing application include metal nanowires [405], graphene [403], carbon nanotubes [404], conductive polymers [405] and their composites. Although, these materials exhibit excellent electrical, thermal and mechanical properties, they are very expensive for developing highly sensitive pressure sensors for practical large scale application due to very complex method and low signal feedback. However, one can say that the novel 2D MXenes, exhibiting high surface hydrophilicity, high metallic conductivity, modifiable and rich surface terminations and extremely large specific surface area of a single nanosheet, will be an alternative to those expensive materials. 2D MXenes are gradually occupying a place in the wearables sector due to their excellent properties. They exhibit comparable bending strength and electronic properties to graphene. Moreover, MXenes have been reported as a room temperature sensing material. The other properties that make MXenes superior to graphene are their electron irradiation and oxidation resistances. MXene based flexible printed wearables have been developed. One of the main advantages of MXene printing is the possibility to select flexible substrates which can be used for the fabrication of flexible electronics devices with applications in biomedical engineering and healthcare. Particularly for printed wearable electronics, flexible substrates are important to use for maximum human comfort. Hence nanostructures with high mechanical flexibility for high stability and highly conductive materials are required. One thing is, although a number of MXene based physiological parameter monitoring sensors are available, the devices developed using printing techniques are limited. The reports available today on printed sensor devices for healthcare monitoring are only pressure sensors for monitoring human body activities. Flexible pressure sensors have wide applications in printed electronics, such as artificial skin, interface surfaces for human machine interaction, touch displays, and smart robots. For example, Y. Guo *et al.*, have been fabricated a wearable transient pressure sensor on a paper substrate using MXenes based screen printable ink (Fig. 16). This MXene based pressure sensor is suitable for

broad-range highly sensitive human–machine interfacing, monitoring of human motion ranges from small distortions to large movements and by touching the surface of the sensor (Fig. 16). [406] Due to the performance of the developed pressure sensor (high sensitivity, biodegradability, lower detection limit (10.2 Pa), fast feedback (11 ms), sensing of ultrasensitive load (2.3 mg), stability cycle over 10,000 cycles and consumption of low power (8–10 W), they suggest that, this is appropriate for broad-range medical monitoring tasks by attaching this to the human body skin, especially, for predicting the potential health states of patients with early stage Parkinson’s disease. They have evaluated its biocompatibility by conducting toxicity tests.

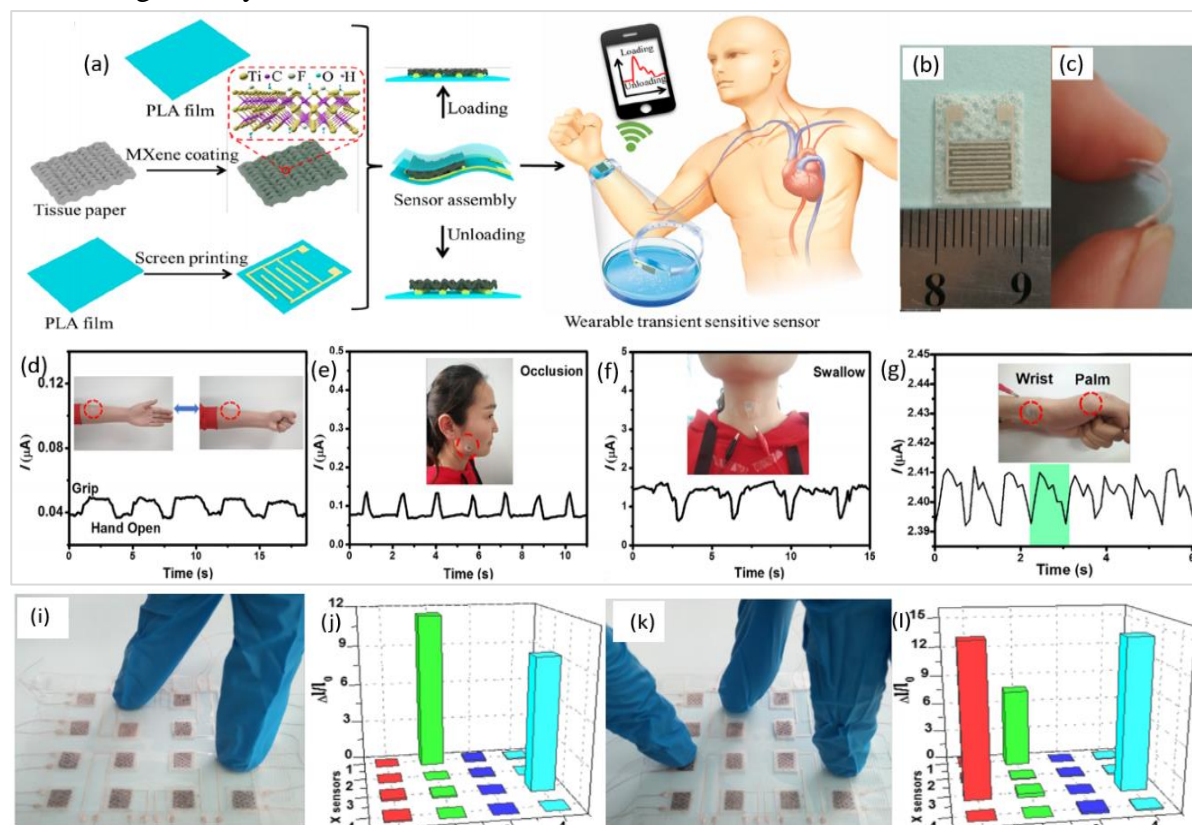


FIGURE 16. Flexible pressure sensor based on MXene. (a) Schematic demonstration of the MXene based wearable and flexible transient pressure sensor fabrication via screen printing and (b, c) image of the screen printed pressure sensor. The performance of the fabricated pressure sensor that is attached to (d) arm (e) cheek (f) throat and (g) wrist. (I, k) images of the E-skins touching with two fingers with their (j, l) corresponding pressure variation mapping from their sensing responses. Reprinted from the Ref. [406] Copyright © 2019 with permission from American Chemical Society.

Very recently, Y. Cheng *et al.*, have inkjet printed MXene based highly sensitive (151.4 kPa^{-1}) piezoresistive pressure sensor to monitor body activities and medical states by placing on either joints or muscles (Fig. 17). [407] The response time of this sensor shows $< 130 \text{ ms}$, means it is very fast and stability cycle is over 10,000 cycles, indicating high stability. Fast response time is one of the key parameters for ensuring timely feedback under pressure. The detection limit of this developed pressure sensor is 4.4 Pa. For developing this pressure sensor, single-layer $\text{Ti}_3\text{C}_2\text{T}_x$ MXene nanosheets, which is generated by the removal of Al layers using the etchants HCl and LiF, were at first spray coated on the microstructured

polydimethylsiloxane (PDMS) and then it is assembled with an interdigitated electrode patterns that are inkjet printed using Ag functional ink on the polyimide (PI) sheet. The flexible spinous microstructures of different heights and roughness on the PDMS are generated by its treatment with an abrasive paper. In their work, Cheng *et al.* have pointed out that the microstructures are critical for achieving sought sensor performance levels. [407]

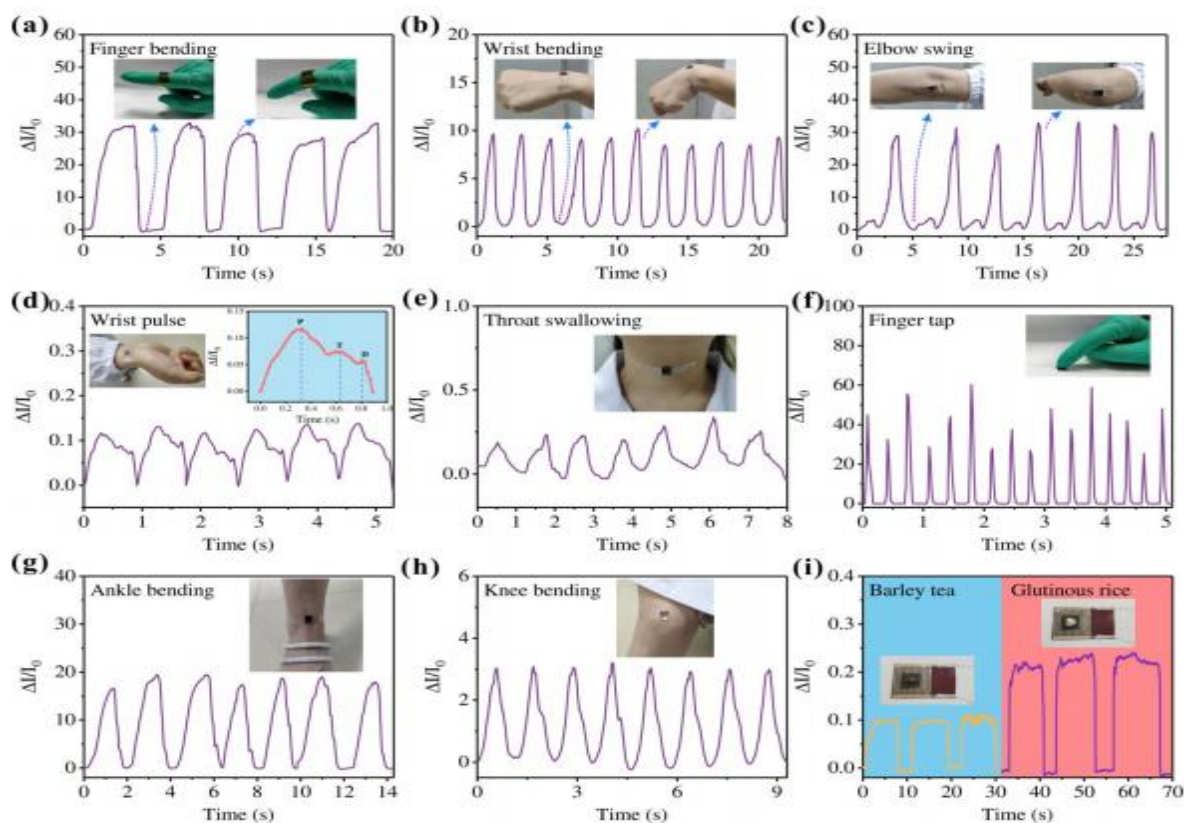


FIGURE 17. MXene based inkjet printed piezoresistive sensor. The signal feedback obtained in the form of changes in current when (a) bend finger, (b) bend wrist, (c) swing elbow, (d) pulse from wrist, (e) signal from throat when swallow, (f) finger tap, (g) bend ankle, (h) bend knee, and (i) barley tea grain and rice on the top of a pressure sensor. Reprinted from the Ref. [407] Copyright © 2020 with permission from American Chemical Society.

In wearable technology, renewable, inexpensive and human body skin friendly textile substrates have a huge role. Since 1980, investigations have been carrying out to incorporate wearable sensor system in garments offering seamless integration of sensors and clothing, *i.e.*, health states and body movements can be monitored directly by the help of the smart cloth we wear. The development of knittable and weavable conductive and stretchable yarns or fibers with high capacitance is still a challenge. To this end, MXene based composites and fibers with high conductivity and stretchability have been reported. [408, 409] These yarns are suitable for the garments based strain sensors. The stretchability in combination with conductivity is the basic requirement to sense physical distortions like strain. Another work proposes spring like core-sheath MXene based yarn for textile humidity and strain sensors. [410] Interestingly, Wen-Tao Cao *et al.*, have reported 3D printed multifunctional fibres and smart textiles using TEMPO (2,2,6,6-tetramethylpiperidine-1-oxyl-radi-cal)-mediated oxidized cellulose nanofibrils (TOCNFs)/ Ti_3C_2 MXene hybrid inks (Fig. 18). [411] The developed MXene hybrid ink exhibiting excellent rheological characteristics can be printed rapidly and develop precise

structures. They pointed out that the 3D printed TOCNFs/Ti₃C₂ smart fibers showed excellent responsiveness to the external multiple stimuli such as, mechanical, electrical or photonic when compared to the traditional synthetic fibers and the electromechanical performances of TOCNFs/Ti₃C₂ textiles can be processed into highly sensitive strain sensors. Such smart textiles and fibres with fast electromechanical, photothermal, and electrothermal, responsiveness may be suitable for wearable next-generation sensing and heating systems. This MXene based smart fiber was 3D printed at room temperature. They conducted atomistic modelling studies (Fig. 18 b) to understand the role of Ti₃C₂ nanolayers and TOCNFs in the mechanical property enhancement of the composite smart fibres.

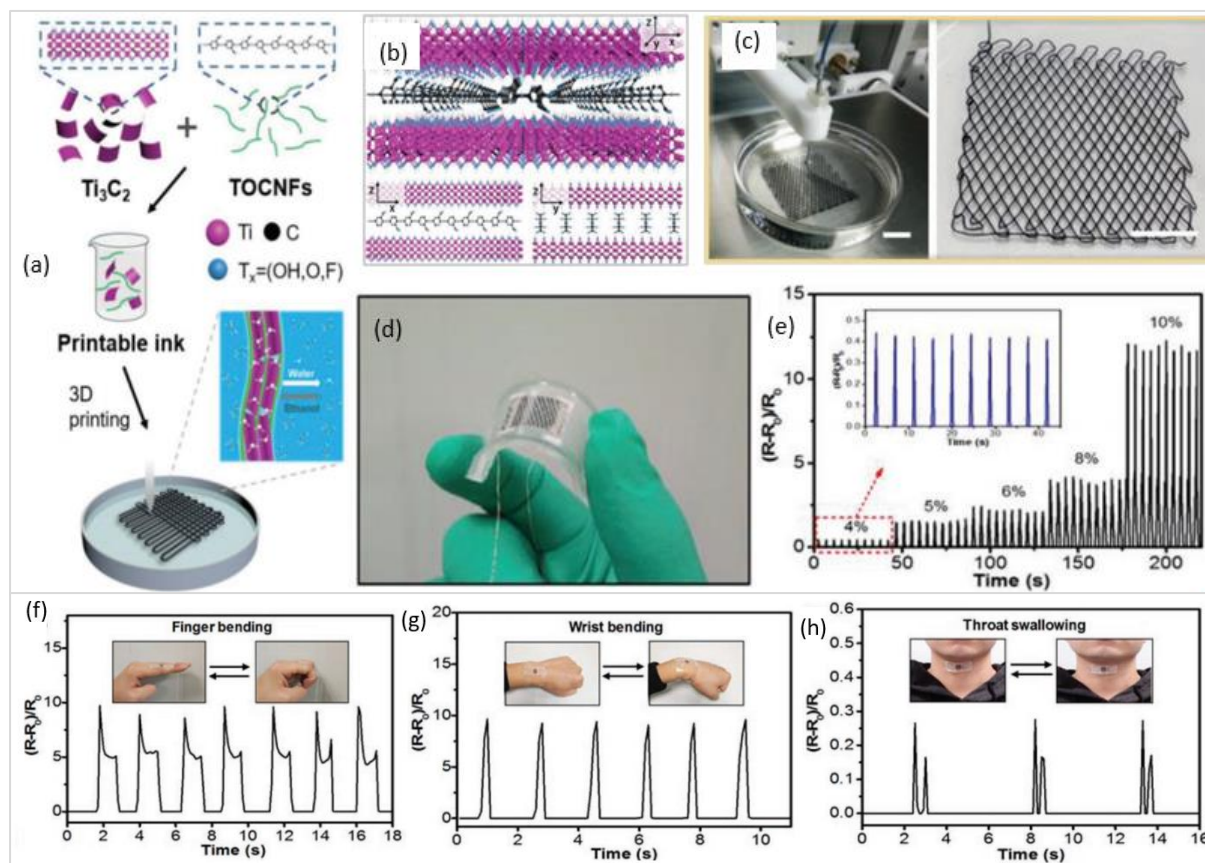


FIGURE 18. MXene based smart textiles and 3D printing. (a) Schematic demonstration of the development of smart textiles and fibers based on TOCNF/Ti₃C₂. (b) The atomistic TOCNF/Ti₃C₂ fiber model. (c) Photograph of the net structure 3D printed using TOCNF/Ti₃C₂ fabric. (d) Image of the textile TOCNF/Ti₃C₂ strain sensor and (e) its relative resistance $((R-R_0)/R_0)$ changes under different cyclic strains. Relative resistance variations when (f) bend finger, (g) bend wrist, and (h) swallow. Reprinted from the Ref. [411] Copyright © 2019 with permission from WILEY-VCH Verlag GmbH & Co. KGaA, Weinheim.

The long term stability and degradation in MXene ink properties, low volume printing processes, use of fluorine based etching method for synthesis, biocompatibility are main limiting factors for MXene, inhibiting large volume fabrication and deployment of MXene materials for mass scale applications. In order to promote the use of MXene based inks for large area printed electronics and mass scale high volume production to manufacture biomedical and healthcare devices, several challenges need to be addressed. For low temperature printing processes, that can be used on a range of substrates, such as plastics,

papers, polymers and textiles, long term ink stability and retention of ink properties are crucial. Oxidation stability of MXenes is challenging given their reactivity with water and oxygen. Therefore, methodologies for long term stability of MXene inks need to be explored to achieve chemical and thermodynamic stability.

3.2. MXene based flexible Energy Storage Devices

The increased demand of portable, wearable and flexible devices for practical application leads to the development of appropriate flexible powering systems such as SCs, LIBs, fuel cells, solar cells, *etc.* Flexible power management systems play a significant role in the fabrication of compatible devices and hence novel energy storage technologies are essential to attain sustainable energy management in the future. In order to fulfill the future high demand energy storage and powering requirements of flexible and PE systems, the development of innovative active materials for high capacity electrodes are important. In the last few years, the use of layered materials from the 2D family exhibit new possibilities in the flexible and printed LIBs and supercapacitors (SCs). The high ion-capacity and rapid ion-diffusion are the peculiarities of these 2D layered materials, that is because of their high surface area and the appearance of unique electrical properties. [412, 413] 2D materials (*e.g.*, TMO, [414, 415] TMD, [416, 417] MXenes [73, 418, 495]) already have exhibited their potential to use as anode materials. In 2D materials, MXene, exhibiting wide structural and chemical varieties and tunability of surface chemistry,

offer unique reaction spaces even at the nanoscale for a chemical reaction and thereby enhance the performance of the storage devices. That makes MXene competitive

with the other materials in the 2D family. [419, 420]

Although MXenes are ceramic, they exhibit inherently high conductivity and super volumetric capacitance due to their molecular layers which are made up of nitrides/carbides/carbonitrides of transition metals (*e.g.* titanium). These properties make them suitable for many important storage devices applications. Both theoretical [73, 74, 421] and experimental [71]

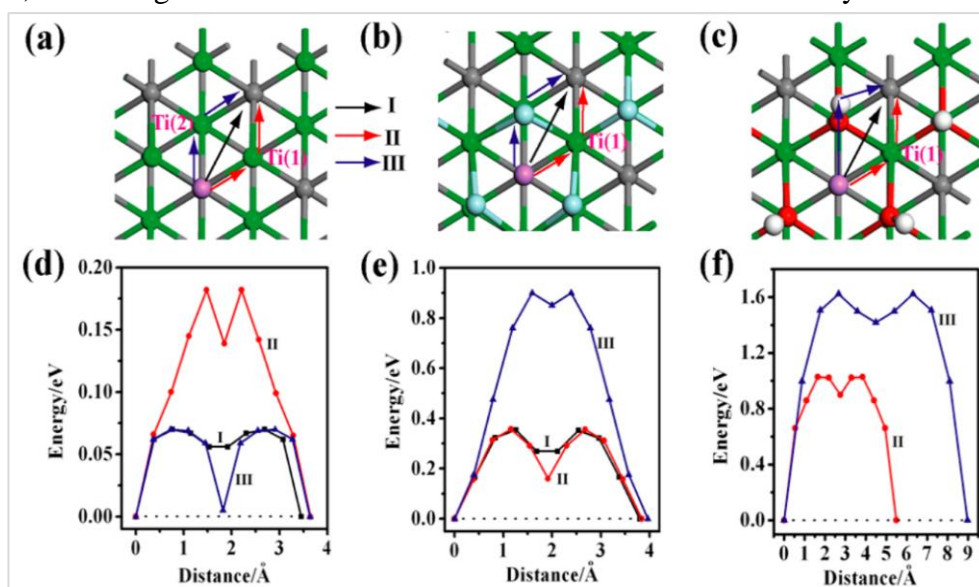


FIGURE 19. Schematic demonstration of Li ions diffusion paths I, II, and III (view from the top) and their corresponding diffusion barrier profiles on the monolayers of (a, d) Ti_3C_2 (b, e) $\text{I-Ti}_3\text{C}_2\text{F}_2$ and (c, f) $\text{I-Ti}_3\text{C}_2(\text{OH})_2$. Reprinted from the Ref. [74] Copyright © 2012 with permission from American Chemical Society.

investigations have shown that 2D MXenes are the potential candidate for novel electrode material in LIBs, and SCs.

Lithium Ion Battery (LIB) and Lithium Ion Capacitor (LIC): For flexible PE systems, LIBs are highly versatile cost effective power sources having longer span of life and excellent energy density. [422-427] Lower self-discharges and large capacity are the key requirements of its anode and cathode materials as these properties strongly affect the LIB performance. Due to the specific capacity and good safety, recyclable LIBs are being examined as advanced next generation powering systems. [428-430] Different architectures of flexible LIBs have already been produced. [324, 426, 431-436] A number of LIB electrodes have been printed successfully via, 3D printing, [324] screen printing [433, 434] and inkjet printing [431, 432] methods. Even though, graphite, having stable and low Li potential, 0.01-0.2 V, high specific capacity and low cost, already occupied LIB anode material's main market, [437, 438] theoretical [439] and experimental [41] studies show the Ti_3C_2 MXene [439-444] is an appropriate and promising material for anodes in LIB's as this exhibits excellent capacity when compared to graphite. [75, 445] Computational studies based on density functional theory (DFT) on the electronic and structural stability properties of Ti_3C_2 monolayer and its hydroxylated (OH-) or fluorinated (F-) derivatives reveals the magnetic metal behaviour of pure Ti_3C_2 and very small band gap semiconductor/ metallic nature of functionalised $\text{Ti}_3\text{C}_2(\text{OH})_2$ and $\text{Ti}_3\text{C}_2\text{F}_2$ in their stable molecular conformations. [74] The electronic properties of MXenes strongly depends on their surface treatments. In the study in 2012, Q. Tang *et al.* [74] reported theoretically that the pure MXene Ti_3C_2 which exhibit high capacity for Li storage (theoretical), low diffusion barrier for Li, small operating voltage, is a potential candidate as anode material to replace the commercial TiO_2 polymorphs [446, 447] in LIB. Moreover, they have suggested to avoid OH- or F- derivatives at synthesis level as these reduce or stop the Li diffusion (Fig. 10) and thereby lower the energy storage capacity. [74] The theoretical [421] investigations showing lower diffusion barriers for ions of Li^+ in MXene materials, are in good agreement with the excellent performances reported in some of the MXenes based on experiments [9, 75, 448]. In another work, Khazaei *et al.* have discussed the electronic properties of several MXenes (M_2N (M = Zr, Ti or Cr) and M_2C (M = Sc, Ti, Cr, Nb, Zr, Ta or V)) having surface treatments using O-, OH- or F-. [10] This work shows the monolayers of all the bare 2D MXenes are metallic and the surface treated MXenes such as $\text{Cr}_2\text{C}(\text{OH})_2$, $\text{Cr}_2\text{N}(\text{OH})_2$, Cr_2NO_2 , Cr_2CF_2 and Cr_2NF_2 become ferromagnetic and $\text{Sc}_2\text{C}(\text{OH})_2$, Zr_2CO_2 , Ti_2CO_2 , Hf_2CO_2 , Sc_2CF_2 and Sc_2CO_2 act as semiconductors with ~0.25–2.0 eV band gaps. The electrochemical experiments conducted to evaluate the performance of Ti_2C as a LIB anode material by Naguib *et al.* [73, 445] shows a retained charge storage capacity even at 1000 charge-discharge cycles. It was found that the functional groups terminated on the layer surfaces strongly affects the Li-ion energy storage capabilities and the highest capacity by theory is achieved with the functional group O-. Based on the theoretical and experimental studies, Yu Xie *et al.*, recommended O-functionalised, free standing bare 2D MXenes with high surface areas for obtaining large Li ion energy storage capacities. [421] The storage device Li Ion Capacitor (LIC) combining a LIB type of anode and a SC type of cathode with a proper electrolyte has received much attraction recently. [449] It is designed for exhibiting high energy density without affecting high power density. For achieving advanced electrochemical charge storage, the hybrid LIC device requires higher capacity anodes with reversible Li ion intercalation. Low life cycle and poor rate capability are its main limitations for the practical application. In this sense, MXenes are one of the potential

candidates for the LIC application due to their excellent properties. MXene materials, such as, V_2CT_x , $Ti_3C_2T_x$, Nb_2CT_x , and Ti_2CT_x exhibit open layer and ultra-thin structure, relieving the slow deintercalation/intercalation kinetics of Li ions. Therefore, MXene materials show non-ideal battery nature but similar to capacitors. [450, 451]

For wearable and printed electronics, flexible LIB provide lightweight and stretchable solution with fast charging capabilities. To produce flexible electrodes and replacement of metallic charge collectors with flexible conductive tracks, 2D materials such as CNTs and graphene have been investigated as conductive material with excellent electrical conductivity. [534-539]. MXenes, in addition to high electrical conductivity provide low lithium ion diffusion barrier and excellent elasticity, thus emerged as excellent candidate for flexible LIBs. [73, 540-542] Even though a number reports have been available on MXene based LIBs and LICs, none of the works show their development using printing techniques and it remains still unexplored.

Super capacitor (SC) and Micro-supercapacitors (MSCs): In energy storage applications, SCs are excellent candidates, in which electrical double layers will be charged *via* fast reversible adsorption of ions on the surface of the electrode materials having large surface area (*e.g.*, CNT, [452] GR [453] and porous carbon [454]) and then energy will be stored. [455-457] SCs offer less internal resistance, reduced weight, long life cycle, wide range of operating temperature, high transient response and high power density. According to the charge storage mechanisms SCs can be classified as pseudocapacitor and electrical double layer capacitor. [458-460] In the latter case, capacitance arises from the electrical double layer at the boundary

between the electrolyte and electrode. In the former condition, capacitance arises because of the Faradic reactions. In acidic electrolytes (*e.g.*, H_2SO_4), MXenes show pseudocapacitance because of their surface redox chemistry (Fig. 20

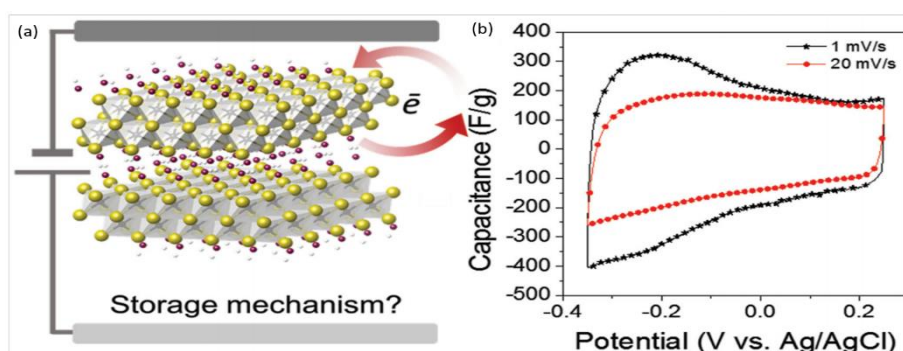


FIGURE 20. (a) $Ti_3C_2(OH)_2$ MXene structure schematic (Ti atoms= yellow colour, C atoms=gray colour, and OH = red colour). (b) MXene electrochemical performance. Reprinted from the Ref. [462] Copyright © 2015 with permission from WILEY-VCH Verlag GmbH & Co. KGaA, Weinheim.

(a, b)). [461-463] For example, $Ti_3C_2T_x$ MXene in 1 M H_2SO_4 show 205 F/g capacitance within -0.35-0.35 V *vs.* Ag/AgCl, [462] and in another example, it is 400 F/g within -0.45 to -0.05 V *vs.* Ag/AgCl. [461] The surface chemistry has a major role on the capacitive feedback in acid electrolytes *i.e.*, when compared to OH and O terminations on the MXene nanosheets, less F terminations show significantly improved specific capacitance. [462] Therefore, MXenes have been widely studied for SC application. [464] The characterization of the pseudocapacitive materials charge kinetics can be carried out by assessing capacitive and flow controlled charge accumulation to the total charges on the electrodes using scan rate dependent cyclic voltametric

data. Normally, the storage mechanism of charges can be determined from the scan rate (v) and current (i) dependencies as, [465]

$$i = av^b \quad (3)$$

where, a and b are controllable parameters, b determines from the slope of $\log(i)$ vs $\log(v)$ plot.

Micro-supercapacitors (MSCs) received much attraction in recent years as an advanced power management system due to its outstanding properties such as high-frequency response, faster rate of charging and discharging, longer cycle of life, safety and excellent power/energy delivery. [466, 467] The MSC concept was first proposed in 2003 by H.-K. Kim, who fabricated successfully a thin film capacitor using LiPON electrolyte and W-RuO₂ electrodes. [468] In 2007, H. Peng *et al.*, have first reported another type of wire shaped MSC. [469] First interdigitated electrode MSC based on carbide-derived carbon films was reported at first in 2010. [470] The GR based MSC showed better performance in this in-plane interdigitated electrode structure compared to what they were and therefore this MSC architectures considered as superior to the traditional sandwich like arranged devices that consist of solid-state electrolytes as the separator and two thin-film electrodes and have observed its wide usage. [470] The evaluation of the performance of SC is based on the power densities, energy and gravimetric capacitance, however, in MSCs, it is assessed by the parameters such as energy, areal/volumetric capacitance and the power density based on area/volume as the active materials mass is very less and space limitation is a major constraint. In 2016, J. Chen *et al.*, have developed flexible MSC with interdigitated electrodes using reduced graphene oxide (rGO)-PEDOT/Poly (styrene sulfonate), that exhibited excellent areal capacitances (84.7 mF/cm² at 5 mV/s and 45.5 mF/cm² at 200 mV/s), high volumetric capacitances (14.5 F/cm³ at 5 mV/s and 7.83 F/cm³ at 200 mV/s) and excellent life cycle stability (capacitance 94.3% after 10000 cycles). [471] In portable devices including wearables, sensors and in miniature electronic devices, the MSCs are the potential candidates to store energy. Their performances are different from the traditional SCs. [423, 472] The remarkable feature of MSCs are their high electrochemical performance and reduced volume. Recently, a huge effort has been focussed toward MSC designing and development using various active materials as electrode (Fig. 20).

MXene based MSCs have been fabricated using printing techniques on flexible substrates. Xu *et al.* have screen printed MXene based coplanar asymmetric microscale hybrid device (MHD). [473] In this case, Ti₃C₂T_x MXene nanolayers were used as negative electrode and Co-Al layered double hydroxide (LDH) nanolayers were used positive electrode. They applied a two-step screen printing process for this MHD development. This microdevice exhibited higher energy density of 8.84 μWh cm⁻² and excellent cyclic stability with the capacitance retention, 92% even after 10,000 cycles. In addition to this device development they have shown its application by integrating it with a flexible force sensor (Fig. 21a-b) which is fabricated on a paper and PET flexible substrates, as a portable source of power unit and they could monitor heart rate by detecting weak vibrations from the finger arteries (Fig. 21c). They also pointed out that this MHD is possible to attach directly on to the human body skin. In another work, MXene-N ink based MSCs with interdigitated electrodes have been screen printed successfully on different flexible substrates including PI, PET, paper, rubber, glass, stainless steel plate and

Cu foil (Fig. 21d). [166] The high structural stability and adhesion of the printed MXene-N electrode patterns on these chosen substrates and its pseudocapacitive nature were confirmed by performing cyclic voltammetry (CV) tests under several bending conditions (Fig. 21f, g) and different scan rates of from 10 mV s^{-1} to 100 mV s^{-1} . [166] The mechanical or structural flexibility is an important factor for MSCs for the integration in flexible and conformable smart wearable devices. When compared to the pure MXene ink based print patterns, this MXene-N based one show superior energy storage nature and provided enhanced areal capacitances that 70.1 mF cm^{-2} at 10 mV s^{-1} and 62.5 mF cm^{-2} at 100 mV s^{-1} (Fig. 21h). The achieved cyclic retention was 92% after 7000 cycles at 5 mA cm^{-2} current density. These capacitance retention and areal capacitance values of this MXene-N based patterns were higher when compared to the exfoliated GR, [474] clay Ti_3C_2 , [475] large flake sized Ti_3C_2 , [168] and Ti_3CN [167] state of the art systems. In another example, MSCs were screen printed on paper substrate using different inks such as pure MXene, M-A, R-M-A, and R@M-A_{0.75:1} inks (Fig. 9a-h). In this case, MSC based on R@M-A_{0.75:1} showed higher energy densities 8.1 to 13.5 mWh cm^{-3} corresponding to the 1.1 W cm^{-3} - 48.5 W cm^{-3} (Fig. 9i), which are higher than the SCs that available commercially. [476] R@M-A_{0.75:1} MSC shows high conductivity and enhanced electrochemical performances. They suggest R@M-A_{0.75:1} MSC is suitable for practical application as this exhibits excellent cyclic stability *i.e.*, 90% remained after 10000 cycles at 100 mV/s (Fig. 9k) and high volumetric capacitances of 864.2 Fcm^{-3} at 1 mV/s (Fig. 9j). This volumetric capacitance value obtained from R@M-A_{0.75:1} MSC is the highest reported value for MSCs based on MXenes [167, 168, 474 477-485] They recommend screen printing process for fabricating miniaturized high performance MXene based storage devices for future flexible wearable systems.

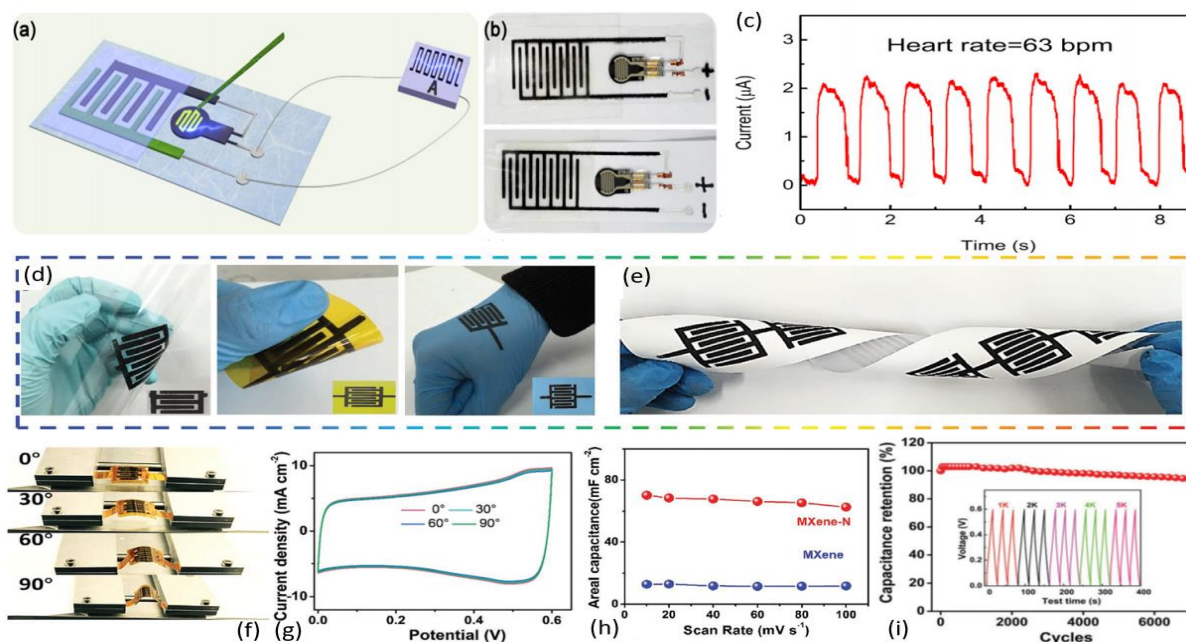


FIGURE 21. Flexible MXene based force sensor fabrication and its characterization. (a) Schematic demonstration of the microscale hybrid device (MHD) integration to the force sensor on flexible PET and paper substrates and its (b) optical image. (c) Heart rate detection using the MHD integrated force sensor. Reprinted from the Ref. [473] Copyright © 2018 with permission from Elsevier. (d-e) Images of the screen printed MSCs using MXene-N ink on different substrates such as PET, PI, Rubber and Paper. (f) CV profiles at different scan rates of screen printed MXene-N MSC. (g) Scan rate dependent

areal capacitance. (h) Cyclic stability of printed MXene-N MSC and (i) Digital pictures of printed MXene-N MSC at different 0° , 30° , 60° , and 90° bending angles. Reprinted from the Ref. [166] Copyright © 2019 with permission from WILEY-VCH Verlag GmbH & Co. KGaA, Weinheim.

One of the very recent work that reported in 2020 shows an inkjet printed flexible and planar MSC with stable and uniform interdigitated MXene based electrodes on a paper substrate. [289] Fabrication of interdigitated electrode pattern using the inkjet printing method is a relatively straightforward and cost effective, and through the repeated and controlled number of print passes, the interdigitated pattern thickness can be controlled at the micro-meter to nano-meter range. When compared to the MXene-MSC works reported previously based on solution spray-coating, [168] hydrothermal, [486] and vacuum-assisted filtration [474] techniques, this water-based SA-MXene ink (Fig. 6c-h) based MSC produced *via* inkjet print technique [289] exhibits comparable or higher volumetric energy density ($\sim 100.2 \text{ mWh cm}^{-3}$) at 1.9 W cm^{-3} power density because of its low oxidation ability, high conductivity (119 S cm^{-1}). The electrode patterns have delivered volumetric capacitance of 720.7 F cm^{-3} , areal capacitance, 108.1 mF cm^{-2} and increased cyclic stability. The current density is almost two fold higher than the pure MXene. This is due to the enhanced capacitance as a result of increased nanolayer spacing which is formed by ascorbate ions. Interestingly, in 2019, C. J. Zhang *et al.*, have fabricated MXene MSCs on flexible paper substrate *via* inkjet printing and extrusion printing (Fig. 22). [140] For this, they have used additive free organic MXene inks for inkjet printing (Fig. 7) and additive free aqueous $\text{Ti}_3\text{C}_2\text{T}_x$ MXene inks for extrusion printing. The MSCs were inkjet printed at ambient environments on AlO_x coated PET flexible substrates. They have shown that these MXene MSCs can be inkjet printed in parallel, series or both (Fig. 22d) and have strong adhesion to the chosen substrate which is confirmed by multiple peels test with a scotch tape (Fig. 22d). The homogenous inkjet patterns were obtained by optimizing print passes ($\langle N \rangle$) and initially achieved 2770 S cm^{-1} electronic conductivity for $\langle N \rangle = 5$. X-ray photoelectron spectroscopy (XPS) study proved the absence of oxide formation on inkjet printed MSC patterns even after six months under ambient laboratory conditions. However, conductivity decreased to 510 S cm^{-1} , that may due to the water molecules trapping between the layers of MXene from the ambient air environment. Substrate deformation upto 1000 bending cycles didn't create any damage to these patterns, *i.e.*, conductivity of these patterns remained completely. The inkjet printed MXene MSCs exhibited pseudocapacitance and achieved 562 F cm^{-3} volumetric capacitance for $\langle N \rangle = 25$. The capacitive retention was $\sim 100\%$ with the current density $14 \mu\text{A/cm}^2$ (Fig. 22f).

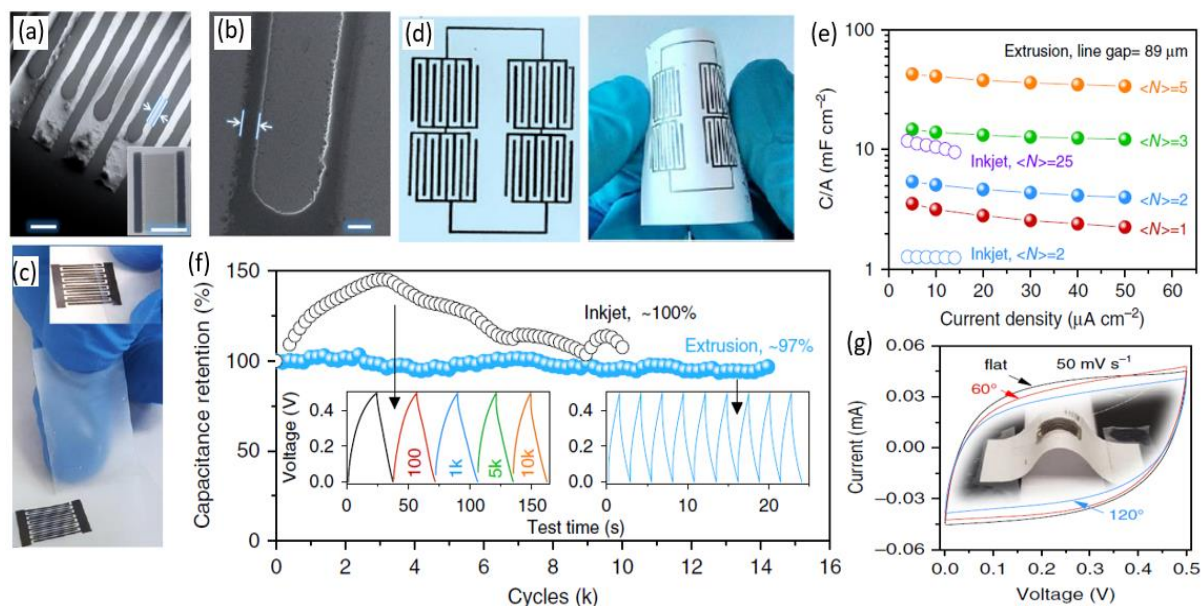


FIGURE 22. Inkjet printed flexible MXene MSC and its properties. SEM optical image of the inkjet printed MSC based on (a) NMP MXene ink (scale bar=200 μm) (b) ethanol MXene ink (scale bar=200 μm). The scale bar of the inset whole device image of the figure (a) is 1 cm. The distance between the marked arrows in (a) is 50 μm and in (b) is 130 μm. (c) Peeling test performed using scotch tape on the inkjet printed MXene MSC shows strong adhesions of the interdigitated patterns that printed on the AlO_x-coated PET. The absence of material on the scotch tape even after ten number of peels indicate excellent adhesion between the inkjet printed patterns and the chosen substrate. (d) 3D printed MXene MSCs on a paper substrate, two makes parallel connection and two in series connection. (e) Extrusion and inkjet printed MXene MSCs areal capacitance for different number of print lines <N>. (f) Capacitance retention extrusion and inkjet printed MXene MSCs as a function of cycle. Inset figures represents capacitive nature in cycling, indicate super electrochemical performances. (g) CV profile of the paper based MXene MSC fabricated *via* extrusion printing under various bend angles. Reprinted from the Ref. [140] Copyright © 2019 with permission from Springer Nature.

For extrusion printing (Fig. 22), they have used additive free aqueous MXene inks. Similar to inkjet printing using organic MXene inks, electrochemical performance of the extrusion printed MXene MSC on paper substrate was tuned by optimizing <N> and patterns gap. Extrusion printed MXene MSC achieved a high rate and

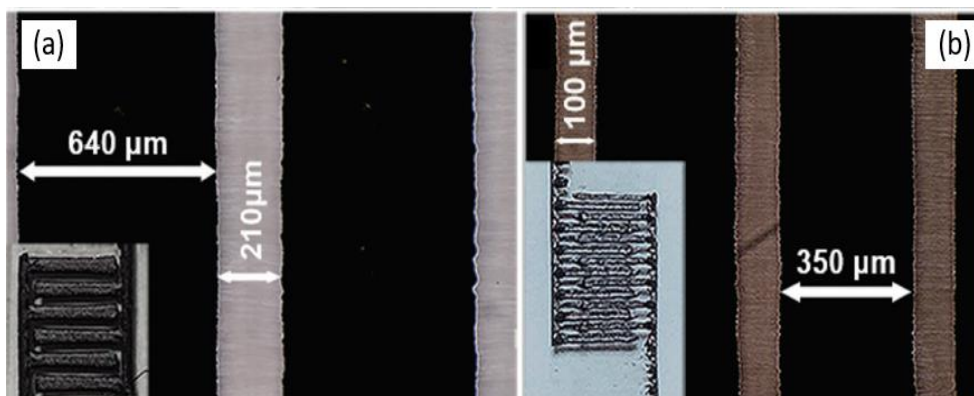


FIGURE 23. 3D printed MXene MSC. (a, b) Optical images and photographs of 3D printed MXene MSC interdigitated patterns. Reprinted from the Ref. [327] Copyright © 2019 with permission from WILEY-VCH Verlag GmbH & Co. KGaA, Weinheim.

pseudocapacitive behaviour at $\langle N \rangle = 3$ and pattern gap = $\sim 89 \mu\text{m}$. This MSC showed $\sim 97\%$ capacitive retention. By analysing Raman peaks, they have confirmed the absence of oxide formation during the extrusion printing process. The obtained areal capacitance of the extrusion printed pattern was 43 mF cm^{-2} for $\langle N \rangle = 5$. They reported an improved pseudocapacitance nature with cycling performance. To check energy storage performance of the printed MXene MSCs, they have evaluated both extrusion printed and inkjet printed MXene MSCs using the electrolyte sulfuric acid (H_2SO_4)-poly (vinylalcohol, PVA) gel. For that coat this electrolyte on the surface of the MSCs, followed by dry those naturally. In another work, Jafar Orangi *et al.*, 3D printed MSC interdigitated electrodes at room temperature using highly viscous $\text{Ti}_3\text{C}_2\text{T}_x$ MXene water based additive free ink (Fig. 23). [141] This interdigitated architecture of the electrode generally provides high volumetric and areal energy densities. In this study, MXene MSC achieved over 2.1 F cm^{-2} areal capacitance at 1.7 mA cm^{-2} . At 4.3 mA cm^{-2} current density, this MXene MSC showed $0.0244 \text{ mWh cm}^{-2}$ energy density and 0.64 mW cm^{-2} power density. These values of MXene MSC are large, offering excellent electrochemical performances.

Table 2 lists the details and the electrochemical performances of the MXene based MSCs developed using printing techniques.

Table 2. Electrochemical performances and details of printed MSC based on MXene.

Ref.	Electrode material	Substrate	Areal capacitance	Volumetric capacitance	Areal energy density	Volumetric energy density	Power density	Formation
Inkjet Printing								
[289]	Sodium ascorbate- $\text{Ti}_3\text{C}_2\text{T}_x$	Paper	108.1 F cm^{-2}	720.7 F cm^{-3}	-	$100.2 \text{ mWh cm}^{-3}$	$1.9 \mu\text{W cm}^{-2}$	Symmetric, planar
[140]	$\text{Ti}_3\text{C}_2\text{T}_x$	AlOx-coated PET	12 F cm^{-2}	562 F cm^{-3}	-	-	-	Symmetric, planar
Screen Printing								
[473]	$\text{Ti}_3\text{C}_2\text{T}_x$ & Co-Al LDH	Paper & PET	28.5 F cm^{-2}	-	$8.84 \mu\text{Wh cm}^{-2}$	-	$230 \mu\text{W cm}^{-2}$	Asymmetric, planar
[166]	N-doped $\text{Ti}_3\text{C}_2\text{T}_x$	PET, Paper Rubber, PI,	70.1 F cm^{-2}	-	-	-	-	Symmetric, planar
[487]	$\text{RuO}_2 \cdot x\text{H}_2\text{O}$ @ $\text{Ti}_3\text{C}_2\text{T}_x$ -Ag NWs	Paper	-	864.2 F cm^{-3}	-	13.5 mWh cm^{-3}	$4.85 \times 10^7 \mu\text{W cm}^{-2}$	Symmetric, planar
[514]	m- $\text{Ti}_3\text{C}_2\text{T}_x$	Paper	158 mF cm^{-2}	-	$1.64 \mu\text{Wh cm}^{-2}$	-	$778.3 \mu\text{W cm}^{-2}$	Asymmetric planar
3D Printing, Extrusion Printing								
[289]	$\text{Ti}_3\text{C}_2\text{T}_x$	Paper	43 F cm^{-2}	-	$0.32 \mu\text{Wh cm}^{-2}$	-	$11.4 \mu\text{W cm}^{-2}$	Symmetric, planar
[166]	N-doped $\text{Ti}_3\text{C}_2\text{T}_x$ AC CNT, GO	PET, Paper Rubber, PI,	8200 F cm^{-2}	-	$420 \mu\text{Wh cm}^{-2}$	0.83 mWh cm^{-3}	-	Symmetric, planar
[327]	$\text{Ti}_3\text{C}_2\text{T}_x$	-	2100 F cm^{-2}	-	$24.4 \mu\text{Wh cm}^{-2}$	-	$640 \mu\text{W cm}^{-2}$	Symmetric, planar
[141]	$\text{Ti}_3\text{C}_2\text{T}_x$	Polymer, Paper	1035 F cm^{-2}	-	$51.7 \mu\text{Wh cm}^{-2}$	-	-	Symmetric, planar

One of the main challenges of the printed energy storage device application of MXene based inks are their short shelf life when compared to the metallic and GR based functional inks.

Although much progress has been made on the development of flexible and printed MXene MSCs having high energy densities suitable to integrate it with high power miniaturized PEs, their scalable production for the practical application is still challenging. Eventhough, the MXene based printed structure shows better oxidation resistance after the solvent evaporation, still advancements are required under exposure to humid environmental conditions.

4. Conclusions

This review article summarises the present position of 2D MXene material based inks and their printing application in the health sector as cost effective printed smart devices have a key role in revolutionizing the health care sector through disease prediction and timely treatment via continuous non-invasive and real time health monitoring. The developments in PE materials and smart printed wearable cost effective devices have the potential to strongly benefit the quality of human living. However, PE technology will be successful and generic in future only if the systems and components are inexpensive, easy to produce, allow low voltage operation, and are possible to make from the stable and environmentally friendly materials. For all the PE device application, materials should exhibit proper mechanical integrity and resistivity while being non-toxic and for sensing application high conductivity is an essential requirement. MXenes have received much attraction due to its excellent mechanical and thermal properties, high ion adsorption abilities and super electric conductivities. In addition to these fascinating properties, the relative ease of the large quantity production of MXene and the possibility of their production in different forms such as pure MXene powders or films or colloidal suspensions, make MXenes very attractive to the scientific community and for practice applications. The surface terminations (-OH, -F and -O) of MXenes make their layered surface hydrophilic and enable them easier to solution-process in organic or aqueous systems. The usage of colloidal MXene materials in printing applications mainly using screen printing, extrusion type 3D printing, and inkjet printing techniques have been increased in recent years. The excellent properties exhibited by MXenes make them suitable for many important PE applications including storage devices, and sensors. It is possible to generate multi layer or single layer nanosheets of MXenes having large surface areas favourable to enhance the performance of the sensors based on MXenes. The unique 2D in-layer nanostructures which are transformable and chemical compositions which are controllable provide 2D MXenes with versatile characteristics benefiting a range of possible biomedical and wearable healthcare applications. Even though multifunctional 2D MXenes and their composites have already been developed for the biomedical application including, biosensing, diagnostic imaging, typical phototherapy of photothermal therapy, antimicrobial, and photothermal/photodynamic/chemo synergistic therapy, the printed biomedical or therapeutic applications of MXene materials are limited. While MXenes are promising 2D materials for printed device applications, the gradual degradation [489-491] of single or multilayer $Ti_3C_2T_x$ nanosheets in humid conditions, either in water or air, can negatively affect their usage in sensing applications as many sensors function in humid environment. When considering energy storage device application, long term storage can similarly be a problem as MXene storage stability has been shown to be weak in an aqueous environment. Another problem that faces MXene synthesis process is the use of HF etchant as this is toxic and raises safety and environmental issues. The introduction of terminal groups during the etching process strongly influences the device performances by enhancing electron transfer rate. Therefore, a good understanding is required on such terminal

groups. MXenes currently used in biomedical device applications exhibit biocompatibility and biodegradability, however, there are no reports discussing their long term biosafety. Effectively integrated energy storage and powering systems have a key role for meeting the growing demand in the flexible and portable PEs. The current challenges for the scalable production of cost effective printed storage devices and components need to be addressed by developing novel active electrode materials exhibiting high performance, as the energy storage properties are strongly dependent on the mechanism of charge storage and intrinsic properties of materials used for fabricating electrodes. Research on printable MXene materials, which have the potential to overcome the limitations of other materials from the 2D family, is still in its early stages with much more research to be performed, but as can be seen from the results presented to date MXenes are a very promising class of 2D materials for PE applications.

Conflicts of interest

There are no conflicts to declare.

Acknowledgements

This work is supported in part by a research grant from Science Foundation Ireland (SFI) under Grant Number 16/RC/3872 and is co-funded under the European Regional Development Fund and by I-Form industry partners.

Reference

- [1] W. Lei, D. Portehault, D. Liu, S. Qin, Y. Chen, *Nat. Commun.* 4 (2013) 1777.
- [2] P. Urbankowski et al., *Nanoscale* 8 (2016) 11385.
- [3] B. Soundiraraju, B. K. George, *ACS Nano* 11 (2017) 8892.
- [4] M. Naguib et al., *ACS Nano* 6 (2012) 1322.
- [5] M. R. Lukatskaya et al., *Science* 341 (2013) 1502.
- [6] R. Meshkian, L.-Å. Naslund, J. Halim, J. Lu, M. W. Barsoum, J. Rosen, *Scr. Mater.* 108 (2015) 147.
- [7] M. Naguib et al., *Adv. Mater.* 23 (2011) 4248.
- [8] B.-M. Jun, S. Kim, J. Heo, C.M. Park, N. Her, M. Jang, Y. Huang, J. Han, Y. Yoon, *Nano Res.* 12 (2019) 471.
- [9] M. Naguib et al., *J. Am. Chem. Soc.* 135 (2013) 15966.
- [10] M. Khazaei et al., *Adv. Funct. Mater.* 23 (2013) 2185.
- [11] M. Ghidui et al., *Chem. Commun.* 50 (2014) 9517.
- [12] B. Anasori et al., *ACS Nano* 9 (2015) 9507.
- [13] Y Gogotsi, *Nat. Mater.* 14 (2015) 1079.
- [14] M. Naguib, V. N. Mochalin, M. W. Barsoum, Y Gogotsi, *Adv. Mater.* 26 (2014) 992.
- [15] C. Dai, H. Lin, G. Xu, Z. Liu, R. Wu, Y. Chen, *Chemistry of Materials* 29 (2017) 8637.
- [16] W. Zheng, P. Zhang, J. Chen, W. Tian, Y. Zhang, Z. Sun, *Journal of Materials Chemistry A* 6 (2018) 3543.
- [17] T. Cai et al., *Applied Catalysis B: Environmental* (2018) 239545.
- [18] M. Kurtoglu, M. Naguib, Y. Gogotsi, M. W. Barsoum, *MRS Commun.* 2 (2012) 133.
- [19] M. Khazaei, M. Arai, T. Sasaki, M. Estili, Y. Sakka, *Phys. Chem. Chem. Phys.* 16 (2014) 7841.
- [20] A. L. Ivanovskii, A. N. Enyashin, *Russ. Chem. Rev.* 82 (2013) 735.
- [21] I. R. Shein, A. L. Ivanovskii, *Comput. Mater. Sci.* 65 (2012) 104.
- [22] G. Gao, G. Ding, J. Li, K. Yao, M. Wu, M. Qian, *Nanoscale* 8 (2016) 8986.
- [23] M. Khazaei et al., *Phys. Rev. B* 93 (2016) 205125.
- [24] A. N. Gandi, H. N. Alshareef, U. Schwingenschlögl, *Chem. Mater.* 28 (2016) 1647.
- [25] A. Enyashin, A. Ivanovskii, *Comp. Theor. Chem.* 989 (2012) 27.
- [26] Y. Lee, S. B. Cho, Y. C. Chung, *ACS Appl. Mater. Interfaces* 6 (2014) 14724.
- [27] Z. Ma, Z. Hu, X. Zhao, Q. Tang, D. Wu, Z. Zhou, L. Zhang, *J. Phys. Chem. C* 118 (2014) 5593.
- [28] S. Zhao, W. Kang, J. Xue, *Appl. Phys. Lett.* 104 (2014) 133106.
- [29] C. Si, J. Zhou, Z. Sun, *ACS Appl. Mater. Interfaces* 7 (2015) 17510.
- [30] H. Weng et al., *Phys. Rev. B* 92 (2015) 075436.
- [31] S. Zhao, W. Kang, J. Xue, *J. Mater. Chem. C* 3 (2015) 879.

- [32] J. Yang, X. Luo, S. Zhang, L. Chen, *Phys. Chem. Chem. Phys.* 18 (2016) 12914.
- [33] V. Mauchamp et al., *Phys. Rev. B* 89 (2014) 235428.
- [34] V. N. Borysiuk, V. N. Mochalin, Y. Gogotsi, *Nanotechnology* 26 (2015) 265705.
- [35] Z. H. Fu et al., *Phys. Rev. B* 94 (2016) 104103.
- [36] U. Yorulmaz, A. Özden, N. K. Perkgöz, F. Ay, C. Sevik, *Nanotechnology* 27 (2016) 335702.
- [37] H. Zhang, G. Yang, X. Zuo, H. Tang, Q. Yang, G. Li, *J. Mater. Chem. A* 4 (2016) 12913.
- [38] P. Urbankowski, et al., *Nanoscale* 9 (2017) 17722.
- [39] C. Zhang et al., *Nat. Com.* 10 (2019) 849.
- [40] Z. Y. Li et al., *Mater. Sci. Eng. B* 191 (2015) 33.
- [41] D. Sun, M. Wang, Z. Li, G. Fan, L.-Z. Fan, A. Zhou, *Electrochemistry Communications* 47 (2014) 80.
- [42] M. Ghidui, M. R. Lukatskaya, M.-Q. Zhao, Y. Gogotsi, M. W. Barsoum, *Nature* 516 (2014) 78.
- [43] J. Halim, *Chem. Mater.* 26 (2014) 2374.
- [44] L. H. Karlsson, J. Birch, J. Halim, M. W. Barsoum, P. O. Persson, *Nano Lett.* 15 (2015) 4955.
- [45] L. Wang et al., *Electron. Mater. Lett.* 12 (2016) 702.
- [46] K. S. Novoselov et al., *Science* 306 (2004) 666.
- [47] M. W. Barsoum, *Physical Properties of the MAX Phases*. In *Encyclopedia of Materials: Science and Technology*; Buschow, K. H. J., Cahn, R., Flemings, M., Ilschner, B., Kramer, E., Mahajan, S., Veysière, P., Eds.; Elsevier, Oxford, 2006; pp 1-11.
- [48] M. W. Barsoum, *MAX Phases: Properties of Machinable Ternary Carbides and Nitrides*, Wiley-VCH Verlag GmbH & Co. KGaA, Weinheim, Germany 2013.
- [49] D. J. Finn et al., *J. Mater. Chem. C* 2 (2014) 925.
- [50] F. Withers et al., *Nano Lett.* 14 (2014) 3987.
- [51] D. McManus et al., *Nat. Nanotechnol.* 12 (2017) 343.
- [52] G. Hu et al., *Nat. Commun.* 8 (2017) 278.
- [53] V. Bianchi et al., *Nat. Commun.* 8 (2017) 15763.
- [54] B. L. Dasaria, J. M. Nouri, D. Brabazon, S. Naher, *Energy* 140 (2017) 766.
- [55] Q. Tang, Z. Zhou, Z. F. Chen, *J. Phys. Chem. C* 115 (2011) 18531.
- [56] W. Chen, Y. F. Li, G. T. Yu, C. Z. Li, S. B. Zhang, Z. Zhou, Z. F. J. Chen, *Am. Chem. Soc.* 132 (2010) 1699.
- [57] Q. Tang, Y. Cui, Y. F. Li, Z. Zhou, Z. F. Chen, *J. Phys. Chem. C* 115 (2011) 1724.
- [58] Y. F. Li, Z. Zhou, S. B. Zhang, Z. F. J. Chen, *Am. Chem. Soc.* 130 (2008) 16739.
- [59] Y. F. Li, D. H. Wu, Z. Zhou, C. R. Cabrera, Z. F. Chen, *J. Phys. Chem. Lett.* 3 (2012) 2221.
- [60] Q. Tang, F. Y. Li, Z. Zhou, Z. F. J. Chen, *Phys. Chem. C* 115 (2011) 11983.
- [61] Q. Tang, Y. F. Li, Z. Zhou, Y. S. Chen, Z. F. Chen, *ACS Appl. Mater. Interfaces* 2 (2010) 2442.
- [62] Y. F. Li, F. Y. Li, Z. Zhou, Z. F. J. Chen, *Am. Chem. Soc.* 133 (2011) 900.
- [63] Q. Tang, Z. Zhou, Z. F. J. Chen, *Phys. Chem. C* 116 (2012) 4119.
- [64] B. Anasori, M. R. Lukatskaya, Y. Gogotsi, *Nat. Rev. Mater.* 2 (2017) 16098.
- [65] F. Shahzad et al., *Science* 353 (2016) 1137.
- [66] H. Wei, M. Wang, W. Zheng, Z. Jiang, Y. Huang, *Ceramics International* 46 (2020) 6199.
- [67] Y.-J. Wan et al., *Composites Part A: Applied Science and Manufacturing* 130 (2020) 105764.
- [68] P. He, M. -S. Cao, Y. -Z. Cai, J. -C. Shu, W. -Q. Cao, J. Yuan, *Carbon* 157 (2020) 80.
- [69] X. Wu et al., *Chemical Engineering Journal* 381 (2020) 122622.
- [70] M. D. Levi et al., *Adv. Energy Mater.* 5 (2015) 1.
- [71] J. Zhou et al., *Angew. Chem. Int. Ed.* 55 (2016) 5008.
- [72] C. Lu, A. Li, T. Zhai, C. Niu, H. Duan, L. Guo, W. Zhou, *Energy Storage Materials* 26 (2020) 472.
- [73] M. Naguib et al., *Electrochem. Commun.* 16 (2012) 61.
- [74] Q. Tang, Z. Zhou, P. J. Shen, *Am. Chem. Soc.* 134 (2012) 16909.
- [75] O. Mashtalir et al., *Nat. Commun.* 4 (2013) 1716.
- [76] X. Li et al., *Journal of Alloys and Compounds* 824 (2020) 153803.
- [77] C. Wei, H. Fei, Y. Tian, Y. An, H. Guo, J. Feng, Y. Qian, *Energy Storage Materials* 26 (2020) 223.
- [78] I. Persson et al., *Adv. Mater.* 31 (2018) 1805472.
- [79] A.-M.-García, A.-F.-Fernández, F. Vines and F. Illas *J. Mater. Chem. A* 6 (2018) 3381.
- [80] Q. Tang, Z. Sun, S. Deng, H. Wang, Z. Wu, *Journal of Colloid and Interface Science* 564 (2020) 406.
- [81] X. Zhang et al., *Angew. Chem., Int. Ed.* 52 (2013) 4361.
- [82] B. Xu, M. Zhu, W. Zhang, X. Zhen, Z. Pei, Q. Xue, C. Zhi, P. Shi, *Adv. Mater.* 28 (2016) 3333.
- [83] X. Zhang, Z. Zhang, J. Li, X. Zhao, D. Wu, Z. Zhou, *J. Mater. Chem. A* 5 (2017) 12899.
- [84] Z. Guo, J. Zhou, L. Zhu, Z. Sun, *J. Mater. Chem. A* 4 (2016) 11446.
- [85] W. Yuan, L. Cheng, Y. An, S. Lv, H. Wu, X. Fan, Y. Zhang, X. Guo, J. Tang, *Adv. Sci.* 5 (2018) 1700870.
- [86] H. Feng et al., *Applied Catalysis B: Environmental* 266 (2020) 118609.
- [87] B. Lia et al., *Applied Catalysis B: Environmental* 266 (2020) 118650.

- [88] X. Han et al., *Applied Catalysis B: Environmental* 265 (2020) 118539.
- [89] Y. Cao, Y. Fang, X. Lei, B. Tan, X. Hu, B. Liu, Q. Chen, *Journal of Hazardous Materials* 387 (2020) 122021.
- [90] X. Zhu et al., *ACS Nano* 11 (2017) 10816.
- [91] M. Ding et al., *Journal of Membrane Science* 600 (2020) 117871.
- [92] E. Y. M. Ang et al., *Journal of Membrane Science* 598 (2020) 117653.
- [93] J. Ma, Y. Cheng, L. Wang, X. Dai, F. Yu, *Chemical Engineering Journal* 384 (2020) 123329.
- [94] L. Ding, L. Li, Y. Liu, Y. Wu, Z. Lu, J. Deng, Y. Wei, J. Caro, H. Wang, *Nature Sustainability* 3 (2020) 296.
- [95] S. Cui, H. Pu, S. A. Wells, Z. Wen, S. Mao, J. Chang, M. C. Hersam, J. Chen, *Nat. Commun.* 6 (2015) 8632.
- [96] X. Liu, T. Ma, N. Pinna, J. Zhang, *Adv. Funct. Mater.* 27 (2017) 1702168.
- [97] A. N. Abbas et al., *ACS Nano* 9 (2015) 5618.
- [98] G. Liu, S. Rumyantsev, C. Jiang, M. Shur, A. Balandin, *IEEE Electron Device Lett.* 36 (2015) 1202.
- [99] S. Zou, J. Gao, L. Liu, Z. Lin, P. Fu, S. Wang, Z. Chen, *Journal of Alloys and Compounds* 817 (2020) 152785.
- [100] S. H. Lee et al., *ACS Appl. Mater. Interfaces* 12 (2020) 10434.
- [101] G. Yang, J. Zhao, S. Yi, X. Wan, J. Tang *Sens. & Act.: B Chem.* 309 (2020) 127735.
- [102] M. D. Levi et al., *Adv. Energy Mater.* 5 (2015) 1400815.
- [103] J. Come, et al., *Nano Energy* 17 (2015) 27.
- [104] H. Lin, X. Wang, L. Yu, Y. Chen, J. Shi, *Nano Lett.* 17 (2017) 384.
- [105] C. Dai, Y. Chen, X. Jing, L. Xiang, D. Yang, H. Lin, Z. Liu, X. Han, R. Wu, *ACS Nano* 11 (2017) 12696.
- [106] Q. Zhang, Q. Guo, Q. Chen, X. Zhao, S. J. Pennycook, H. Chen, *Adv. Sci.* 7 (2020) 1902576.
- [107] M. Soleymaniha et al., *Adv. Healthc. Mater.* 8 (2019) 1801137.
- [108] H. L. Chia et al., *Anal. Chem.* 92 (2020) 2452.
- [109] X. Maa et al., *Sensors and Actuators B: Chemical* 309 (2020) 127815.
- [110] K. Chen et al., *ACS Biomater. Sci. Eng.* 3 (2017) 2293
- [111] F. Veronesi et al., *Mater. Sci. Eng. C* 70 (2017) 264.
- [112] Z. Li, H. Zhang, J. Han, Y. Chen, H. Lin, T. Yang, *Adv. Mater.* 30 (2018) 1706981.
- [113] X. Han, J. Huang, H. Lin, Z. Wang, P. Li, Y. Chen, *Adv. Healthcare Mater.* 7 (2018) 1701394.
- [114] K. Rasool, M. Helal, A. Ali, C. E. Ren, Y. Gogotsi, K. A. Mahmoud, *ACS Nano* 10 (2016) 3674.
- [115] F. Alimohammadi et al., *Langmuir* 34 (2018) 7192.
- [116] H. Lin, Y. Wang, S. Gao, Y. Chen, J. Shi, *Adv. Mater.* 30 (2018) 1703284.
- [117] Y. Hernandez et al., *Nat. Nanotechnol.* 3 (2008) 563.
- [118] W. Zhao, M. Fang, F. Wu, H. Wu, L. Wang and G. Chen, *J. Mater. Chem.* 20 (2010) 5817.
- [119] K. R. Paton et al., *Nat. Mater.* 13 (2014) 624.
- [120] X. Li, G. Zhang, X. Bai, X. Sun, X. Wang, E. Wang, H. Dai, *Nat. Nanotechnol.* 3 (2008) 538.
- [121] C. Valles et al., *J. Am. Chem. Soc.* 130 (2008) 15802.
- [122] S. Stankovich et al., *Carbon* 45 (2007) 1558.
- [123] J. N. Coleman et al., *Science* 331 (2011) 568.
- [124] E. Varrla et al., *Chem. Mater.* 27 (2015) 1129.
- [125] L. H. Li, Y. Chen, G. Behan, H. Zhang, M. Petracic, A. M. Glushenkov, *J. Mater. Chem.* 21 (2011) 11862.
- [126] Y. Yao, Z. Lin, Z. Li, X. Song, K.-S. Moon, C.-P. Wong, *J. Mater. Chem.* 22 (2012) 13494.
- [127] J. Zheng et al., *Nat. Commun.* 5 (2014) 3905.
- [128] G. Eda, H. Yamaguchi, D. Voiry, T. Fujita, M. Chen, M. Chhowalla, *Nano Lett.* 11 (2011) 5111.
- [129] D. Hanlon et al., *Nat. Commun.* 6, (2015) 8563.
- [130] J. Kang et al., *Proc. Natl. Acad. Sci. U. S. A.* 13 (2016) 11688.
- [131] J. Kang, J. Wood, S. Wells, J.-H. Lee, X. Liu, K.-S. Chen, M. Hersam, *ACS Nano* 9 (2015) 3596.
- [132] R. C. T. Howe, G. Hu, Z. Yang, T. Hasan, *SPIE Nanosci. Eng.* (2015) 95530R.
- [133] F. Bonaccorso, A. Bartolotta, J. N. Coleman, C. Backes, *Adv. Mater.* 28 (2016) 6136.
- [134] Z. Cui, *Printed electronics: Materials, technologies and applications*, John Wiley & Sons Singapore Pvt. Ltd, Singapore, 1st edn, 2016, p. 360.
- [135] C. Casiraghi et al., *Carbon* 129 (2018) 462.
- [136] T. Vuorinen, J. Niittynen, T. Kankkunen, T.M. Kraft, M. Mäntysalo, *Sci. Rep.* 6 (2016) 35289.
- [137] A. M. Joseph, B. Nagendra, E. B. Gowd, K. P. Surendran, *ACS Omega* 1 (2016) 1220.
- [138] P. He, J. R. Brent, H. Ding, J. Yang, D. J. Lewis, P. O. Brien, B. Derby, *Nanoscale* 10 (2018) 5599.
- [139] D. McManus et al., *Flex. Print. Electron.* 3, (2018) 034005.
- [140] C. J. Zhang et al., *Nat. Commun.* 10 (2019) 1795.
- [141] J. Orangi, F. Hamade, V. A. Davis, M. Beidaghi, *ACS Nano* 14 (2020) 640.
- [142] N. Zhao, M. Chiesa, H. Sirringhaus, Y. Li, Y. Wu, B. Ong, *Journal of Applied Physics* 101 (2007) 064513.
- [143] X. Yang et al., *Science China Materials* 63 (2020) 392.
- [144] J. Guo et al., *Biosensors (Basel)* 9 (2019) 112.
- [145] P. He et al., *ACS Appl. Mater. Interfaces* 11 (2019) 32225.

- [146] E. Yakimchuk, R. Soots, I. Kotin, I. Antonova, *Current Applied Physics* 17 (2017) 1655.
- [147] A. Kosmala, R. Wright, Q. Zhang, P. Kirby, *Mater. Chem. Phys.* 129 (2011) 1075.
- [148] Y. Z. Zhao, D. X. Du, Y. H. Wang, *International Journal of Modern Physics B* 33 (2019) 1950385.
- [149] H. Shahariar, I. Kim, H. Soewardiman, J. S. Jur, *ACS Appl. Mater. Interfaces* 11 (2019) 6208.
- [150] D. Juric, S. Hämmerle, K. Gläser, W. Eberhardt, A. Zimmermann, *IEEE Transactions on Components, Packaging and Manufacturing Technology* 9 (2019) 156.
- [151] Z. Zhang, T. Si, J. Liu, *Nanotechnology* 29 (2018) 415603.
- [152] M. Tavakoli et al., *Adv. Mater.* 19 (2018) 1801852.
- [153] K. Zhu et al., *Adv Funct Mater.* 27 (2017) 1605352.
- [154] M. Borzenkov et al., *ACS Appl. Mater. Interfaces* 8 (2016) 9909.
- [155] M. Abulikemu, et al., *Ang. Che. -Int.* 53 (2014) 420.
- [156] P. T. Bishop et al., *Gold Bulletin* 43 (2010) 181.
- [157] C.-J. Lee, B.-G. Park, K.-H. Jung, Y. Kim, S.-B. Jung, *Science of Advanced Materials* 12 (2020) 594.
- [158] J. Sarfraz, A. Fogde, P. Ihalainen, J. Peltonen, *Applied Surface Science* 445 (2018) 89.
- [159] Y. S. Rosen et al., *Flexible and Printed Electronics* 2 (2017) 035007.
- [160] H. Lei, Z. Hang, L. Yinxiang, *Journal of materials science-materials in electronics* 28 (2017) 4219.
- [161] Y. Wang et al., *Electrochimica Acta* 218 (2016) 24.
- [162] E. Y. Wang, Xuezhao Li, Y. N. Duan, *Applied Nanoscience* 6 (2016) 575.
- [163] Y. Zhang, L. Wang, N. Zhang, Z. Zhou, *RSC Adv.* 8 (2018) 19895.
- [164] D.-H. Kim, R. Ghaffari, N. Lu, J. A Rogers, *Annu Rev Biomed Eng.* 14 (2012) 113.
- [165] <https://www.flexenable.com/blog/five-benefits-of-flexible-electronics-for-displays-and-sensors/> (accessed on 15/10/2020)
- [166] L. Yu, Z. Fan, Y. Shao, Z. Tian, J. Sun, Z. Liu, *Adv. Energy Mater.* 9 (2019) 1901839.
- [167] C. Zhang et al., *Adv. Funct. Mater.* 28 (2018) 1705506.
- [168] Y.-Y. Peng et al., *Energy Environ. Sci.* 9 (2016) 2847.
- [169] E. Quain et al., *Adv. Mater. Technol.* 4 (2019) 1800256.
- [170] J. Perelaer et al., *J. Mater. Chem.* 20 (2010) 8446.
- [171] A. Kamyshny, S. Magdassi, *Small* 10 (2014) 3515.
- [172] R. Abbel et al., *Transl. Mater. Res.* 1, (2014) 015002.
- [173] G. Grau et al., *Flexible Printed Electron.* 1 (2016) 023002.
- [174] M. Layani, A. Kamyshny, S. Magdassi, *Nanoscale* 6 (2014) 5581.
- [175] P. V. Zant, *Microchip Fabrication* 5th ed. New York: McGraw-Hill, (2004).
- [176] T. Leng et al., *2D Mater.* 7 (2020) 024004.
- [177] Y. Wang et al., *Journal of Power Sources* 450 (2020) 227685.
- [178] S. Chen, Y. Song, F. Xu, *ACS Appl. Mater. Interfaces* 10 (2018) 34646.
- [179] J. Ferri, C. P. Fuster, R. L. Llopis, J. Moreno, E. Garcia-Breijo, *Sensors (Basel)*. 18 (2018) 3313.
- [180] N.T. Furtak, E. Skrzetuska, I. Krucinska, *Fibres Text. Eastern Europe* 21 (2013) 84.
- [181] J. Ferri, J. V. Lidón-Roger, J. Moreno, G. Martinez, E. Garcia-Breijo, *Materials* 10 (2017) 1450.
- [182] Z. Zhou et al., *J. Mater. Chem. C* 6 (2018) 13120.
- [183] S. Cui, Z. Dai, Q. Tian, J. Liu, X. Xiao, C. Jiang, W. Wu, V. A. L. Roy, *J. Mater. Chem. C* 4 (2016) 6371.
- [184] R. Zhang, B. Peng, Y. Yuan, *Composites Sci. Technol.* 168 (2018) 118.
- [185] Y. Yuan, B. Peng, H. Chi, C. Li, R. Liu, X. Liu, *RSC Adv.* 6 (2016) 113298.
- [186] S. Harada, K. Kanao, Y. Yamamoto, T. Arie, S. Akita, K. Takei, *ACS Nano* 8 (2014) 12851.
- [187] S. Bielska, M. Sibinski, A. Lukasik, *Mater. Sci. Eng. B* 165 (2009) 50.
- [188] P. Jolke, E. H. Chris, W. M. D. L. Antonius, S. S. Ulrich, *Nanotechnology* 20 (2009) 165303.
- [189] S. H. Ko et al., *Sensors and Actuators, A: Physical* 134 (2007) 161.
- [190] M. Borghetti, M. Serpelloni, E. Sardini, S. Pandini, *Sensors and Actuators A: Physical* 243 (2016) 71.
- [191] S. Khan, L. Lorenzelli, R. S. Dahiya, *IEEE Sensors Journal* 15 (2015) 3164.
- [192] H.-Y. Mi, Z. Li, L.-S. Turng, Y. Sun, S. Gong, *Materials & Design* 56 (2014) 398.
- [193] J. Y. Lim, S. Y. Kim, *Polymer Journal* 36 (2004) 769.
- [194] J. H. Waller, L. Lalonde, Y. Leterrier, J.-A. E. Månson, *Thin Solid Films* 519 (2011) 4249.
- [195] I. U. Ahad et al., *Acta Physica Polonica A* 129 (2016) 241.
- [196] I. U. Ahad et al., *AIP Conference Proceedings* 2146 (2019) 020022.
- [197] N. Q. Balaban et al., *Nature Cell Biol.* 3 (2001) 466.
- [198] Y. Chan, Y. Mi, D. Trau, P. Huang, E. Chen, *Polymer* 2006, 47, 5124.
- [199] G. Schwartz et al., *Nat. Commun.* 4 (2013) 1859.
- [200] S. C. B. Mannsfeld et al., *Nat. Mater.* 9 (2010) 859.
- [201] X. Lin, J. Kavalakkatt, M. C. Lux-Steiner, A. Ennaoui, *Adv. Sci.* 2 (2015) 1500028.
- [202] T. Carey, *Nat. Commun.* 8 (2017) 1202.

- [203] G. Vescio, J. Lopez-Vidrier, R. Leghrib, A. Cornet, A. Cirera, *J. Mater. Chem. C* 4 (2016) 1804.
- [204] J. S. Gebauer, V. Mackert, S. Ognjanović, M. Winterer, *J. Colloid and Interface Science* 526 (2018) 400.
- [205] J.J. Schneider et al., *J. Mater. Chem.* 19 (2009) 1449.
- [206] J. Li, M. M. Naiini, S. Vaziri, M. C. Lemme, M. Östling, *Adv. Funct. Mater.* 24 (2014) 6524.
- [207] R. Guo et al., *Adv. Mater.* 25 (2013) 3343.
- [208] K. Takei, W. Honda, S. Harada, T. Arie, S. Akita, *Adv. Healthcare Mater.* 4 (2015) 487.
- [209] M. D. Dankoco, G. Y. Tesfay, E. Benevent, M. Bendahan, *Mater. Sci. Eng. B* 205 (2016) 1.
- [210] L. Basiricó, Inkjet printing of organic transistor devices [thesis]. University of Cagliari, (2012).
- [211] K. Baggaa et al., *J. Colloid and Interface Science*, 447 (2015) 263.
- [212] K. Sugauma, *Introduction to printed electronics*, 74 ed., Springer New York, US, (2014) p. 132.
- [213] E. W. Flick, *Printing ink and overprint varnish formulations*, William Andrew, Norwich, US, 2nd edn, (1999) p. 127.
- [214] P. De Gennes, F. Brochard-Wyart, D. Quééré, *Capillarity: Deformable interfaces*, in: *Capillarity and Wetting Phenomena: Drops, Bubbles, Pearls, Waves*, Springer Science and Business Media, Inc., New York, USA, (2004) pp. 2-3.
- [215] Y. Xu et al., *Adv. Energy Mater.* 3 (2013) 1035.
- [216] W. J. Hyun, E. B. Secor, M. C. Hersam, C. D. Frisbie, L. F. Francis, *Adv. Mater.* 27 (2015) 109.
- [217] K. Arapov, E. Rubingh, R. Abbel, J. Laven, G. de With, H. Friedrich, *Adv. Funct. Mater.* 26 (2016) 586.
- [218] P. G. Karagiannidis et al., *ACS Nano* 11 (2017) 2742.
- [219] J. Baker, D. Deganello, D. T. Gethin, T. M. Watson, *Mater. Res. Innovations* 18 (2014) 86.
- [220] E. B. Secor, S. Lim, H. Zhang, C. D. Frisbie, L. F. Francis, M. C. Hersam, *Adv. Mater.* 26 (2014) 4533.
- [221] J. Niittynen, E. Sowade, H. Kang, R. R. Baumann, M. Mäntysalo, *Sci. Rep.* 5 (2015) 8832.
- [222] Del Carro et al., *IEEE Trans. Components, Packag. Manuf. Technol.* 9 (2019) 1.
- [223] J. W. Boley, E. L. White, R. K. Kramer, *Adv. Mater.* 27, (2015) 2355.
- [224] N.-G. Park, K. M. Kim, M. G. Kang, K. S. Ryu, S. H. Chang, Y.-J. Shin, *Adv. Mater.* 17 (2005) 2349.
- [225] W. Shou, B. K. Mahajan, B. Ludwig, X. Yu, J. Staggs, X. Huang, H. Pan, *Adv. Mater.* 29 (2017) 1700172.
- [226] M. Dexter, Z. Gao, S. Bansal, C. H. Chang, R. Malhotra, *Sci. Rep.* 8 (2018) 2201.
- [227] A. S. G. Reddy et al., *Procedia Engineering* 25 (2011) 120.
- [228] M. Bariya et al., *ACS Nano* 12 (2018) 6978.
- [229] J. Courbat, Y.B. Kim, D. Briand, N.F. de Rooij, *Actuators and Microsystems Conference (TRANSDUCERS)*, (2011) T3P.089
- [230] S. P. Sreenilayam, I. Ul Ahad, V. Nicolosi, V. A. Garzon, D. Brabazon, *Materials Today* 32 (2020) 147.
- [231] H. Siringhaus et al., *Science* 290 (2000) 2123.
- [232] B. J. DeGans, P. Duineveld, U. Schubert, *Adv. Mater.* 16 (2004) 203.
- [233] Z. P. Yin, Y. Huang, N. Bu, X. Wang, Y. Xiong, *Chinese Science Bulletin* 55 (2010) 3383.
- [234] Y. S. Rim, S.-H. Bae, H. Chen, N. De Marco, Y. Yang, *Adv. Mater.* 28 (2016) 4415.
- [235] R. G. Scalisi, et al. *Organic Electronics* 18 (2015) 89.
- [236] D. Stuwe, D. Mager, D. Biro, J. G. Korvink, *Adv. Mater.* 27 (2015) 599.
- [237] Y. Sun, Y. Zhang, Q. Liang, Y. Zhang, H. Chi, Y. Shi, D. Fang, *RSC Adv.* 3 (2013) 11925.
- [238] B. Kang, W. H. Lee, K. Cho, *ACS Appl. Mater. Interfaces* 5 (2013) 2302.
- [239] P. F. Moonen, I. Yakimets, J. Huskens, *Adv. Mater.* 24 (2012) 5526.
- [240] B. H. Kim, et al. *Nano Lett.* 15 (2015) 969.
- [241] J. Song, H. Zeng, *Angew. Chem. Int. Ed.* 54 (2015) 9760.
- [242] B. Kim, et al. *Nano Lett.* 14 (2014) 3683.
- [243] H. M. Dong, W. W. Carr, J. F. Morris, *Phys. Fluids* 18 (2006) 072102.
- [244] T. H. J. V. Osch, J. Perelaer, A. W. M. de Laat, U. S. Schubert, *Adv. Mater.* 20 (2008) 343.
- [245] A. A.-Halhouli, H. Qitouqa, A. Alashqar, J. A.-Khalaf, *Sensor Review* 38 (2018) 438.
- [246] B. Derby, *Annu. Rev. Mater. Res.* 40 (2010) 395.
- [247] A. C. Arias, J. D. MacKenzie, I. McCulloch, J. Rivnay, A. Salleo, *Chem. Rev.* 110 (2010) 3.
- [248] C. Ruiz, E. M. García-Frutos, G. Hennrich, B. Gómez-Lor, *J. Phys. Chem. Lett.* 3 (2012) 1428.
- [249] C. Wang, K. Takei, T. Takahashi, A. Javey, *Chem. Soc. Rev.* 42 (2013) 2592.
- [250] K. Kordás et al., *Small* 2 (2006) 1021.
- [251] H. Okimoto et al., *Adv. Mater.* 22 (2010) 3981.
- [252] T. Takenobu et al., *Appl. Phys. Express* 2 (2009) 025005.
- [253] A. L. Dearden et al., *Macromol. Rapid Commun.* 26 (2005) 315.
- [254] S. Gamerith et al., *Adv. Funct. Mater.* 17 (2007) 3111.
- [255] B. K. Park, D. Kim, S. Jeong, J. Moon, J. S. Kim, *Thin Solid Films* 515 (2007) 7706.
- [256] <https://www.novacentrix.com/> (accessed on 11/08/2020)
- [257] F. Torrisi et al., *ACS Nano* 6 (2012) 2992.

- [258] J. Li, F. Ye, S. Vaziri, M. Muhammed, M. C. Lemme, M. Östling, *Adv. Mater.* 25 (2013) 3985.
- [259] K. Arapov, R. Abbel, G. De With, H. Friedrich, *Faraday Discuss* 173 (2014) 323.
- [260] Y. Gao, W. Shi, W. Wang, Y. Leng, Y. Zhao, *Ind. Eng. Chem. Res.* 53 (2014) 16777.
- [261] A. Capasso et al., *Solid State Commun.* 224 (2015) 53.
- [262] M. Singh, H. M. Haverinen, P. Dhagat, G. E Jabbour, *Adv. Mater.* 22 (2010) 673.
- [263] B. Derby, N. Reis, *MRS Bull.* 28 (2003) 815.
- [264] G. K. Batchelor, *An Introduction to Fluid Dynamics*, Cambridge University Press, (1967).
- [265] N. Reis, B. Derby, *M. R. S. Symp. Proc.* 624 (2000) 65.
- [266] *Inkjet technology for digital fabrication*, ed. I.M. Hutchings, G.D. Martin, John Wiley & Sons, Ltd, Chichester, UK, (2012) p. 390.
- [267] V Bergeron, D Bonn, J. Y. Martin, L Vovelle, *Nature* 405 (2000) 772.
- [268] O. Reynolds, *Philos. Trans. R. Soc.* 174 (1883) 935.
- [269] G. H. McKinley, M. Renardy, *Phys. Fluids* 23 (2011) 127101.
- [270] J. E. Fromm, *IBM J. Res. Dev.* 28 (1984) 322.
- [271] D. Tian, Y. Song, L. Jiang, *Chem. Soc. Rev.* 42 (2013) 5184.
- [272] N. Reis, B. Derby, *Mater. Res. Soc. Symp. Proc.* 625 (2000) 117.
- [273] D. Jang, D. Kim, J. Moon, *Langmuir* 25 (2009) 2629.
- [274] N. Luechinger, A. E. K. Athanassiou, W. J. Stark, *Nanotechnology* 19 (2008) 445201.
- [275] C.-L. Lee, C.-H. Chen, C.-W. Chen, *Chem. Eng. J.* 230 (2013) 296.
- [276] S. Wang, P. K. Ang, Z. Wang, A. L. L. Tang, J. T. L. Thong, K. P. Loh, *Nano Lett.* 10 (2010) 92.
- [277] L. Huang, Y. Huang, J. Liang, X. Wan, Y. Chen, *Nano Res.* 4 (2011) 675.
- [278] Y. M. Jo, S. Yoon, J.-H. Lee, S.-J. Park, S. R. Kim, *In, Chem. Lett.* 40 (2011) 54.
- [279] L. T. Le, M. H. Ervin, H. Qiu, B. E. Fuchs, W. Y. Lee, *Electrochem. Commun.* 13 (2011) 355.
- [280] K. Y. Shin, J.-Y. Hong, J. Jang, *Adv. Mater.* 23 (2011) 2113.
- [281] K. Y. Shin, J.-Y. Hong, J. Jang, *Chem. Commun.* 47 (2011) 8527.
- [282] D. Kong, L. T. Le, Y. Li, J. L. Zunino, W. Lee, *Langmuir* 28 (2012) 13467.
- [283] F. J. Tölle, M. Fabritious, R. Mülhaupt, *Adv. Funct. Mater.* 22 (2012) 1136.
- [284] H. Zhang, A. Xie, Y. Shen, L. Qiu, X. Tian, *Phys. Chem. Chem. Phys.* 14 (2012) 12757.
- [285] Y. Su, J. Du, D. Sun, C. Liu, H. Cheng, *Nano Res.* 6 (2013) 842.
- [286] Y. Su, S. Jia, J. Du, J. Yuan, C. Liu, W. Ren, H. Cheng, *Nano Res.* 8 (2015) 3954.
- [287] Y. Yoon, et al. *Sci. Rep.* 5 (2015) 14177.
- [288] W. Zhang, E. Bi, M. Li, L. Gao, *Colloids Surf. A* 490 (2016) 232.
- [289] C.-W. Wu et al., *Energy Storage Materials* 25 (2020) 563.
- [290] D. Tobjörk, R. Österbacka, *Adv. Mater.* 23 (2011) 1935.
- [291] F. C. Krebs, et al. *Solar Energy Materials and Solar Cells* 93 (2009) 422.
- [292] Y. J. Kwack, W. S. Choi, *J. Korean, Physiological Society* 59 (2011) 3410.
- [293] W. Y. Chang, T. H. Fang, S. H. Yeh, Y. C. Lin, *Sensors* 9 (2009) 1188.
- [294] S. Scherp, S. J. D. Ericsson, *US Patent* (1981) US4267773.
- [295] R. R. Søndergaard, et al. *Journal of Polymer Science Part B: Polymer Physics* 51 (2013) 16.
- [296] D. Novaković, N. Kašiković, G. Vladić, M. Pál, 15 - Screen Printing, in: J. Izdebska, S. Thomas (ed.), *Printing on Polymers*, William Andrew Publishing, (2016) pp. 247-261.
- [297] X. Cao, H. Chen, X. Gu, B. Liu, W. Wang, Y. Cao, F. Wu, C. Zhou, *ACS Nano* 8 (2014) 12769.
- [298] R. H. Leach, R. J. Pierce, E. P. Hickman, M. J. Mackenzie, H. G. Smith, *The printing ink manual*, ed. Springer Netherlands, Dordrecht, the Netherlands, 5th edn, (1993).
- [299] A. Goldschmidt, H.-J. Streitburger, *BASF Handbook on Basics of Coating Technology*, William Andrew, Hannover, Germany, (2003).
- [300] Z. Żolek-Tryznowska, 6 - Rheology of Printing Inks, in: J. Izdebska, S. Thomas (ed.), *Printing on Polymers*, William Andrew Publishing, (2016) 87.
- [301] A. Tyagi, K. M. Tripathi, R. K. Gupta, *J. Mater. Chem. A* 3 (2015) 22507.
- [302] T. Sekine et al., *Sci. Rep.* 8 (2018) 4442.
- [303] I. Shitanda et al., *ChemElectroChem* 4 (2017) 2460.
- [304] Q. Lu, L. Liu, S. Yang, J. Liu, Q. Tian, W. Yao, Q. Xue, M. Li, W. Wua, *J. Power Sources* 361 (2017) 31.
- [305] S. Liu et al., *J. Mater. Chem. A* 2 (2014) 18125.
- [306] H.-W. Lin, C.-P. Chang, W.-H. Hwu, M.-D. Ger, *J. Materials Processing Technology* 197 (2008) 284.
- [307] H. Li, X. Li, J. Liang, Y. Chen, *Adv. Energy Mater.* 9 (2019) 1803987.
- [308] N. A. Kyeremateng, T. Brousse, D. Pech, *Nat. Nanotechnol.* 12 (2016) 7.
- [309] H. Xiao, Z. S. Wu, L. Chen, F. Zhou, S. Zheng, W. Ren, H. M. Cheng, X. Bao, *ACS Nano* 11 (2017) 7284.
- [310] K.-H. Choi, J. T. Yoo, C. K. Lee, S.-Y. Lee, *Energy Environ. Sci.* 9 (2016) 2812.
- [311] W. J. Hyun et al., *Adv. Energy Mater.* 7 (2017) 1700285.

- [312] G. Cai, J.-H. Ciou, Y. Liu, Y. Jiang, P. S. Lee, *Sci. Adv.* 5 (2019) eaaw7956.
- [313] P. Jiang, Z. Ji, X. Zhang, Z. Liu, X. Wang, *Prog. Addit. Manuf.* 3 (2018) 65.
- [314] E. MacDonald, R. Wicker, *Science* 353 (2016) aaf2093.
- [315] Y. Xu, X. Wu, X. Guo, B. Kong, M. Zhang, X. Qian, S. Mi, W. Sun, *Sensors* 17 (2017) 1166.
- [316] K. Shen, J. Ding, S. Yang, *Adv. Energy Mater.* 8 (2018) 1800408.
- [317] T.-S. Wei, B. Y. Ahn, J. Grotto, J. A. Lewis, *Adv. Mater.* 30 (2018) 1703027.
- [318] P. Chang, H. Mei, S. Zhou, K. G. Dassios, L. Cheng, *J. Mater. Chem. A* 7 (2019) 4230.
- [319] K. Sun, T.-S. Wei, B. Y. Ahn, J. Y. Seo, S. J. Dillon, J. A. Lewis, *Adv. Mater.* 25 (2013) 4539.
- [320] B. C. Gross, J. L. Erkal, S. Y. Lockwood, C. Chen, D. M. Spence, *Anal. Chem.* 86 (2014) 3240.
- [321] B. G. Compton, J. A. Lewis, *Adv. Mater.* 26 (2014) 5930.
- [322] J. A. Lewis, *Adv. Funct. Mater.* 16 (2006) 2193.
- [323] J. A. Lewis, G. M. Gratson, *Mater. Today* 7 (2004) 32.
- [324] K. Fu et al., *Adv. Mater.* 28 (2016) 2587.
- [325] F. Zhang, M. Wei, V. V. Viswanathan, B. Swart, Y. Shao, G. Wu, C. Zhou, *Nano Energy* 40 (2017) 418.
- [326] A. Zhakeyev, P. Wang, L. Zhang, W. Shu, H. Wang, J. Xuan, *Adv. Sci.* 4 (2017) 1700187.
- [327] W. Yang et al., *Adv. Mater.* 31 (2019) 1902725.
- [328] H. Liu, C. Duan, C. Yang, W. Shen, F. Wang, Z. Zhu, *Sensors and Actuators B: Chemical* 218 (2015) 60.
- [329] F. Wang et al., *J. The Electrochemical Society* 162 (2015) B16.
- [330] E. Lee et al., *ACS Appl Mater Interfaces* 9 (2017) 37184.
- [331] L. Lorencova et al., *Electrochimica Acta* 235 (2017) 471.
- [332] A. Byeon et al., *ACS Appl Mater Interfaces* 9 (2017) 4296.
- [333] J. Zheng et al., *J. Electrochem. Soc.* 165 (2018) B227.
- [334] F. Wang, C. H. Yang, M. Duan, Y. Tang, J. F. Zhu, *Biosens. Bioelectron.* 74 (2015) 1022.
- [335] L. Lorencova et al., *Sens. Actuators B* 263 (2018) 360.
- [336] H. Liu, C. Duan, C. Yang, X. Chen, W. Shen, Z. Zhu, *Mater Sci Eng C* 53 (2015) 43.
- [337] J. Liu et al., *Adv. Funct. Mater.* 29 (2019) 1807326.
- [338] S. S. Shankar, R. M. Shereema, R. B. Rakhi, *ACS Appl. Mater. Interfaces* 10 (2018) 43343.
- [339] L. Wu, X. Lu, Dhanjai, Z.eS. Wu, Y. Do, *Biosens. Bioelectron.* 107 (2018) 69.
- [340] S. Kumar et al., *Biosens. Bioelectron.* 121 (2018) 243.
- [341] R. B. Rakhi, P. Nayuk, C. Xia, H. N. Alshareef, *Sci. Rep.* 6 (2016) 36422.
- [342] Y. Lei et al., *Small* 15, (2019) 1901190.
- [343] Y. Zhang, X. Jiang, J. Zhang, H. Zhang, Y. Li, *Biosens Bioelectron.* 130, (2019) 315.
- [344] H. Wang, H. Li, Y. Huang, M. Xiong, F. Wang, C. Li, *Biosens Bioelectron.* 142 (2019) 111531.
- [345] Y. Fang, X. Yang, T. Chen, G. Xu, M. Liu, J. Liu, Y. Xu, *Sens Actuators B Chem* 263 (2018) 400.
- [346] M. Sawangphruk et al., *Carbon* 70 (2014) 287.
- [347] X. Sun, S. Guo, Y. Liu, S. Sun, *Nano Letters* 12 (2012) 4859.
- [348] W. Dorge, H. M. Schipper, *Aging Cell* 6 (2007) 361.
- [349] S. DiMauro, E. A. Schon, *Annu. Rev. Neurosci.* 31 (2008) 91.
- [350] D. J. Rossi, C. H. M. Jamieson, I. L. Weissman, *Cell* 132 (2008) 681.
- [351] A. Sevanian, P. Hochstein, *Annu. Rev. Nutr.* 5 (1985) 365.
- [352] E. A. L. Martins, R. Meneghini, *Biochem. J.* 299 (1994) 137.
- [353] F. Ghorbani-Bidkorbeh et al., *Electrochem. Acta* 55 (2010) 2752.
- [354] R. Manjunatha, G. S. Suresh, J. S. Melo, S. F. D'Souza, *Electrochim. Acta* 56 (2011) 6619.
- [355] N. S. Anuar et al., *Sens. Actuators B-Chem.* 266 (2018) 375.
- [356] Z. Guo, Z. Y. Wang, H. H. Wang, G. Q. Huang, M. M. Li, *Mater. Sci. Eng. C* 57 (2015) 197.
- [357] G. Absalan, M. Akhond, M. Soleimani, H. Ershadifar, *J. Electroanal. Chem.* 761 (2016) 1.
- [358] B. Devadas, S. Cheemalapati, S. M. Chen, M. A. Ali, F. M. A. Al-Hemaid, *Ionics* 21 (2015) 547.
- [359] S. Cheemalapati, S. M. Chen, M. A. Ali, F. M. A. Al-Hemaid, *Colloid Surf. B* 121 (2014) 444.
- [360] S. Pan, J. Yin, L. Yu, C. Zhang, Y. Zhu, Y. Gao, Y. Chen, *Adv. Sci.* 7 (2020) 1901511.
- [361] S. Eosoly, S. Lohfeld, D. Brabazon, *Key Engineering Materials* 396 (2009) 659.
- [362] M. Lipowiecki, M. Ryvolova, A. Tottosi, S. Naher, D. Brabazon, *Adv. Mater. Res.* 445 (2012) 607.
- [363] T. D. Szucs, D. Brabazon, *Key Engineering Materials* 396 (2008) 663.
- [364] Marcin Lipowiecki, Dermot Brabazon, *Advanced Materials Research* 83 (2010) 914.
- [365] J. Xuan et al., *Angew. Chem.* 128 (2016) 14789.
- [366] Y. Bai, Y. Deng, Y. Zheng, Y. Li, R. Zhang, Y. Lv, Q. Zhao, S. Wei, *Mater. Sci. Eng. C* 2016, 59, 565.
- [367] R. C. Webb et al., *Nat. Mater.* 12 (2013) 938.
- [368] N. T. Tien et al., *Adv. Mater.* 26 (2014) 796.
- [369] B. Yin, X. Liu, H. Gao, T. Fu, J. Yao, *Nat. Commun.* 9 (2018) 5161.
- [370] A. H. A. Razak, A. Zayegh, R. K. Begg, Y. Wahab, *Sensors* 12 (2012) 9884.

- [371] X. Wang, Y. Gu, Z. Xiong, Z. Cui, T. Zhang, *Adv. Mater.* 26 (2014) 1336.
- [372] J. Hughes, F. Iida, *Sensors* 18 (2018) 3822.
- [373] Y. Wanga, S. Ali, J. Wijekoon, R. H. Gong, A. Fernando, *Sensors and Actuators A* 282 (2018) 215.
- [374] H. Liu, Z. Zhang, J. Gea, X. Lin, X. Ni, H. Yang, L. Yang, *J. Mater. Sci. Technol.* 35 (2019) 176.
- [375] K. H. Shelley, *Anesth. Analg.* 105 (2007) S31.
- [376] S. Gong et al., *Nat. Commun.* 5 (2014) 3132.
- [377] K. Hantanasirisakul, Y. Gogotsi, *Adv. Mater.* 30 (2018) 1804779.
- [378] Y-Z. Zhang et al., *Adv. Mater.* 32 (2020) 1908486.
- [379] J. Pang et al., *Chem. Soc. Rev.* 48 (2019) 72.
- [380] J. Kang, V. K. Sangwan, J. D. Wood, M. C. Hersam, *Acc. Chem. Res.* 50 (2017) 943.
- [381] E. Kayali, A. VahidMohammadi, J. Orangi, M. Beidaghi, *ACS Appl. Mater. Interfaces* 10 (2018) 25949.
- [382] C. C. Lai et al., *Acta Mater.* 99 (2015) 157.
- [383] C. Hu, et al., *Chem. Commun.* 51 (2015) 6560.
- [384] C. C. Lai et al., *Nanoscale* 9 (2017) 17681.
- [385] R. Meshkian et al., *Scr. Mater.* 108 (2015) 147.
- [386] Y. Zang, F. Zhang, C.-a. Di, D. Zhu, *Mater. Horiz.* 2 (2015) 140.
- [387] G. Ge, H. Wei, S. Jinjun, Xiaochen, D. J. Semicond. 39 (2018) 011012.
- [388] Y. Ding, J. Yang, C. R. Tolle, Z. Zhu, *ACS Appl. Mater. Interfaces* 10 (2018) 16077.
- [389] T. Yang, D. Xie, Z. Li, H. Zhu, *Mater. Sci. Eng. R* 115 (2017) 1.
- [390] T. Q. Trung, L. Nae Eung, *Adv. Mater.* 28 (2016) 4338.
- [391] N. N. Jason, M. D. Ho, W. Cheng, *Resistive Electronic Skin. J. Mater. Chem. C* 5 (2017) 5845.
- [392] F. R. Fan, T. Wei, W. Z. Lin, *Adv. Mater.* 28 (2016) 4283.
- [393] R. Zhang, R. Hu, X. Li, Z. Zhen, Z. Xu, N. Li, L. He, H. Zhu, *Adv. Funct. Mater.* 28 (2018) 1705879.
- [394] G. Zhu et al., *Nano Lett.* 14 (2014) 3208.
- [395] C. Mu et al., *ACS Applied Nano Materials* 1 (2018) 274.
- [396] D. Kwon et al., *ACS Appl. Mater. Interfaces* 8 (2016) 16922.
- [397] M. Kang, J. Kim, B. Jang, Y. Chae, J.-H. Kim, J.-H. Ahn, *ACS Nano* 11 (2017) 7950.
- [398] L. Qiu, M. B. Coskun, Y. Tang, J. Z. Liu, T. Alan, J. Ding, V. T. TruongD. Li, *Adv. Mater.* 28 (2016) 194.
- [399] L. Lv, P. Zhang, T. Xu, L. Qu, *ACS Appl. Mater. Interfaces* 9 (2017) 22885.
- [400] X. Dong, Y. Wei, S. Chen, Y. Lin, L. Liu, J. Li, *Compos. Sci. Technol.* 155 (2018) 108.
- [401] X. Zang, X. Wang, Z. Yang, X. Wang, R. Li, J. Chen, J. Ji, M. Xue, *Nanoscale* 9 (2017) 19346.
- [402] E. Strelcov, Y. Lilach, A. Kolmakov, *Nano Lett.* 9 (2009) 2322.
- [403] W. Li et al., *ACS Nano* 5 (2011) 6955.
- [404] D. J. Lipomi et al., *Nat. Nanotechnol.* 6 (2011) 788.
- [405] J. Janata, M. Josowicz, *Nat. Mater.* 2 (2003) 19.
- [406] Y. Guo, M. Zhong, Z. Fang, P. Wan, G. Yu, *Nano Lett.* 19 (2019) 1143.
- [407] Y. Cheng et al., *ACS Nano* 14 (2020) 2145.
- [408] S. Seyedin et al., *Adv. Mater.* 30 (2020) 1910504.
- [409] H. Li, Z. Du, *ACS Appl. Mater. Interfaces* 11 (2019) 49.
- [410] L. Wang, M. Tian, Y. Zhang, F. Sun, X. Qi, Y. Liu, L. Qu, *Journal of Materials Science* 55 (2020) 6187.
- [411] W.-T. Cao, C. Ma, D.-S. Mao, J. Zhang, M.-G. Ma, F. Chen, *Adv. Funct. Mater.* 29 (2019) 1905898.
- [412] R. Mas-Balleste, C. Gomez-Navarro, J. Gomez-Herrero, F. Zamora, *Nanoscale* 3 (2011) 20.
- [413] J. Lu, Z. Chen, F. Pan, Y. Cui, K. Amine, *Energy Rev.* 1 (2018) 35.
- [414] Y. Jiang, M. Hu, D. Zhang, T. Yuan, W. Sun, B. Xu, M. Yan, *Nano Energy* 5 (2014) 60.
- [415] J. Rockenberger, E. C. Scher, A. P. Alivisatos, *J. Am. Chem. Soc.* 121 (1999) 11595.
- [416] H. Wang, H. Feng, J. Li, *Small* 10 (2014) 2165.
- [417] W. Choi, N. Choudhary, G. H. Han, J. Park, D. Akinwande, Y. H. Lee, *Mater. Today* 20 (2017) 116.
- [418] H. Wu, Z. Guo, J. Zhou, Z. Sun, *Appl. Surf. Sci.* 488 (2019) 578.
- [419] F. Bonaccorso et al., *Science* 347 (2015) 1246501.
- [420] F. Feng, J. Wu, C. Wu, Y. Xie, *Small* 11 (2015) 654.
- [421] Y. Xie et al., *J. Am. Chem. Soc.* 136 (2014) 6385.
- [422] W. Liu, M. S. Song, B. Kong, Y. Cui, *Adv. Mater.* 29 (2017) 1603436.
- [423] Y. Gogotsi, P. Simon, *Science* 334 (2011) 917.
- [424] Q. Cheng, Z. Song, T. Ma, B. B. Smith, R. Tang, H. Yu, H. Jiang, C. K. Chan, *Nano Lett.* 13 (2013) 4969.
- [425] A. M. Zamarayeva et al., *Sci. Adv.* 3 (2017) e1602051.
- [426] L. Noerochim et al., *J. Mater. Chem.* 22 (2012) 11159.
- [427] L. Li, Z. Wu, S. Yuan, X. B. Zhang, *Energy Environ. Sci.* 7 (2014) 2101.
- [428] S. Goriparti et al., *J. Power Sources* 257, (2014) 421.
- [429] D. Deng, *Energy Sci. Eng.* 3 (2015) 385.

- [430] A. Opitz, P. Badami, L. Shen, K. Vignarooban, A. M. Kannan, *Sust. Energy Rev.* 68 (2017) 685.
- [431] J. Huang, J. Yang, W. Li, W. Cai, Z. Jiang, *Thin Solid Films* 516 (2008) 3314.
- [432] Y. Zhao, G. Liu, L. Liu, Z. Jiang, *Journal of Solid State Electrochemistry* 13 (2008) 705.
- [433] R. E. Sousa, et al., *Electrochimica Acta* 196 (2016) 92.
- [434] M.-S. Park, S.-H. Hyun, S.-C. Nam, *Electrochimica Acta* 52, (2007) 7895.
- [435] J. Ren, L. Li, C. Chen, X. Chen, Z. Cai, L. Qiu, Y. Wang, X. Zhu, H. Peng, *Adv. Mater.* 25 (2013) 1155.
- [436] G. Qian, X. Liao, Y. Zhu, F. Pan, X. Chen, Y. Yang, *ACS Energy Lett.* 4 (2019) 690.
- [437] K. Persson et al., *J. Phys. Chem. Lett.* 1 (2010) 1176.
- [438] L. Ji, Z. Lin, M. Alcoutlabi, X. Zhang, *Energy Environ. Sci.* 4 (2011) 2682.
- [439] D. Er, J. Li, M. Naguib, Y. Gogotsi, V.B. Shenoy, *ACS Appl. Mater. Interfaces* 6 (2014) 11173.
- [440] T. Bo et al., *Phys. Chem. Chem. Phys.* 20 (2018) 22168.
- [441] Q. Wan, S. Li, J. B. Liu, *ACS Appl. Mater. Inter.* 10 (2018) 6369.
- [442] D. Wang et al., *J. Phys. Chem. C* 121 (2017) 13025.
- [443] D. Wang, Z. H. Sun, D. X. Han, L. Liu, L. Niu, *RSC Adv.* 7 (2017) 11834.
- [444] X. Chen, Z. Kong, N. Li, X. Zhao, C. Sun, *Phys. Chem. Chem. Phys.* 18 (2016) 32937.
- [445] J. Come et al., *J Electrochem Soc.* 159 (2012) A1368.
- [446] Z. Yang et al., *Power Sources* 192 (2009) 588.
- [447] Z. Chen, I. Belharouak, Y. -K. Sun, K. Amine, *Adv. Funct. Mater.* 23 (2013) 959.
- [448] X. Wang et al., *Nat. Commun.* 6 (2015) 6544.
- [449] P. Yu, G. Cao, S. Yi, X. Zhang, C. Li, X. Sun, K. Wang, Y. Ma, *Nanoscale* 10 (2018) 5906.
- [450] A. Byeon et al., *Power Sources* 326 (2016) 686.
- [451] J. Li, N. Kurra, M. Seredych, X. Meng, H. Wang, Y. Gogotsi, *Nano Energy* 56 (2019) 151.
- [452] B. J. Yoon, S. H. Jeong, K. H. Lee, H. S. Kim, C. G. Park, J. H. Han, *Chem. Phys. Lett.* 388 (2004) 170.
- [453] X. W. Yang, C. Cheng, Y. F. Wang, L. Qiu, D. Li, *Science* 341 (2013) 534.
- [454] J. Chmiola, G. Yushin, Y. Gogotsi, C. Portet, P. Simon, P. L. Taberna, *Science* 313 (2006) 1760.
- [455] S.W. Zhang, B. S. Yin, X. X. Liu, D. M. Gu, H. Gong, Z. B. Wang, *Nano Energy.* 59 (2019) 41.
- [456] X. Fu et al., *Appl. Surf. Sci.* 507 (2020) 145135.
- [457] Q. Zhu, D. Zhao, M. Cheng, J. Zhou, K.A. Owusu, L. Mai, Y. Yu, *Adv. Energy Mater.* 9 (2019) 1.
- [458] M. Zhi, C. Xiang, J. Li, M. Li, N. Wu, *Nanoscale* 5, (2013) 72.
- [459] G. Wang, L. Zhang, J. Zhang, *Chem. Soc. Rev.* 41 (2012) 797.
- [460] Y. Wang, Y. Xia, *Adv. Mater.* 25, (2013) 5336.
- [461] M. M. Hu, Z. J. Li, T. Hu, S. H. Zhu, C. Zhang, X. H. Wang, *ACS Nano* 10 (2016) 11344.
- [462] M. R. Lukatskaya et al., *Adv. Energy Mater.* 5 (2015) 1500589.
- [463] M. R. Lukatskaya et al., *Nat. Energy* 2 (2017) 17105.
- [464] M. Hu, Z. Li, H. Zhang, T. Hu, C. Zhang, Z. Wuab, X. Wang, *Chem. Commun.* 51 (2015) 13531.
- [465] X. Wang, G. Yushin, *Energy Environ. Sci.*, 8 (2015) 1889.
- [466] W. Gao et al., *Nat. Nanotechnol.* 6 (2011) 496.
- [467] Z. Su et al., *Energy Environ. Sci.* 7 (2014) 2652.
- [468] H.-K. Kim, S.-H. Cho, Y.-W. Ok, T.-Y. Seong, Y. S. Yoon, *J. Vac. Sci. Technol. B* 21 (2003) 949.
- [469] Z. Cai, L. Li, J. Ren, L. Qiu, H. Lin, H. Peng, *J. Mater. Chem. A* 1 (2013) 258.
- [470] J. Chmiola, C. Largeot, P.-L. Taberna, P. Simon, Y. Gogotsi, *Science* 328 (2010) 480.
- [471] Y. Liu et al., *J. Chen. Adv. Mater. Tech.* 1 (2016) 1600166.
- [472] M. Beidaghi, Y. Gogotsi, *Energy Environ. Sci.* 7 (2014) 867.
- [473] S. Xu, Y. Dall'Agnese, G. Wei, C. Zhang, Y. Gogotsi, W. Han, *Nano Energy* 50 (2018) 479.
- [474] H. Li, Y. Hou, F. Wang, M. R. Lohe, X. Huang, L. Niu, X. Feng, *Adv. Energy Mater.* 7 (2017) 1601847.
- [475] H. Wang, Y. Wu, X. Yuan, G. Zeng, J. Zhou, X. Wang, J. W. Chew, *Adv. Mater.* 30 (2018) 1704561.
- [476] D. Yu, K. Goh, H. Wang, L. Wei, W. Jiang, Q. Zhang, L. Dai, Y. Chen, *Nat. Nanotechnol.* 9 (2014) 555.
- [477] H. Hu, Z. Bai, B. Niu, M. Wu, T. Hua, *J. Mater. Chem. A* 6 (2018) 14876.
- [478] C. Couly et al., *Adv. Electron. Mater.* 4 (2018) 1700339.
- [479] Q. Jiang et al., *Nano Energy* 45 (2018) 266.
- [480] N. Kurra, B. Ahmed, Y. Gogotsi, H. N. Alshareef, *Adv. Energy Mater.* 6 (2016) 1601372.
- [481] H. Hu, Y. Hua, *J. Mater. Chem. A* 5 (2017) 19639.
- [482] Q. Jiang, N. Kurra, M. Alhabeab, Y. Gogotsi, H. N. Alshareef, *Adv. Energy Mater.* 8 (2018) 1703043.
- [483] B.-S. Shen, H. Wang, L.-J. Wu, R.-S. Guo, Q. Huang, X.-B. Yan, *Chin. Chem. Lett.* 27 (2016) 1586.
- [484] H. Huang et al., *Adv. Electron. Mater.* 4 (2018) 1800179.
- [485] P. Salles, E. Quain, N. Kurra, A. Sarycheva, Y. Gogotsi, *Small* 14 (2018) 1802864.
- [484] Q. X. Xia, J. Fu, J. M. Yun, R. S. Mane, K. H. Kim, *RSC Adv.* 7 (2017) 11000.
- [487] Z. Fu et al., *Chem. Rev.* 119 (2019) 11980.
- [488] Chen X, Villa N S, Zhuang Y, Chen L, Wang T, Li Z, Kong T 2019 *Adv. Energy Mater.* 10 (2019) 1902769.

- [489] I.-M. Low, *Mater.* 12 (2019) 473.
- [490] S. Huang, V. N. Mochalin, *Inorg. Chem.* 58 (2019) 1958.
- [491] C. Zhang et al., *Chem. Mater.* 29 (2017) 4848.
- [492] P. Eklund, M. Beckers, U. Jansson, H. Högberg, L. Hultman, *Thin Solid Films* 518 (2010) 1851.
- [493] Y.-Z. Zhang et al., *Sci. Adv.* 4 (2018) eaat0098.
- [494] D. P. Dubal, N. R. Chodankar, D. H. Kim, P. Gomez-Romero, *Chem. Soc. Rev.* 47 (2018) 2065.
- [495] X. Zhang et al., *Journal of Energy Chemistry* 27 (2018) 73.
- [496] G. Lv et al., *Materials Letters* 219 (2018) 45.
- [497] C. Xing et al., *ACS Appl. Mater. Interfaces* 10 (2018) 27631.
- [498] L. Wu et al., *Laser Photonics Rev.* 12 (2018) 1800215.
- [499] Q. Wu et al., *Adv. Mater.* 4 (2019) 1800532.
- [500] C. Wang et al., *Adv. Opt. Mater.* 7 (2019) 1900060.
- [501] Y. Song et al., *Adv. Opt. Mater.* 7 (2019) 1801777.
- [502] Y. Song et al., *Adv. Opt. Mater.* 6 (2018) 1701287.
- [503] X. Jiang et al., *Physics Reports* 848 (2020) 1-58.
- [504] Y. Zang et al., *Biosensors and Bioelectronics* 130 (2019) 315.
- [505] M. M. Arafat, et al., *Sensors* 12 (2012) 7207.
- [506] N. Barsan et al., *Sens. Actuators B* 121 (2007) 18.
- [507] S. Yang et al., *Sensors and Actuators B* 226 (2016) 478.
- [508] J. Kim, H. Kim, W. J. Kim, *Small* 12 (2016) 1184.
- [509] Q. Weng, et al., *ACS Nano* 8 (2014) 6123.
- [510] W. Yin et al., *ACS Nano* 8 (2014) 6922.
- [511] W. Sun et al., *Journal of Materials Chemistry A*, 5 (41) (2017) 21663.
- [512] S. Yang et al., *Angewandte Chemie*, 130 (47) (2018) 15717.
- [513] B. Akuzum et al., *ACS Nano* 12 (2018) 2685.
- [514] S. Abdolhosseinzadeh et al., *Adv. Mater.* 32 (2020) 2000716.
- [515] T. Zhang et al., *J. Alloys Compd.* 695 (2017) 818.
- [516] B. Behera et al., *Institute of Physics Publishing* 13 (2019) 024001.
- [517] W. Yuan et al., *J. Mater. Chem. A* 6 (2018) 18116.
- [518] L. Gao et al., *Chem. Mater.* 32 (2020) 1703.
- [519] L. Zhao and B. Tungsten, 2 (2020) 176.
- [520] A. Liu et al., *Advanced Functional Materials* 30 (2020) 2003437.
- [521] M. Jeon et al., *Chemosphere* 261 (2020) 127781.
- [522] Y. A. J. Al-Hamadani et al., *Chemosphere* 254. (2020) 126821.
- [523] B. M. Jun et al., *Nano Research* 12 (2019) 471.
- [524] K. Rasool et al., *Materials Today* 30 (2019) 80.
- [525] K. Kannan, K. K. Sadasivuni, A. M. Abdullah, B. Kumar, *Catalysts* vol. 10 (2020) 495.
- [526] R. Garg, A. Agarwal, M. Agarwal, *Materials Research Express* 7 (2020) 22001.
- [527] M. K. Aslam, M. Xu, *Nanoscale* 12 (2020) 15993.
- [528] U. Yorulmaz, İ. Demiroğlu, D. Çakir, O. Gülseren, C. Sevik, *J. Phys. Energy* 2 (2020) 032006.
- [529] K. Deshmukh et al., *Coordination Chemistry Reviews* 424 (2020) 213514.
- [530] T. Li et al., *Angew. Chemie - Int. Ed.* 57 (2018) 6115.
- [531] X. Wang et al., *J. Mater. Chem. A* 5 (2017) 22012.
- [532] M. Alhabeb et al., *Angew. Chemie - Int. Ed.* 57 (2018) 5444.
- [533] M. Hu et al., *Chemical Society reviews* 49 (2020) 6666.
- [534] L. Jin et al., *Energy Storage Mater.* 23 (2019) 409.
- [535] K. Jayaramulu et al., *Adv. Funct. Mater.* 29 (2019) 1902539.
- [536] Y. Shi et al., *Sci. Rep.* 3 (2013) 1.
- [537] X. Jia et al., *Chem. Commun.* 47 (2011) 9669.
- [538] S. Ko, J. I. Lee, H. S. Yang, S. Park, and U. Jeong, *Adv. Mater.* 24 (2012) 4451.
- [539] X. Jia, Y. Kan, X. Zhu, G. Ning, Y. Lu, and F. Wei, "Nano Energy 10 (2014) 344.
- [540] C. Wei et al., *Small* 15 (2019) 1903214.
- [541] Q. Zhao et al., *Small* 15 (2019) 1904293.
- [542] Y. Wang, Y. Zheng, J. Zhao, Y. Li, *Energy Storage Mater.* 33 (2020) 82.
- [543] X.-R. Wang, et al. *Journal of Materials Processing Technology* 241 (2017) 93.

- [544] M. A. Worsley, *et al.* Chemical Communications 48 (2012) 8428.
- [545] X. Xiao *et al.*, ACS Nano 11 (2017) 2180.
- [546] A. VahidMohammadi, *et al.*, ACS Nano 11 (2017) 11135.
- [547] S. Abdolhosseinzadeh *et al.*, J. Phys. Energy 2 (2020) 031004.
- [548] A. Lipatov *et al.*, Adv. Electron. Mater. 2 (2016) 1600255.
- [549] M. A. Hope *et al.*, Phys. Chem. Chem. Phys. 18 (2016) 5099.
- [550] D. Magne *et al.*, Physical Chemistry Chemical Physics, 18 (2016) 30946.
- [551] H. Wang *et al.*, Applied Surface Science, 384 (2016) 287.
- [552] K. Hantanasirisakul *et al.*, Adv. Electron. Mater. 2 (2016) 1600050.
- [553] X. Y. Feng *et al.*, Laser Phys. Lett. 15 (2018) 085805.
- [554] S. Cho, M. Kim, J. Jang, ACS Appl. Mater. Interfaces, 7 (2015) 10213.
- [555] W. S. Brett and A. L. Jennifer, J. Am. Chem. Soc., 2012, 134, 1419.
- [556] D. S. Wang *et al.*, J. Mater. Chem. A 3 (2015) 2407.
- [557] Y. Liu *et al.*, Adv. Funct. Mater., 28 (2018) 1706592.
- [558] L. Li *et al.*, Adv. Energy Mater. 6 (2016) 1600909.
- [559] J. Li *et al.*, ACS Nano 11 (2017) 8249.
- [560] L. Liu *et al.*, Adv. Mater. Technol. 3, (2018) 1700206.
- [562] S. Liu *et al.*, Nanoscale 10 (2018) 20096.
- [563] Z. Ling *et al.*, Proc. Natl. Acad. Sci. U. S. A. 111, (2014) 16676.
- [564] K. J. Harris *et al.*, J. Phys. Chem. C 119 (2015) 13713-13720.
- [565] A Sugahara *et al.*, Nat. Commun. 10 850 (2019) 1.
- [566] K. Takeshi *et al.*, J. Phys. Chem. C 124 (2020) 13649.
- [567] B. Yang *et al.*, Adv. Mater. 30 (2018) 1705611.